AD_____

Award Number:

W81XWH-11-1-0803

TITLE:

Muscle Stem Cell Therapy for the Treatment of DMD Associated Cardiomyopathy

PRINCIPAL INVESTIGATOR:

Johnny Huard, Ph.D.

CONTRACTING ORGANIZATION:

**University of Pittsburgh
Pittsburgh, PA 15260**

REPORT DATE:

October 2012

TYPE OF REPORT:

Annual

PREPARED FOR:

**U.S. Army Medical Research and Materiel Command
Fort Detrick, Maryland 21702-5012**

DISTRIBUTION STATEMENT:

Approved for Public Release; Distribution Unlimited

The views, opinions and/or findings contained in this report are those of the author(s) and should not be construed as an official Department of the Army position, policy or decision unless so designated by other documentation.

REPORT DOCUMENTATION PAGE

1. REPORT DATE	2. REPORT TYPE	3. DATES COVERED
1 Oct 2012	Annual	30 Sep 2011 to 29 Sep 2012

4. TITLE AND SUBTITLE

Muscle Stem Cell Therapy for the Treatment of DMD Associated Cardiomyopathy

Ù˘à]¦[þ&oáFↄkÁT˘•&|^ÁŮc^{ ÁÔ^||Á/@¦aj^Á[¦Áó@Á/¦^æ{ ^}o{-ÁÖT ÖÁ/Œ•[&æœ^å

Subproject 2: Human hepatocytes for treatment of life-threatening liver injury

5a. CONTRACT NUMBER

5b. GRANT NUMBER

W81XWH-11-1-0803

5c. PROGRAM ELEMENT NUMBER

6. AUTHOR(S)

Johnny Huard, Ph.D.
Ira Fox, M.D.
David Perlmutter, M.D.

E-Mail: jhuard@pitt.edu

5d. PROJECT NUMBER

5e. TASK NUMBER

5f. WORK UNIT NUMBER

7. PERFORMING ORGANIZATION NAME(S) AND ADDRESS

University of Pittsburgh
Pittsburgh, PA 15219

8. PERFORMING ORGANIZATION REPORT NUMBER

9. SPONSORING / MONITORING AGENCY

U.S. Army Medical Research and Materiel Command
Fort Detrick, Maryland 21702-5012

10. SPONSOR/MONITOR'S ACRONYM(S)

11. SPONSOR/MONITOR'S REPORT NUMBER(S)

12. DISTRIBUTION / AVAILABILITY STATEMENT

Approved for Public Release; Distribution Unlimited

13. SUPPLEMENTARY NOTES

14. ABSTRACT

See next page

15. SUBJECT TERMS Project 1: Duchenne muscular dystrophy, Cardiomyopathy, Cell Therapy, Cellular cardiomyoplasty, Pericytes, myo-endothelial cells, Angiogenesis, Project 2: Liver disease, Cirrhosis, Hepatocyte isolation, Hepatocyte transplantation, Induced Pluripotent Stem (iPS) cells

16. SECURITY CLASSIFICATION OF:			17. LIMITATION OF ABSTRACT	18. NUMBER OF PAGES	19a. NAME OF RESPONSIBLE PERSON USAMRMC
a. REPORT	**b. ABSTRACT**	**c. THIS PAGE**			
U	U	U	UU	83	**19b. TELEPHONE NUMBER** *(include area code)*

ABSTRACT:

Project 1: Dilated cardiomyopathy affects approximately 1 in 2,500 individuals in the United States and is the 3rd most common cause of heart failure and the most frequent cause of heart transplantation. Patients that suffer from various muscle diseases, including Duchenne muscular dystrophy (DMD), develop progressive cardiomyopathy. Cellular cardiomyoplasty, which involves the transplantation of exogenous cells into the heart, is a possible approach by which to repair diseased or injured myocardium and improve cardiac function. Though there are a number of drugs prescribed to treat dilated cardiomyopathy, there is no cure and individuals eventually require a heart transplant; therefore the use of cardiomyoplasty to repair the hearts of individuals suffering from cardiomyopathy could possibly be an effective alternative to heart transplantation. Technical Objective #1: To investigate the effect of cell survival, proliferation, and differentiation on the regeneration/repair capacity of various human MDSC populations implanted into the heart of mdx/SCID mice. Technical Objective #2: To investigate the role that angiogenesis plays in the regeneration/repair capacity of human MDSCs injected into the hearts of mdx/SCID mice.

 Project 2: This project will determine the extent to which novel sources of hepatocytes can be used for regeneration and repair of injuries to the liver and liver failure. A more complete understanding of the extent to which donor liver cells can be resuscitated from non-traditional sources and expanded for application to reduce liver injury and toxin and/or cancer risk should enhance the number of areas where hepatic stem cell transplantation might be effectively applied.   Technical Objective #1: To characterize and expand hepatocytes from patients with cirrhosis and end-stage liver disease in immune deficient hosts whose livers permit extensive repopulation with donor cells. Technical Objective #2: To determine the extent to which transplantation with human hepatocytes can reverse hepatic failure in a clinically relevant non-human primate model of this process.

Table of Contents

Sub-project 1: Muscle Stem Cell Therapy for the Treatment of

DMD Associated Cardiomyopathy

PI: Johnny Huard

INTRODUCTION:

Cardiomyopathy is a serious disease of the heart muscle that can lead to congestive heart failure, a condition in which the heart can no longer effectively pump blood. Dilated cardiomyopathy affects approximately 1 in 2,500 individuals in the United States and is the 3rd most common cause of heart failure and the most frequent cause of heart transplantation. Patients that suffer from some diseases of the cytoskeleton, such as the progressive muscular dystrophies, often develop cardiomyopathy. Duchenne muscular dystrophy (DMD), one of the progressive muscular dystrophies, is an X-linked muscle disease caused by mutations in the dystrophin gene. This devastating disease is characterized by progressive muscle weakness due to a lack of dystrophin expression at the sarcolemma of muscle fibers. DMD patients usually develop symptoms of dilated cardiomyopathy in their early teens, and these symptoms steadily progress with age. This dilated cardiomyopathy is characterized by an enlarged ventricular chamber, wall thinning, and systolic dysfunction. Histological examination of a human DMD cardiomyopathic heart reveals fibrosis, degeneration, and fatty infiltration. The lack of dystrophin has consequently been linked to the cardiomyopathy that develops in DMD. In the hearts of mdx, dystrophin-deficient, mice (a murine model of DMD), especially in aged mdx mice, fibrosis and degeneration of the myocardium are evident upon histological examination. Because the mammalian heart possesses only a limited capacity to regenerate new cardiac muscle after injury and disease, noncontractile scar tissue eventually replaces the injured and diseased myocardium. Cellular cardiomyoplasty, which involves the transplantation of exogenous cells into the heart, is a possible approach by which to repair diseased or injured myocardium and improve cardiac function. Though there are a number of drugs prescribed to treat dilated cardiomyopathy, there is no cure and individuals eventually require a heart transplant; therefore the use of cardiomyoplasty to repair the hearts of individuals suffering from cardiomyopathy could possibly be an effective alternative to heart transplantation.

Technical Objectives

Technical Objective #1: To investigate the effect of cell survival, proliferation, and differentiation on the regeneration/repair capacity of various human MDSC populations implanted into the heart of mdx/SCID mice.

Hypothesis: After implantation into the heart, the human muscle derived cells abilities to survive and undergo long-term proliferation play a role in their efficient regeneration and repair of diseased cardiac tissue.

Technical Objective #2: To investigate the role that angiogenesis plays in the regeneration/repair capacity of human MDSCs injected into the hearts of mdx/scid mice.

Hypothesis: Enhancing angiogenesis will increase the regeneration/repair capacity of human muscle derived cells injected into the hearts of mdx mice.

BODY:

Progress made from: 10-1-11 to 9-30-12

1) Double Utrophin/dystrophin knockout mice (dKO mice) develop a more severe cardiomyopathy than the mdx mice.

DMD patients die of cardiac or respiratory failure in their 3rd decade (1). The *Mdx* mouse model has near-normal cardiac function until very late in life; therefore, we aimed to determine if dystrophin-/-utrophin+/- (double knock-out, DKO het) mice might represent a superior model of DMD associated cardiomyopathy, and test it to see if we could eventually treat DMD associated heart failure via cell therapy. Some hallmarks of cardiomyopathy include inflammation and fibrosis which leads to decreased contractility and thus dysfunction of the heart. Left ventricle dilation and wall thinning which leads to a decreased ability to pump blood (contractile dysfunction), decreased angiogenesis, which leads to greater cell death due to a of lack of appropriate nutrients and oxygen ,

Figure 1

and arrhythmias (2). First we assayed and compared the amount of fibrosis in the hearts of mdx and DKO het mice at the ages of 10 weeks to 17 months. We found similar levels of fibrosis in mdx mice at 10 weeks and DKO het mice at 14 weeks (**Figure 1A and B**); however, the DKO het mice appeared to accumulate cardiac fibrosis more rapidly than mdx mice. The DKO het mice at 8 months had similar fibrosis levels to mdx mice at 17 months (**Figure 1C -F**).
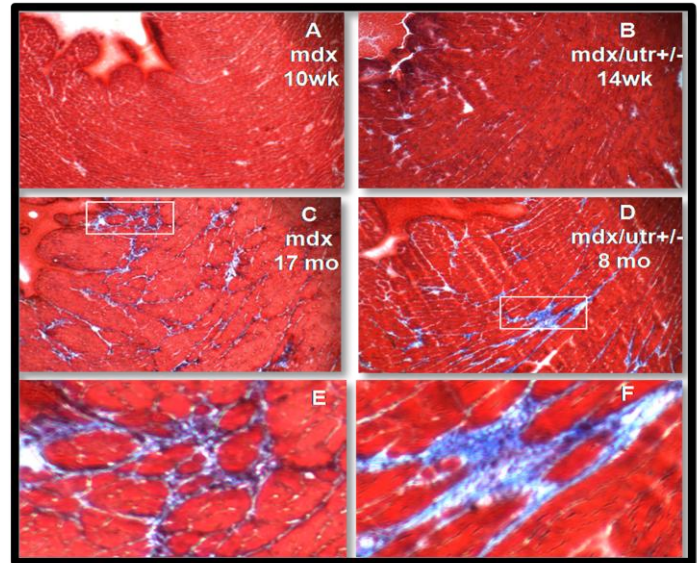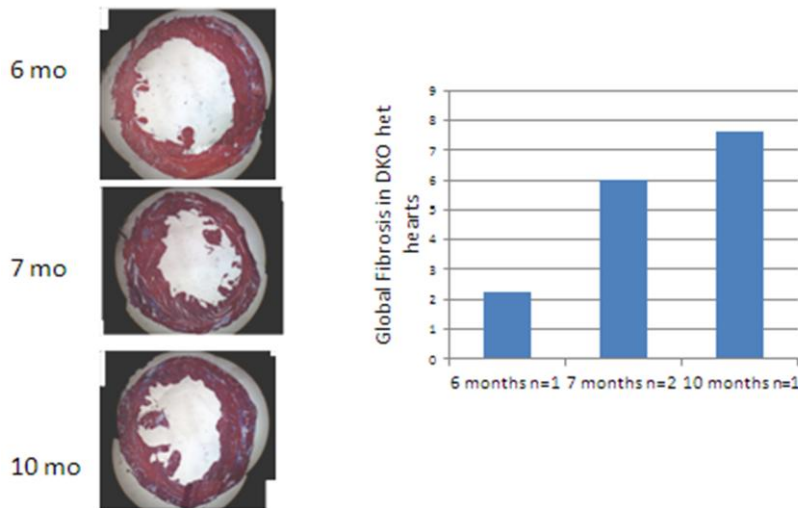
Figure 2

Therefore we went on to further characterize the hallmarks of cardiomyopathy in DKO het mice aged 6-10 months. First we looked at global fibrosis from 6-10 months and found rapidly increasing fibrosis levels (**Figure 2**). Next, we characterized the cardiac function looking at end diastolic area and fractional area change. Dilation of the hearts increased with the age of the mice

which is shown in **Figure 3** and quantified in **Figure 4** as end diastolic area. Correspondingly, the cardiac functional parameter fractional area change decreases from 6-10 months (**Figure 4**).

Figure 3

LV dilation of DKO hets

6 mo

7 mo

10 mo

Figure 4

DKO het ECHO analysis

End Diastolic Area (EDA)

Fractional Area Change (FAC)
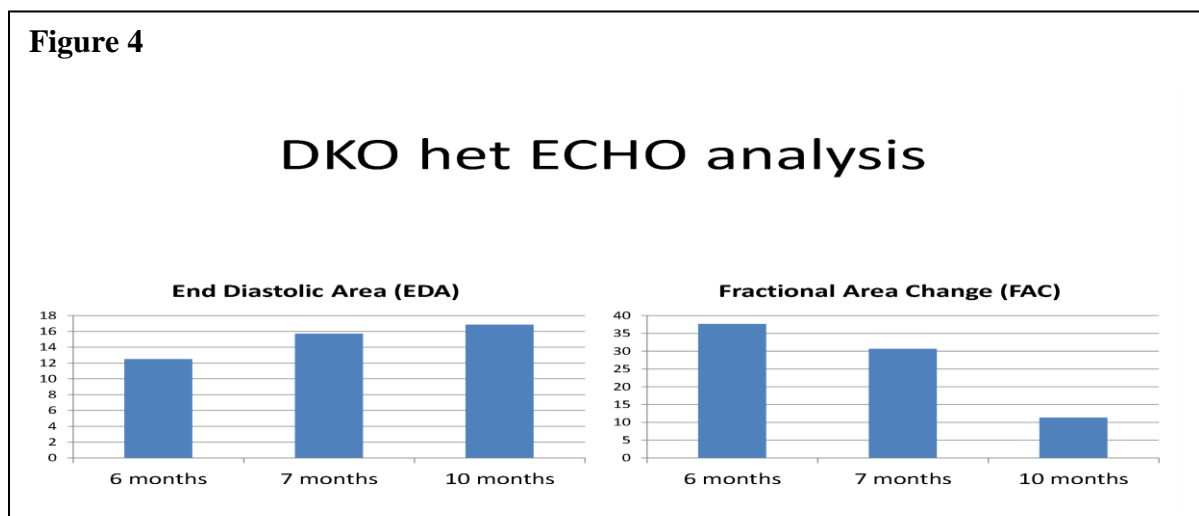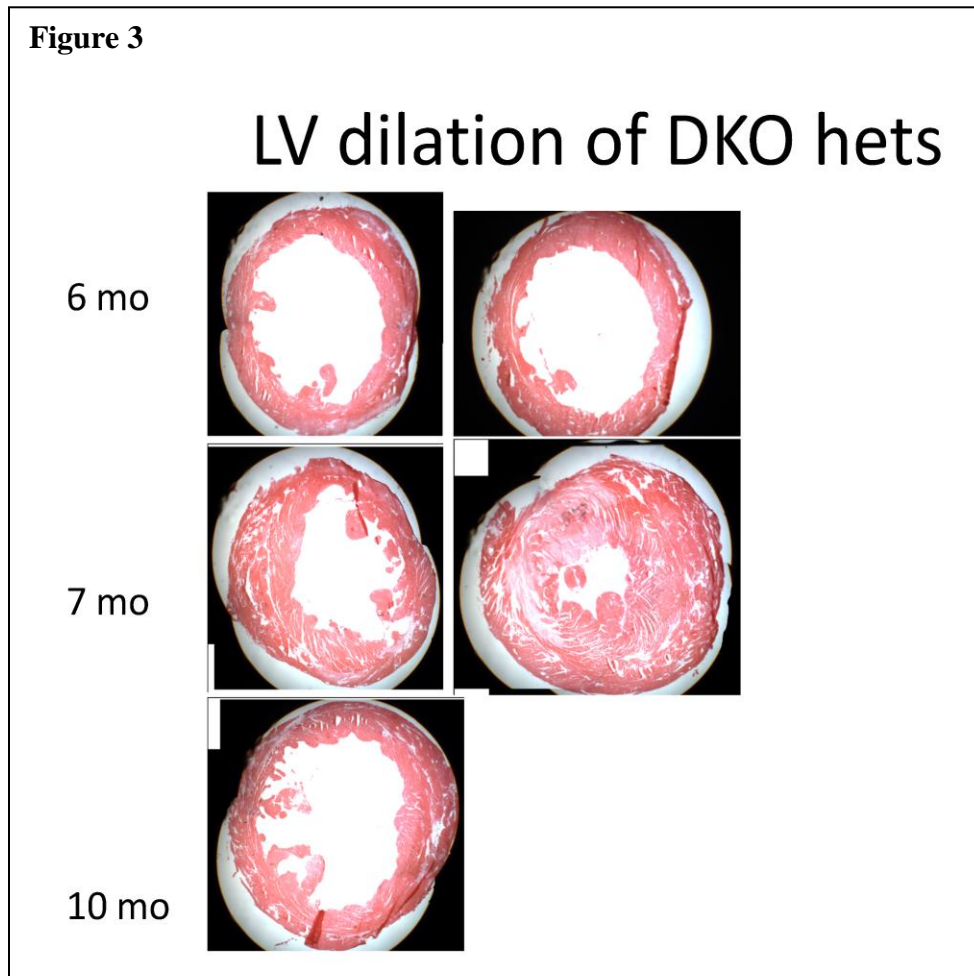
Finally, we examined angiogenesis in the DKO het hearts and found that the percent area of CD31+ endothelial cells increased at 10 months; however, the number of alpha smooth muscle actin positive cells, which marks more mature vascular structures, decreased from 6-7 months and then remained fairly constant through to 10 months (**Figure 5).**

In conclusion, as DKO mice age cardiac fibrosis levels, dilation, and FAC get progressively worse making them a better model for DMD associated cardiomyopathy than the mdx mice, which do not develop severe cardiomyopathy until much later in life. Therefore, we have selected to use the DKO mouse model for the remaining of the experimental objectives which aim to develop biological approaches based on muscle derived

Figure 5

Angiogenesis: CD31 and ASMA
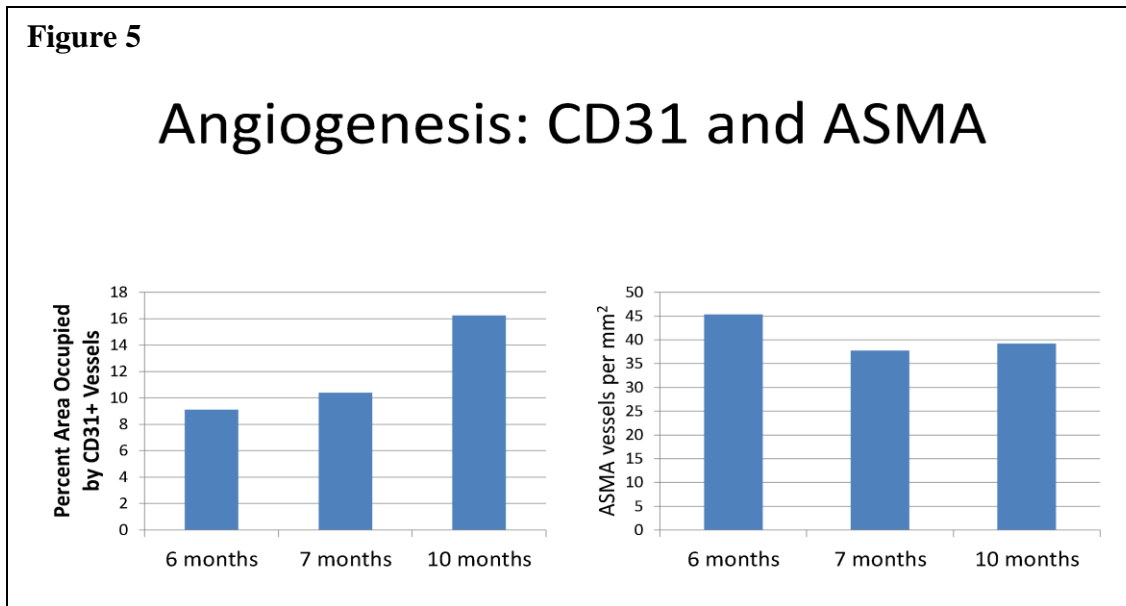
stem cells to improve cardiac function after cardiomyopathy.

2) Intramyocellular lipid accumulation, fibrosis and HO in cardiac muscle of dKO mice are more extensive then in mdx mice: *The role of RhoA in the cardiac histopathology observed in dKO mice.* **(Appendix 1)**

Heterotopic ossification (HO) or ectopic fatty infiltration often occurs in muscle tissues in various disease states, and can contribute to impaired metabolism, muscle force production, and mobility function (3, 4). HO is a process where bone tissue forms in soft tissues, which can be caused by trauma, surgery, neurologic injury and genetic abnormalities (4). Bone Morphogenetic Proteins (BMPs) are known to be responsible for the induction of HO in damaged skeletal muscle (5). Previous studies in our laboratory demonstrated that HO induced by BMP-4, demineralized bone matrix, and trauma in skeletal muscle mouse model could be repressed by overexpressing Noggin, a BMP antagonist (6). Fatty infiltration is the accumulation of fat cells outside the typical fat stores underneath skin, and has been reported to be associated with aging, inactivity, obesity, and diseases like diabetes (3, 7, 8). Fatty infiltration into skeletal muscle (intramuscular adipose tissue, IMAT) is often associated with disorders in lipid metabolism (7-9); however, disorders in lipid metabolism in skeletal muscle can often cause another type of abnormal lipid deposition: intramyocellular lipid accumulation (10-12). More important for the current proposal, intramyocellular lipid accumulation also occurs in cardiac muscle (intramyocardial lipid accumulation) which can also be similarly caused by disorders in lipid metabolism or lipid overload, which leads to lipotoxicity and cardiac dysfunction, and can be a sign of myocardial degradation during the progression of cardiac dysfunction *(13-17).* Intramyocellular lipid accumulation in cardiac muscle (intramyocardial lipid accumulation) has been observed in DMD patients, especially in the most damaged area

of the heart (18, 19). Here we suggest that intramyocellular lipid accumulation may occur in the cardiac muscles of DKO mice as well and could be correlated with the progress of phenotypes such as fibrosis formation.

RhoA is a small G-protein in the Rho family that regulates cell morphology and migration in response to extracellular signals, via reorganizing actin cytoskeleton (20, 21). The RhoA-Rho kinase (ROCK) signaling pathway functions as a commitment switch for osteogenic and adipogenic differentiation of mesenchymal stem cells (MSCs) (22). Activation of RhoA-ROCK signaling in cultured MSCs *in vitro* induces their osteogenesis but inhibits the potential of adipogenesis, while the application of Y-27632, a specific inhibitor of ROCK, reversed the process (22-24). RhoA-ROCK inhibitor Y-27632 was found to induce adipogenic differentiation of myofiber-derived muscle cells *in vitro,* and resulted in fatty infiltration in skeletal muscle (25). Meanwhile, RhoA was shown to be activated by Wnt5a in inducing osteogenic differentiation and repressing adipogenic differentiation of human Adipose Stem Cells (ASCs) (26). Furthermore, the role of RhoA signaling in inflammatory reactions has been demonstrated, for example, TNF-α induces activation of RhoA signaling in smooth muscle cells (27), and RhoA was found to regulate Cox-2 activity in fibroblasts (28). In addition, an important role of RhoA in myogenic differentiation has also been demonstrated where the sustained activation of the RhoA pathway can block muscle differentiation by inhibiting myoblast fusion (29-31).

Trichrome staining of cardiac muscles from WT, mdx and dKO mice (8-weeks old) was conducted to characterize extracellular matrix (ECM) collagen deposition in the muscles. Our findings showed that fibrosis formation was generally very severe in dKO mice, mild in mdx mice, and absent in WT mice (**Figure 6A**). Alizarin Red staining of the cardiac muscle also revealed the occurrence of HO in the cardiac muscle of dKO mice (**Figure 6B**), but not in WT and mdx mice (data not shown). Meanwhile, we did not observe obvious fatty infiltration in the cardiac muscle of any of the three mouse models (data not shown). Intramyocardial lipid accumulation was observed at 1 week of age in all 3 mouse models (**Figure 6C**); however, intramyocardial lipid accumulation in fetal WT mice is known to be common, because unlike the adult hearts, the fetal heart uses glucose and not fatty acids as sources of energy (32, 33). Intramyocardial lipid accumulation was found

Figure 6

A — Trichrome stain 8W: WT, mdx, dKO. B — Alizarin Red: dKO.

C — AdipoRed / DAPI: 1W, 4W, 8W; WT, mdx, dKO.

D — Intramyocardial lipid accumulation. Percentage of area (WT, mdx, dKO); 1W, 4W, 8W.

E — mRNA of cardaic muscle (4W). WT mdx dKO: GAPDH, RhoA, TNF, IL-6, Klotho, PPAR-γ.

to decrease rapidly in WT mice from one week after birth, and became nearly non-detectable by 4 weeks of age (**Figure 6C**); however, both the mdx and dKO mouse models still exhibited extensive amounts of intramyocardial lipid (**Figure 6C, D)**, which was far more pronounced in the DKO mice than the mdx mice

(**Figure 6C, D**). Compared to WT and mdx mice, the expression of RhoA and inflammatory signaling genes (TNF-α and IL-6) was found to be more up-regulated in the cardiac muscle of dKO mice, while the expression of Klotho gene was down-regulated (**Figure 6E**). We suggest that the activation of RhoA and inflammatory signaling may account for the higher levels of HO, intramyocardial lipid accumulation and fibrosis observed in the DKO cardiac muscles.

In vivo RhoA inactivation in DKO mice reduces intramyocellular lipid accumulation fibrosis, and HO in cardiac muscle. (**Appendix 2**)

We hypothesized that RhoA inactivation could reduce HO, intramyocellular lipid accumulation and fibrosis in the cardiac muscles of DKO mice. To verify this hypothesis, Y-27632 was injected intraperitoneally (IP) to achieve systematic inhibition of RhoA signaling in DKO mice (4-week old). After 3 weeks of continuous IP injection, the skeletal muscle phenotype of the DKO mice was found to be similarly improved as when we performed local injection of Y-27632 into skeletal muscle (data not shown). As anticipated the intramyocellular lipid accumulation, fibrosis and HO in cardiac muscle was also reduced (**Figure 7A-E**). Semi-quantitative PCR studies on the cardiac muscle tissues further revealed that, the expression of RhoA and inflammatory factors was down-regulated with Y-27632 administration and the expression of Klotho and PPARγ was up-regulated (**Figure 7F**).


Figure 7
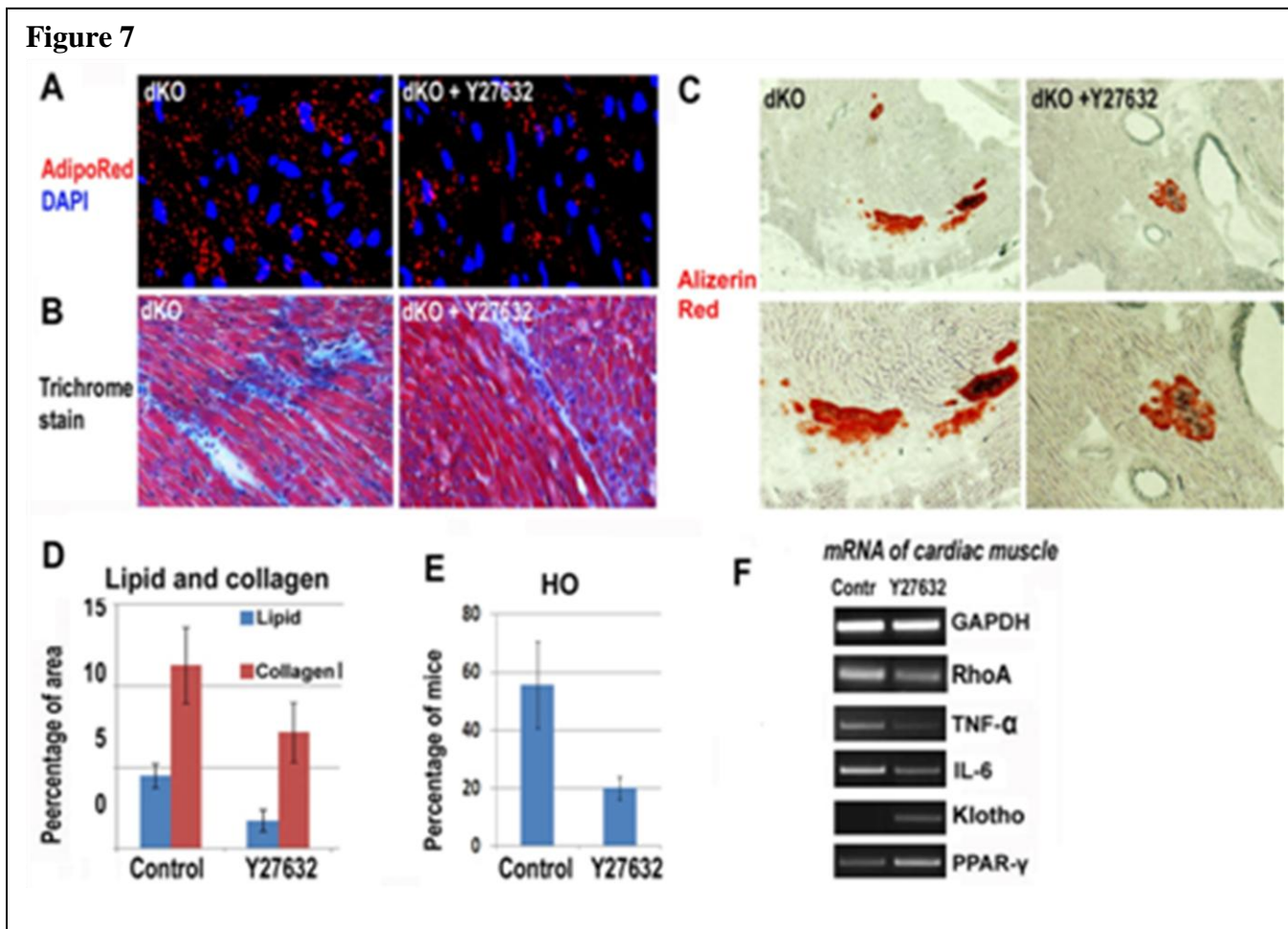
3) The identification of human muscle progenitor cells for dystrophic heart repair and regeneration.

Human myo-endothelial cells repair injured cardiac tissue effectively

The potential of human myo-endothelial cells (MECs, CD34+/144+/56+/45-) to repair the injured heart was demonstrated in our recent study. When transplanted intramyocardially into acutely infarcted immunodeficient hearts of young adult mice, MECs more effectively restored cardiac function, reduced scar tissue formation, and stimulated angiogenesis than purified conventional myoblasts and endothelial cells (34). This is presumably attributed to, at least in part, the augmented angiogenesis, resulted from more vascular endothelial growth factor (VEGF), a potent angiogenic factor, secreted by MECs under hypoxia. Similar to murine MDSCs, MECs regenerated significantly more fast-skeletal MHC-positive myofibers in the ischemic heart. A small fraction of engrafted MECs expressed cardiomyocyte markers, cardiac troponin-T and –I, indicating the likely cardiac differentiation and/or cell fusion in the injured heart. MECs also promoted proliferation and prevented apoptosis of endogenous cardiomyocytes. These results suggest that human MECs are an ideal donor cell population for cardiac repair.

Human pericytes restored the function of the injured heart through paracrine effect and cellular interaction

Human microvascular pericytes (CD146$^+$/34$^-$/45$^-$/56$^-$), with their inherent vascular functions and recently documented multipotency, matched the scope of ideal cells for cardiac repair. (35). Transplantation of cultured human muscle pericytes into acutely infarcted hearts of immunodeficient mice significantly improved cardiac contractility and reduced heart dilatation, superior to CD56+ myogenic progenitor transplantation (**Figure 8**). Pericytes exhibited cardio-protective effects such as promotion of angiogenesis, decrease of chronic inflammation, and reduction of scar formation (36) (**Appendix 3**). Under hypoxia, pericytes suppressed murine fibroblast proliferation and macrophage proliferation *in vitro* through a paracrine mechanism. Pericytes demonstrated expression of a number of immunoregulatory molecules, including IL-6, LIF, COX-2 and HMOX-1, even under hypoxia. Pericytes not only supported microvascular structure formation in three-dimensional co-cultures but also significantly enhanced host angiogenesis *in vivo*. Under hypoxia, pericytes dramatically increased expression of VEGF-A, PDGF-β, TGF-β1.

Figure 8
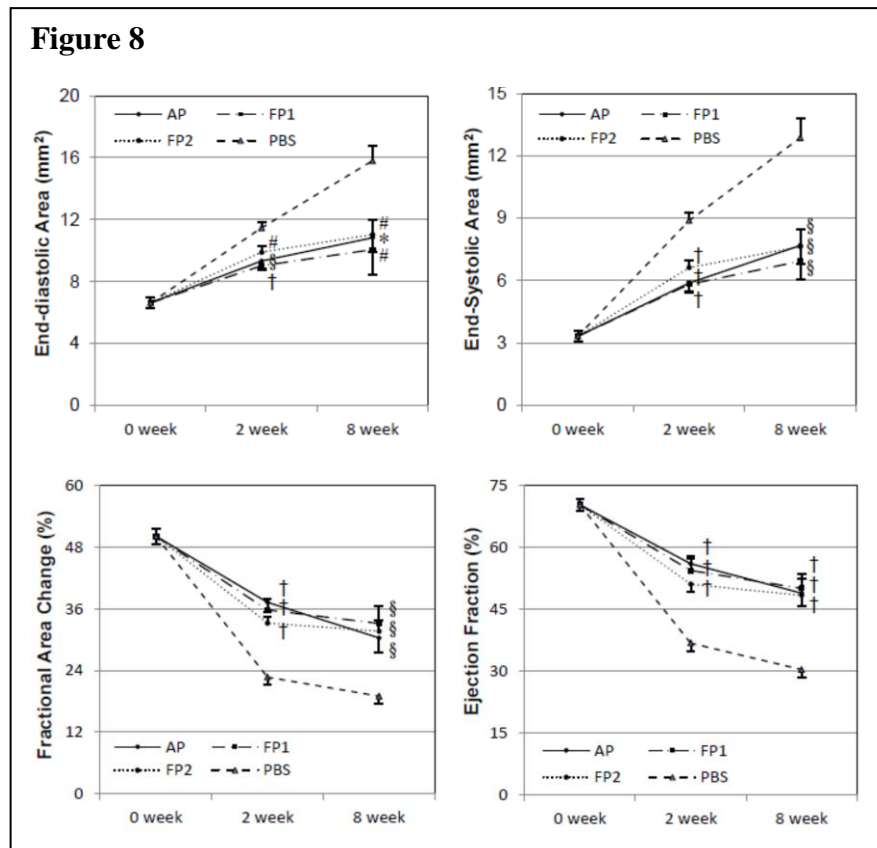
In conclusion, intramyocardial transplantation of purified human muscle pericytes promotes functional and structural recovery, attributable to multiple mechanisms involving paracrine effects and cellular interactions.

Currently, to examine whether donor pericyte-derived VEGF is the primary molecular mediator required for the

Figure 9
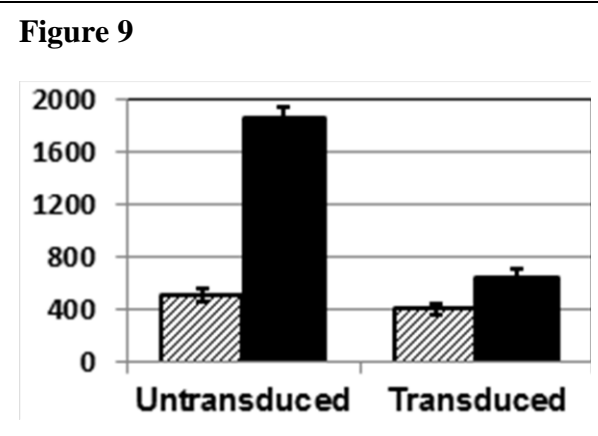
promotion of host angiogenesis, we used anti-human $VEGF_{165}$ shRNA to block VEGF secretion from donor pericytes. The angiogenic effect of transduced pericytes with VEGF blockage as well as their overall therapeutic benefits post-transplantation will be assessed. Human muscle pericytes were successfully transduced by lentiviral anti-VEGF-shRNA-eGFP vector. The transduction rate was roughly 70-80%. We observed no significant change to cell growth and phenotypes after transduction. To further purify transduced pericytes, we plan to use FACS to sort GFP-positive pericytes to homogeny. *In vitro* hypoxia assay showed that although anti-VEGF-shRNA transduction only reduced VEGF secretion from pericytes by 22.3% under normoxia, it effectively inhibited their VEGF secretion by 65.2% under hypoxia, as revealed by ELISA (**Figure 9**). To examine whether their vessel-forming capacity is affected by VEGF blockage, the Matrigel culture assay using pericytes has been performed and the data is currently being analyzed.

Pre-plated human muscle cells display a differential cardiac repair capacity (**Appendix 4**)

Very recently, we applied the modified pre-plate technique to separate freshly dissociated human muscle cells into rapid- and slowly-adhering cell populations, equivalent to the murine early and late pre-plating cells. The slowly-adhering cells (SACs) displayed not only a greater myogenic potential but also better cell survival under oxidative and inflammatory


Figure 10
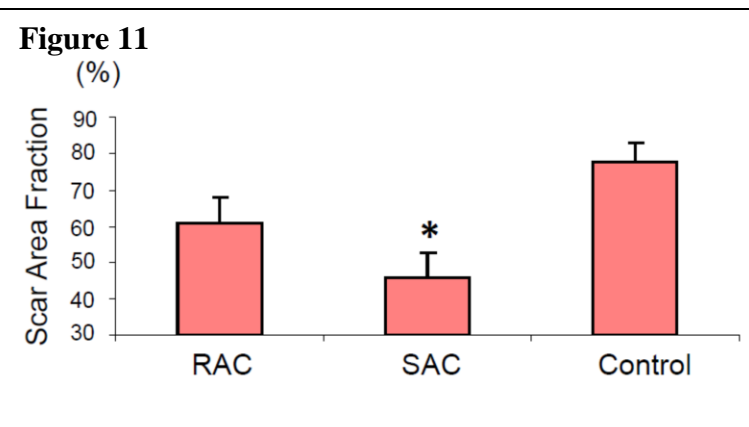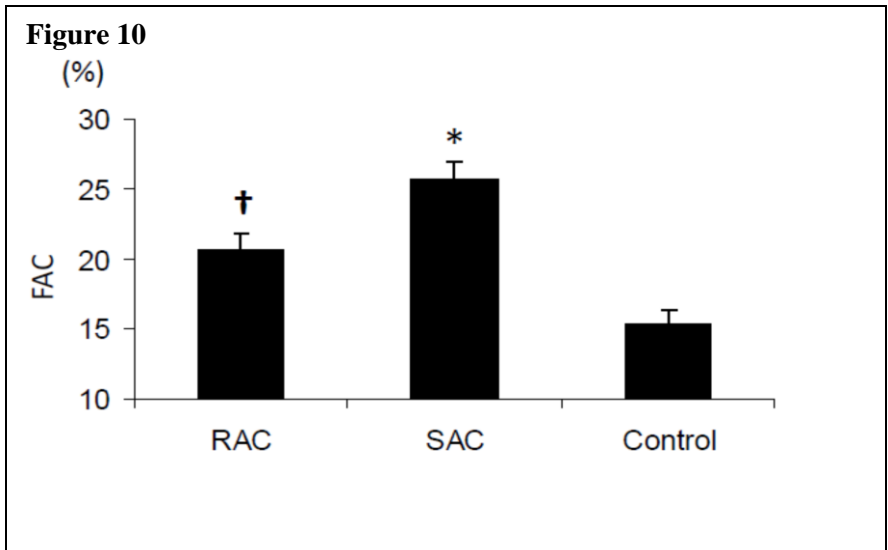
stresses *in vitro* than rapidly-adhering cells (RACs), similar to murine MDSCs (Okada, Payne et al., Mol. Ther. 2012) (**Appendix 4**) . We have investigated the therapeutic potential of human muscle pre-plating cells for the treatment of myocardial injury. The intramyocardial injection of SACs into the acutely infracted immunodeficient murine heart improved cardiac contractility more effectively than the injection of RACs (**Figure 10**; (37)) (**Appendix 4**). The functional recovery likely resulted from the decreased myocardial fibrosis (**Figure 11**), higher cell proliferation, reduction of

Figure 11

cardiomyocyte apoptosis and increased revascularization (**Figure 12**) in SAC-injected hearts, similar to the therapeutic capacity of murine MDSCs.

Figure 12

RAC   SAC   Control
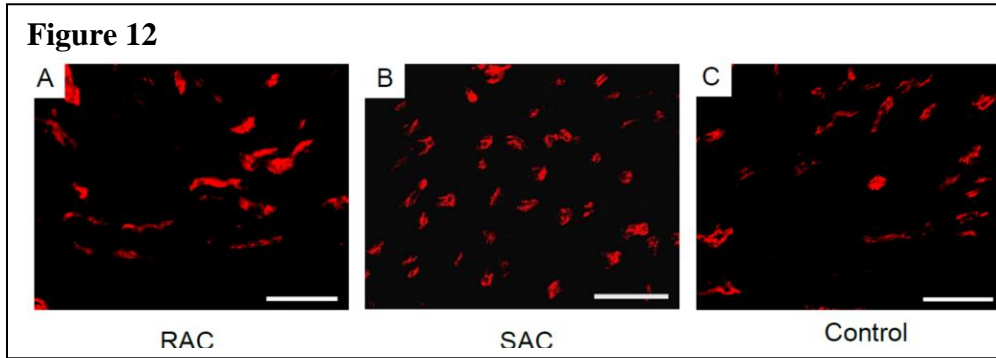
Technical Issues

As described elsewhere in this report, during the investigation, we identified that our young adult mdx/scid mice do not exhibit prominent loss of cardiac function and dystrophic phenotypes in the cardiac tissue. Consequently we aged these animals to nearly 2 years old in order to obtain dystrophic symptoms in the heart similar to the DMD patients. Nevertheless, the aging process significantly weakened the ability of the mdx/scid mice to withstand the invasive and traumatic open-chest surgery and intramyocardial injection of human cells. Therefore, in addition to the usage of the new dKO heterozygous mouse model, we herein propose to switch the injection route of human cells from intramyocardial to intra-peritoneal (IP) in order to circumvent the invasive surgery. We will label human cells with GFP reporter gene and track the migration of transplanted cells to the diseased cardiac tissue.

Future Direction

1)   **We are proposing to further investigate the dKO animal model as a suitable model for cardiomyopathy.** We are also proposing to further investigate the role of RhoA in the cardiomyopathy observed in the dKO model as well as the use of parabiosis and transplantation of human muscle derived cells to improve cardiac function in the dKO model. Specifically we propose the following set of experiments:

2)   **To investigate the effect of cell survival, proliferation, and differentiation on the regeneration/repair capacity of various human MDSC populations (preplate cells, myo-endothelial cells and pericytes) implanted into the heart of dKO mice.**

3)   **To investigate the role that angiogenesis plays in the regeneration/repair capacity of human MDSCs injected into the hearts of dKO mice.**

4)   **Potential benefit of parabiosis for cardiac repair in dKO mice:** Based on the positive effect of RhoA inactivation in cardiac muscle of dKO mice, we are proposing to conduct parabiotic pairings of dKO mice with normal mice which could help repress the activation of RhoA signaling in the cardiac muscles of dKO mice, and therefore improve their defective muscle phenotype.
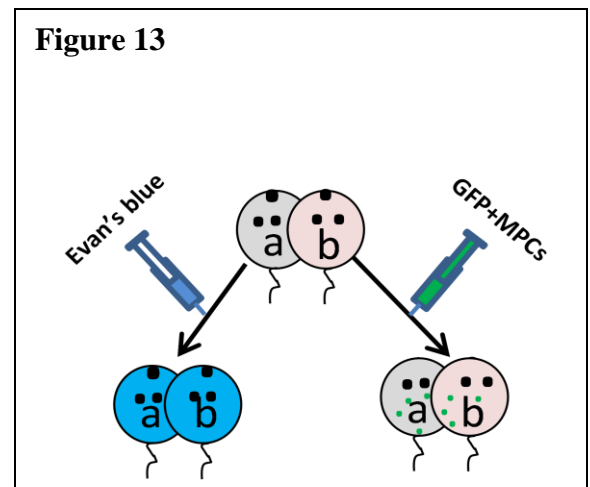

Figure 13

Figure 13 shows a schematic of the proposed experiments that we plan to perform during the next period of funding. We will verify the development of cross-circulation between the animals, via the intravascular injection of Evan's Blue. After injection into one animal of the pair,

the Evan's Blue dye should flush the same animal (**a**) and progressively spread through the common vascular tree at the junction to its partner (**b**). We also propose to investigate if MPCs can travel from mouse (**a**) to the parabiotic partner (**b**) when GFP labeled cells are intravenously into mouse (**a**).

KEY RESEARCH ACCOMPLISHMENTS:

- **Identified and characterized a superior model of dystrophic related cardiomyopathy (the dKO mouse).**
- **Identified the relationship between the activation of RhoA and inflammatory signaling which appears to account for the higher levels of heterotopic ossification (HO), intramyocardial lipid accumulation and fibrosis observed in the dKO cardiac muscles.**
- **Demonstrated that in vivo RhoA inactivation with Y-27632 in dKO mice reduces intramyocellular lipid accumulation fibrosis, and HO in cardiac muscle.**
- **Demonstrated that purified human pericytes could restore the function of the injured heart through paracrine effects and cellular interaction**
- **Demonstrated that the intramyocardial injection of preplate isolated SACs into the acutely infracted immunodeficient murine heart improved cardiac contractility more effectively than the injection of RACs**

REPORTABLE OUTCOMES:

1. **RhoA signaling regulates heterotopic ossification and fatty infiltration in dystrophic skeletal muscle.** Xiaodong Mu, Arvydas Usas, Ying Tang, Aiping Lu, Jihee Sohn, Bing Wang, Kurt Weiss, and Johnny Huard. Orthopaedic Research Society; 2013 ORS Annual Meeting; January 26-29, 2013; San Antonio, TX. (**Appendix 1**)
2. **RhoA inactivation represses BMP-induced heterotopic ossification (HO) in skeletal muscle and potential for HO treatment.** Xiaodong Mu, Kurt Weiss, and Johnny Huard. Orthopaedic Research Society; 2013 ORS Annual Meeting; January 26-29, 2013; San Antonio, TX. (**Appendix 2**)
3. **Human Pericytes for Ischemic Heart Repair.** Chien-Wen Chen, Masaho Okada, Jonathan D. Proto, Xueqin Gao, Naosumi Sekiya, Sarah A. Beckman, Mirko Corselli, Mihaela Crisan, Arman Saparov, Kimimasa Tobita, Bruno Péault, Johnny Huard. Stem Cells, In Press. (**Appendix 3**)
4. **Human skeletal muscle cells with a slow adhesion rate after isolation and enhanced stress resistance improve functions if ischemic heart.** Okada M, Payne T, Drowley L, Jankowski R, Momoi N, Beckman S, Chen C, Keller B, Tobita K, **Huard J**. Mol Ther 2012 Jan; 20(1):138-45. PMID: 22068427 (**Appendix 4**)

CONCLUSIONS:

Our current results demonstrated that we could isolate and deliver both purified human pericytes and human preplate isolated slowly adhering cells (SACs) to the ischemic hearts of mice. The deliveries of these cells were shown to have a significantly positive effect on heart function. We also identified and characterized a superior model of dystrophic cardiomyopathy in the dKO mouse, which will be exploited in over the next year via experiments where we will perform IP injections to compare the efficiency of the cells to impart a positive paracrine effect on the functionality of the hearts of these

mice. We also demonstrated that the RhoA pathway plays a critical role in the formation of HO, intramyocardial lipid accumulation and fibrosis observed in the dKO cardiac muscles. We were also able to demonstrate that blocking RhoA with Y-27632 could reduce intramyocellular lipid accumulation fibrosis, and HO in the cardiac muscle of dKO mice.

REFERENCES:

1. Deconinck N, Dan B. Pathophysiology of duchenne muscular dystrophy: current hypotheses. Pediatr Neurol. 2007;36(1):1-7. Epub 2006/12/13. doi: S0887-8994(06)00624-2 [pii]10.1016/j.pediatrneurol.2006.09.016. PubMed PMID: 17162189.
2. Towbin JA, Bowles NE. The failing heart. Nature. 2002;415(6868):227-33. Epub 2002/01/24. doi: 10.1038/415227a415227a [pii]. PubMed PMID: 11805847.
3. Marcus RL, Addison O, Kidde JP, Dibble LE, Lastayo PC. Skeletal muscle fat infiltration: impact of age, inactivity, and exercise. J Nutr Health Aging. 2010;14(5):362-6. Epub 2010/04/29. PubMed PMID: 20424803.
4. Cipriano CA, Pill SG, Keenan MA. Heterotopic ossification following traumatic brain injury and spinal cord injury. J Am Acad Orthop Surg. 2009;17(11):689-97. Epub 2009/11/03. doi: 17/11/689 [pii]. PubMed PMID: 19880679.
5. Shi S, de Gorter DJ, Hoogaars WM, t Hoen PA, Ten Dijke P. Overactive bone morphogenetic protein signaling in heterotopic ossification and Duchenne muscular dystrophy. Cell Mol Life Sci. 2012. Epub 2012/07/04. doi: 10.1007/s00018-012-1054-x. PubMed PMID: 22752156.
6. Hannallah D, Peng H, Young B, Usas A, Gearhart B, Huard J. Retroviral delivery of Noggin inhibits the formation of heterotopic ossification induced by BMP-4, demineralized bone matrix, and trauma in an animal model. J Bone Joint Surg Am. 2004;86-A(1):80-91. Epub 2004/01/09. PubMed PMID: 14711949.
7. Miljkovic-Gacic I, Wang X, Kammerer CM, Gordon CL, Bunker CH, Kuller LH, et al. Fat infiltration in muscle: new evidence for familial clustering and associations with diabetes. Obesity (Silver Spring). 2008;16(8):1854-60. Epub 2008/06/07. doi: oby2008280 [pii]10.1038/oby.2008.280. PubMed PMID: 18535552; PubMed Central PMCID: PMC2895815.
8. Zoico E, Rossi A, Di Francesco V, Sepe A, Olioso D, Pizzini F, et al. Adipose tissue infiltration in skeletal muscle of healthy elderly men: relationships with body composition, insulin resistance, and inflammation at the systemic and tissue level. J Gerontol A Biol Sci Med Sci. 2010;65(3):295-9. Epub 2009/10/30. doi: glp155 [pii]10.1093/gerona/glp155. PubMed PMID: 19864639.
9. Corcoran MP, Lamon-Fava S, Fielding RA. Skeletal muscle lipid deposition and insulin resistance: effect of dietary fatty acids and exercise. Am J Clin Nutr. 2007;85(3):662-77. Epub 2007/03/09. doi: 85/3/662 [pii]. PubMed PMID: 17344486.
10. Savage DB, Petersen KF, Shulman GI. Disordered lipid metabolism and the pathogenesis of insulin resistance.Physiol Rev. 2007;87(2):507-20. Epub 2007/04/13. doi: 87/2/507 [pii]10.1152/physrev.00024.2006. PubMed PMID: 17429039; PubMed Central PMCID: PMC2995548.
11. Laforet P, Vianey-Saban C. Disorders of muscle lipid metabolism: diagnostic and therapeutic challenges. Neuromuscul Disord. 2010;20(11):693-700. Epub 2010/08/10. doi: S0960-8966(10)00540-7 [pii]10.1016/j.nmd.2010.06.018. PubMed PMID: 20691590.
12. Hulver MW, Dohm GL. The molecular mechanism linking muscle fat accumulation to insulin resistance. Proc Nutr Soc. 2004;63(2):375-80. Epub 2004/08/06. doi: S0029665104000515 [pii]. PubMed PMID: 15294058.

13. Schulze PC. Myocardial lipid accumulation and lipotoxicity in heart failure. J Lipid Res. 2009;50(11):2137-8. Epub 2009/08/19. doi: jlr.R001115 [pii]10.1194/jlr.R001115. PubMed PMID: 19687505; PubMed Central PMCID: PMC2759818.

14. Axelsen LN, Lademann JB, Petersen JS, Holstein-Rathlou NH, Ploug T, Prats C, et al. Cardiac and metabolic changes in long-term high fructose-fat fed rats with severe obesity and extensive intramyocardial lipid accumulation. Am J Physiol Regul Integr Comp Physiol. 2010;298(6):R1560-70. Epub 2010/04/02. doi: ajpregu.00392.2009 [pii]10.1152/ajpregu.00392.2009. PubMed PMID: 20357025.

15. Ruberg FL. Myocardial lipid accumulation in the diabetic heart. Circulation. 2007;116(10):1110-2. Epub 2007/09/05. doi: 116/10/1110 [pii]10.1161/CIRCULATIONAHA.107.721860. PubMed PMID: 17768302.

16. Zhou YT, Grayburn P, Karim A, Shimabukuro M, Higa M, Baetens D, et al. Lipotoxic heart disease in obese rats: implications for human obesity. Proc Natl Acad Sci U S A. 2000;97(4):1784-9. Epub 2000/03/04. doi: 97/4/1784 [pii]. PubMed PMID: 10677535; PubMed Central PMCID: PMC26513.

17. Sharma S, Adrogue JV, Golfman L, Uray I, Lemm J, Youker K, et al. Intramyocardial lipid accumulation in the failing human heart resembles the lipotoxic rat heart. FASEB J. 2004;18(14):1692-700. Epub 2004/11/04. doi: 18/14/1692 [pii]10.1096/fj.04-2263com. PubMed PMID: 15522914.

18. Saini-Chohan HK, Mitchell RW, Vaz FM, Zelinski T, Hatch GM. Delineating the role of alterations in lipid metabolism to the pathogenesis of inherited skeletal and cardiac muscle disorders: Thematic Review Series: Genetics of Human Lipid Diseases. J Lipid Res. 2012;53(1):4-27. Epub 2011/11/09. doi: jlr.R012120 [pii]10.1194/jlr.R012120. PubMed PMID: 22065858; PubMed Central PMCID: PMC3243479.

19. Tahallah N, Brunelle A, De La Porte S, Laprevote O. Lipid mapping in human dystrophic muscle by cluster-time-of-flight secondary ion mass spectrometry imaging. J Lipid Res. 2008;49(2):438-54. Epub 2007/11/21. doi: M700421-JLR200 [pii]10.1194/jlr.M700421-JLR200. PubMed PMID: 18025000; PubMed Central PMCID: PMC2438276.

20. Ridley AJ. Rho GTPases and cell migration. J Cell Sci. 2001;114(Pt 15):2713-22. Epub 2001/10/31. PubMed PMID: 11683406.

21. Luo L. Rho GTPases in neuronal morphogenesis. Nat Rev Neurosci. 2000;1(3):173-80. Epub 2001/03/22. doi: 10.1038/35044547. PubMed PMID: 11257905.

22. McBeath R, Pirone DM, Nelson CM, Bhadriraju K, Chen CS. Cell shape, cytoskeletal tension, and RhoA regulate stem cell lineage commitment. Dev Cell. 2004;6(4):483-95. Epub 2004/04/08. doi: S1534580704000759 [pii]. PubMed PMID: 15068789.

23. Khatiwala CB, Kim PD, Peyton SR, Putnam AJ. ECM compliance regulates osteogenesis by influencing MAPK signaling downstream of RhoA and ROCK. J Bone Miner Res. 2009;24(5):886-98. Epub 2008/12/31. doi: 10.1359/jbmr.081240. PubMed PMID: 19113908; PubMed Central PMCID: PMC2672206.

24. Meyers VE, Zayzafoon M, Douglas JT, McDonald JM. RhoA and cytoskeletal disruption mediate reduced osteoblastogenesis and enhanced adipogenesis of human mesenchymal stem cells in modeled microgravity. J Bone Miner Res. 2005;20(10):1858-66. Epub 2005/09/15. doi: 10.1359/JBMR.050611. PubMed PMID: 16160744; PubMed Central PMCID: PMC1351020.

25. Hosoyama T, Ishiguro N, Yamanouchi K, Nishihara M. Degenerative muscle fiber accelerates adipogenesis of intramuscular cells via RhoA signaling pathway. Differentiation. 2009;77(4):350-9. Epub 2009/03/14. doi: S0301-4681(08)00052-2 [pii]10.1016/j.diff.2008.11.001. PubMed PMID: 19281783.

26. Santos A, Bakker AD, de Blieck-Hogervorst JM, Klein-Nulend J. WNT5A induces osteogenic differentiation of human adipose stem cells via rho-associated kinase ROCK. Cytotherapy. 2010;12(7):924-32. Epub 2010/05/01. doi: 10.3109/14653241003774011. PubMed PMID: 20429785.

27. Goto K, Chiba Y, Sakai H, Misawa M. Tumor necrosis factor-alpha (TNF-alpha) induces upregulation of RhoA via NF-kappaB activation in cultured human bronchial smooth muscle cells. J Pharmacol Sci.

2009;110(4):437-44. Epub 2009/07/16. doi: JST.JSTAGE/jphs/09081FP [pii]. PubMed PMID: 19602845.

28. Slice LW, Bui L, Mak C, Walsh JH. Differential regulation of COX-2 transcription by Ras- and Rho-family of GTPases. Biochem Biophys Res Commun. 2000;276(2):406-10. Epub 2000/10/12. doi: 10.1006/bbrc.2000.3487S0006-291X(00)93487-9 [pii]. PubMed PMID: 11027488.

29. Charrasse S, Comunale F, Grumbach Y, Poulat F, Blangy A, Gauthier-Rouviere C. RhoA GTPase regulates M-cadherin activity and myoblast fusion. Mol Biol Cell. 2006;17(2):749-59. Epub 2005/11/18. doi: E05-04-0284 [pii]10.1091/mbc.E05-04-0284. PubMed PMID: 16291866; PubMed Central PMCID: PMC1356585.

30. Castellani L, Salvati E, Alema S, Falcone G. Fine regulation of RhoA and Rock is required for skeletal muscle differentiation. J Biol Chem. 2006;281(22):15249-57. Epub 2006/04/01. doi: M601390200 [pii]10.1074/jbc.M601390200. PubMed PMID: 16574652.

31. Beqaj S, Jakkaraju S, Mattingly RR, Pan D, Schuger L. High RhoA activity maintains the undifferentiated mesenchymal cell phenotype, whereas RhoA down-regulation by laminin-2 induces smooth muscle myogenesis. J Cell Biol. 2002;156(5):893-903. Epub 2002/03/06. doi: 10.1083/jcb.200107049jcb.200107049 [pii]. PubMed PMID: 11877460; PubMed Central PMCID: PMC2173321.

32. Lindegaard ML, Nielsen LB. Maternal diabetes causes coordinated down-regulation of genes involved with lipid metabolism in the murine fetal heart. Metabolism. 2008;57(6):766-73. Epub 2008/05/27. doi: S0026-0495(08)00049-8 [pii]10.1016/j.metabol.2008.01.016. PubMed PMID: 18502258.

33. Lehman JJ, Kelly DP. Transcriptional activation of energy metabolic switches in the developing and hypertrophied heart. Clin Exp Pharmacol Physiol. 2002;29(4):339-45. Epub 2002/05/03. PubMed PMID: 11985547.

34. Okada M, Payne TR, Zheng B, Oshima H, Momoi N, Tobita K, et al. Myogenic endothelial cells purified from human skeletal muscle improve cardiac function after transplantation into infarcted myocardium. Journal of the American College of Cardiology. 2008;52(23):1869-80. Epub 2008/11/29. doi: 10.1016/j.jacc.2008.07.064. PubMed PMID: 19038685; PubMed Central PMCID: PMC2719893.

35. Crisan M, Yap S, Casteilla L, Chen CW, Corselli M, Park TS, et al. A perivascular origin for mesenchymal stem cells in multiple human organs. Cell stem cell. 2008;3(3):301-13. Epub 2008/09/13. doi: 10.1016/j.stem.2008.07.003. PubMed PMID: 18786417.

36. Chen CW, Okada M, Proto JD, Gao X, Sekiya N, Beckman SA, et al. Human pericytes for ischemic heart repair. Stem Cells. 2012. Epub 2012/11/21. doi: 10.1002/stem.1285. PubMed PMID: 23165704.

37. Okada M, Payne TR, Drowley L, Jankowski RJ, Momoi N, Beckman S, et al. Human skeletal muscle cells with a slow adhesion rate after isolation and an enhanced stress resistance improve function of ischemic hearts. Molecular therapy : the journal of the American Society of Gene Therapy. 2012;20(1):138-45. Epub 2011/11/10. doi: 10.1038/mt.2011.229. PubMed PMID: 22068427; PubMed Central PMCID: PMC3255579.

Sub-project 2: Human hepatocytes for treatment of life-threatening liver injury

PI's: Ira Fox, MD and David Perlmutter, MD

INTRODUCTION:

These studies are focused on expanding human hepatocytes from control, marginal quality and cirrhotic livers for the treatment of life-threatening acute liver failure. Two technical objectives were proposed: 1) to characterize and expand hepatocytes from patients with cirrhosis and end-stage liver disease in immune deficient hosts whose livers permit extensive repopulation with donor cells, and 2) to determine the extent to which transplantation with human hepatocytes can reverse hepatic failure in a clinically relevant non-human primate model of this process. In order to accomplish these objectives, we have expanded human hepatocytes in FRG mice and have isolated the human hepatocytes for use in a non-human primate model of acute liver failure. We have also performed additional studies on hepatocytes isolated from the livers of rats with end-stage cirrhosis, identified a target molecule that controls liver-specific gene expression in these cells and demonstrated that re-expression of this gene, HNF4α, results in normalization of hepatocyte function in vitro and in vivo. We have also induced acute liver failure in two monkeys and transplanted one of these animals with human hepatocytes. While we were unsuccessful in correcting liver failure in this animal, we have made progress in optimizing the protocol for inducing acute liver failure, and we have demonstrated that we can recover an adequate number of human hepatocytes from repopulated FRG mice for transplantation in a primate model.

Body:

Technical Objective #1: To characterize and expand hepatocytes from patients with cirrhosis and end-stage liver disease in immune deficient hosts whose livers permit extensive repopulation with donor cells.

Hypothesis: Human hepatocytes derived from poor quality human cadaver donors can be resuscitated and expand in numbers that can be used for clinical application in the livers of immune deficient hosts where there is a selective repopulation advantage to transplanted donor hepatocytes.

Recently, we have almost exclusively performed transplants on children with liver-based metabolic disorders rather than on children with cirrhosis. As transplantation from the waiting list is based solely on donor availability and MELD score, this situation sometimes occurs. As a result, we have followed two approaches to advancing Technical Objective #1.

1.1. Expanding human hepatocytes in FRG mice.

We have performed primary transplants using human hepatocytes from non-cirrhotic donors as a source of cells for Technical Objective #2 in 3 FRG mice. Human hepatocytes from the explanted liver of two patients with ornithine transcarbamylase (OTC) deficiency were transplanted into 3 immune-deficient mice with hereditary tyrosinemia (FAH-/-; FRG). The level of human serum albumin (HSA) in the peripheral blood of all three animals was greater than 1.5mg/ml, indicating at least 20% of the liver was replaced with human hepatocytes. One recipient animal was sacrificed, and approximately 50% engraftment was confirmed by immunohistochemistry. We then isolated hepatocytes from the remaining repopulated FRG mice and secondary

transplants were performed with the recovered cells in 5 naïve FRG mice. The HSA levels in the transplanted mice were detectable 4 weeks after transplant, with a mean HSA level of 6.87 ± 0.91 ug/ml. This level of re-population, at this time point, is as expected based on the literature. In addition, we transplanted 6 immune deficient mice with alpha-1-antitrypsin deficiency (PiZ-NSG) using human hepatocytes derived from a liver resection specimen from a patient with metastatic colon cancer. The HSA levels in the transplanted mice were detectable 6 weeks after transplant (6.84 ± 1.9 ug/ml). These experiments are ongoing. We intend to transplant and repopulate additional immune deficient mice to generate cells for the non-human primate acute liver failure studies outlined in Technical Objective #2.

1.2. Normalization of end-stage decompensated hepatocyte function in vitro and in vivo by re-expression of HNF4α.

In a continuation of studies to determine the extent to which hepatocytes derived from livers with severe chronic injury could be resuscitated for use in clinical hepatocyte transplantation, we isolated hepatocytes from the livers of Lewis rats with compensated and end-stage decompensated cirrhosis. To assess the extent to which hepatocyte-specific characteristics are affected by cirrhosis and liver failure, mRNA from isolated hepatocytes derived from cirrhotic and control livers were compared for gene expression by microarray analysis. As noted previously, hierarchical cluster analysis demonstrated significant gene expression differences among groups depending on the extent of cirrhosis from which the hepatocytes were derived. As expected, there were progressive changes in the expression of genes representing signals promoting proliferation and regeneration, apoptosis, and cell-death, most likely mediated by inflammation and oxidative stress, and progressive loss of gene expression representing worsening of metabolic function. This work has now been published (**Liu, et al. The microenvironment in hepatocyte regeneration and function in rats with advanced cirrhosis. Hepatology 2012; 55(5): 1529-39**). Microarrays also showed marked decreases in the expression of HNF4α, Foxa2, C/EBPα, and HNF1α, DNA binding proteins that are part of the network of hepatocyte-enriched transcription factors, sequentially established during development, that regulate the mature hepatocyte phenotype, controlling expression of proteins of coagulation, biliary metabolism, and lipid metabolism.

Since transcription factor deficiency could explain hepatocyte impairment, we investigated the therapeutic effects of forced re-expression. HNF4α was chosen for this therapy because it is the central regulator of the adult hepatocyte transcription factor network, has no other hepatocyte-expressed homolog, and showed the greatest reduction in the decompensated hepatocyte. We therefore performed a detailed analysis of the expression of HNF4α and its target genes in isolated hepatocytes and liver tissue. qRT-PCR analysis confirmed severe downregulation of HNF4α expression, and quantification of HNF4α in hepatocytes by western blot and by immunofluorescent staining of cytospin samples gave similar results. Thus, a significant decrease of HNF-4α in hepatocytes correlated with decompensation in cirrhosis.

To assess whether forced re-expression of HNF4α could affect the function of cirrhotic hepatocytes, we first used an *in vitro* culture system. Hepatocytes, isolated from animals with cirrhosis and decompensated liver function, were transduced with adeno-associated virus (AAV) vectors to express HNF4α and GFP or GFP alone. At 48 hours, qRT-PCR analysis showed HNF4α re-expression restored to nearly normal levels the network transcription factors C/EBPα, HNF1α, and PPARα, and the phenotypic target genes important for liver-specific activity. HNF4α expression also improved secretion of albumin into the culture supernatant—severely

impaired in hepatocytes isolated from decompensated cirrhosis —and activity of Cytochrome P450 3A4, a major enzyme of xenobiotic metabolism. Animals with liver failure and cirrhosis were then transduced to re-express HNF4α in their hepatocytes by intravenous infusion of 3×10^{11} AAV-HNF4α-GFP genomes. Animals sacrificed two weeks after infusion demonstrated high transduction efficiency uniformly distributed in most hepatocytes. Moreover, the impaired albumin expression of decompensated cirrhosis was dramatically improved and its expression increased until the time of sacrifice at 100 days following AAV treatment. Administration of the AAV-GFP control vector did not affect liver function. Finally, pathophysiologic testing showed striking and persistent improvement in liver function, ascites, activity, and neurologic function, and survival was prolonged to the end-point of the study at 100 days post AAV treatment. Functional analysis of cells isolated from treated animals showed significant improvement of albumin secretion and CYP3A4 activity. In addition, there was improvement in expression levels of HNF4α target genes and decreased expression of the hepatic progenitor cell markers AFP, CD44, and EpCAM. The healing effects of HNF4α re-expression did not depend on proliferation, since there was no increase apparent in Ki67 staining. HNF4α did not significantly augment TERT expression and telomere length in the cirrhotic hepatocytes remained critically short. Thus, HNF4α acted by phenotypically correcting diseased hepatoctyes, not by stimulating their replacement.

These studies show that down-regulation of HNF4α has a profound effect on the end-stage cirrhotic hepatocyte in vitro, since replenishment of this single factor immediately revitalizes function. Moreover, transduction of hepatocytes in cirrhotic animals with apparently irreversible decompensated function produced a profound and immediate improvement in hepatic function. Normalization of function took place in two weeks. It is likely that cytokine/injury effects alter expression of the hepatocyte transcription factor network by extrinsic mechanisms, with the result that network factors establish a new steady-state equilibrium in the dysfunctional hepatocyte that can no longer compensate to restore normal gene expression. This possibility has important therapeutic implications, because it may require only transient therapy with HNF4α to restore the transcription factor network once the injury has been moderated. These studies suggest that in addition to regeneration mediated by expansion of mature hepatocytes or differentiation and expansion of induced progenitors, normalized function can be accomplished by transcriptional reprograming with reversal of de-differentiation but not senescence. The results also suggest HNF4α therapy could be effective in treating advanced liver cirrhosis with impaired hepatic function as a bridge to organ transplantation or possibly even as destination therapy. We will examine whether this therapy is effective in human hepatocytes from end-stage cirrhotic livers. If so, they may also be useful as a source of hepatocytes for cell therapy.

Technical Objective #2: To determine the extent to which transplantation with human hepatocytes can reverse hepatic failure in a clinically relevant non-human primate model of this process.

Hypothesis: Human hepatocytes derived from human cadaver donors or possibly from human stem cells can reverse hepatic failure.

2.1. Acute hepatic failure in a non-human primate model.
We have treated two additional non-human primates (NHP) with whole liver radiation therapy followed by total parenteral nutrition (TPN) in preparation for transplantation studies. The work has now been incorporated in a

manuscript that has been submitted for publication (**Yannam GR, et al. Tolerable limits to whole liver irradiation in non-human primates. Hepatology. Submitted**).

Unfortunately, there has been a small setback in the ability to complete the transplant studies. The first NHP was irradiated with a dose of 40Gy to the whole liver. For logistical reasons, we delayed instituting TPN to induce acute liver failure. This has not been an issue in the past. In this case, however, it resulted in generating unanticipated non-lethal radiation induced liver disease (RILD) in the animal, which altered the architecture and vascular structure of the liver. We isolated human hepatocytes from several repopulated FRG mice to transplant into this animal, as outlined in the grant proposal. Because of the altered vascular structure we visualized severe shunting during the course of the hepatocyte transplant procedure by contrast imaging. Thus, no cells could be engrafted. The animal was electively euthanized and the liver histology confirmed the RILD and failure to engraft cells because of the altered vascular architecture. A dose of 35Gy to the whole liver was used on a second NHP. This dose was successful and the second animal was electively euthanized when we had determined that the RT dose was effective at ultimately inducing acute liver failure but did not lead to RILD. Now that the issue has been resolved, we should be able to proceed with transplant studies for the treatment of acute liver failure.

KEY RESEARCH ACCOMPLISHMENTS:

1.   Engraftment and proliferation of human hepatocytes in immune-deficient FAH k/o transgenic (FRG) mice.

2.   Identification of a key transcription regulator of hepatocyte function in end-stage decompensated hepatocytes from cirrhotic livers.

3.   Demonstration that re-expression of HNF4α in decompensated cirrhotic hepatocytes leads to normalization of function in vitro and in vivo.

4.   Optimization of the non-human primate model of acute liver failure.

5.   Isolation of an adequate supply of human hepatocytes from repopulated FRG mice for transplantation in NHP with acute liver failure.

REPORTABLE OUTCOMES:

1.   Liu,L, Yannam GR, Nishikawa T, Yamamoto T, Basma H, Ito R, Nagaya M, Dutta-Moscato J, Stolz DB, Duan F, Kaestner KH,Vodovotz Y, Soto-Gutierrez A, Fox IJ.The microenvironment in hepatocyte regeneration and function in rats with advanced cirrhosis. Hepatology 2012;55(5):1529-39.

2. Zhou H, Dong X, Kabarriti R, Chen Y, Avsar Y, Wang X, Ding J, Liu L, Fox IJ, Roy-Chowdhury J, Roy-Chowdhury N, Guha C. Single liver lobe repopulation with wildtype hepatocytes using regional hepatic irradiation cures jaundice in Gunn rats. PLoS One 2012;7(10):e46775.

3. Nishikawa T, Bell A, Brooks JM, Setoyama K, Kaestner KH, Vodovotz Y, Locker J, Soto-Gutierrez A, Fox IJ. Resetting the transcription network using a single factor reverses liver failure in end-stage cirrhosis. Science (submitted).

4. Yannam R, Han B, Setoyama K, Yamamoto T, Ito R, Brooks JM, Guzman-Lepe J, Galambos C, Fong JV, Deutsch M, Quader MA, Yamanouchi K, Mehta K, Soto-Gutierrez A, Roy-Chowdhury J, Locker J, Abe M, Enke CA, Baranowska-Kortylewicz J, Solberg TB, Guha C, Fox IJ. Tolerable limits to whole liver irradiation in non-human primates. (submitted).

5. Setoyama K, Fong JV, Han B, Ito R, Nagaya M, Ross M, Fukumitsu K, Gramignoli R, Rosensteel S, Strom SC, Stolz DB, Quader MA,Deutsch M, Baskin KM, Roy-Chowdhury J, Guha C, Soto-Gutierrez A, Fox IJ. 10-15% donor cell liver repopulation in non-human primates by low dose directed (right lobe) radiation therapy: a preclinical study. Hepatology 2011;54(S1):172A.

6. Yannam GR, Han B, Setoyama K, Yamamoto T, Ito R, Brooks JM, Guzman-Lepe J, Galambos C, Fong JV, Deutsch M, Quader MA, Yamanouchi K, Mehta K, Soto-Gutierrez A, Roy-Chowdhury J, Locker J, Abe M, Enke CA, Baranowska-Kortylewicz J, Solberg TD, Guha C, Fox IJ. Tolerable limits to whole liver irradiation in non-human primates. Hepatology 2012;56(S1):972A-973A.

7. NishikawaT, Bellance N, Damm A, Soto-Gutierrez A, Fox IJ, Nagrath D. Changes in Glycolysis are an Important Mechanism for Maintaining Cell Survival in Hepatic Failure in Advanced Cirrhosis. Hepatology 2012;56(S1):785A-786A.

8. Taichiro Nishikawa; Jenna M. Brooks; Yoram Vodovotz; Alejandro Soto-Gutierrez; Aaron W. Bell; Ira J. Fox 1284. Rescue of hepatic function in rats with advanced cirrhosis and end-stage liver failure following delivery of HNF4a. Hepatology 2012;56(S1):800A-801A.

9.   Invited Speaker, Research Seminar Series in Developmental and Regenerative Biology, University of Kansas Medical Center, ―Use of hepatocytes and stem cells to study and treat liver disease", Kansas City, Kansas, November 9-10, 2011.

10.   Keynote Speaker, ISMRM Workshop on MRI-based cell tracking ―Hepatocyte transplantation and the need to track engrafted cells", Miami Beach, Florida, January 29 – February 1, 2012.

11.   Invited Speaker, American Society of Gene & Cell Therapy 15th Annual Meeting, ―Overcoming barriers to successful cell therapy to treat liver disease", Philadelphia, PA May 16-19, 2012

12.   Moderator, Mid-day Symposium: ―Allotransplants, Cellular Transplants, Organ Repair, and Xenotransplants? A Debate about the Future of Organ Transplantation", American Transplant Congress, Boston, MA, June 2-6, 2012.

13. Invited Speaker, Liver Biology: Fundamental Mechanisms & Translational Application, FASEB Summer Research Conference, ―Hepatocyte, stem cell transplantation, tissue engineering", Snowmass Village, Colorado, July 29 – August 3, 2012.

14. Invited Speaker, 8th Royan International Congress on Stem Cell Biology and Technology, ―Overcoming barriers to the use of hepatocytes and stem cells in treating patients with liver diseases" and ―Use of hepatocytes and stem cells in understanding and treating liver failure and cirrhosis", Tehran, Iran, September 5-7, 2012.

15. Invited Speaker, Masters of Surgery lecture series, Montefiore Medical Center, The University Hospital for Albert Einstein College of Medicine, ―Bench to bedside: finding alternatives to organ transplantation for patients with life-threatening liver disease", New York, NY, November 4-5, 2012.

16. Faculty Member, American Association for the Study of Liver Diseases 2012 Postgraduate Course, ―Tissue engineering and liver cell replacement – liver stem cells on the horizon", Boston, MA, November 10, 2012.

CONCLUSIONS:

The outcomes of our studies are being accomplished.

RhoA signaling regulates heterotopic ossification and fatty infiltration in dystrophic skeletal muscle

Xiaodong Mu, Arvydas Usas, Ying Tang, Aiping Lu, Jihee Sohn, Bing Wang, Kurt Weiss, and Johnny Huard
Stem Cell Research Center, Department of Orthopaedic Surgery, University of Pittsburgh

Introduction: Frequent heterotopic ossification (HO) or fatty infiltration is observed in the dystrophic muscle of many animal models of human Duchenne muscular dystrophy (DMD); however, little is known about the correlated molecular mechanisms involved in the process. The RhoA-Rho kinase (ROCK) signaling pathway has been shown to function as a commitment switch of the osteogenic and adipogenic differentiation of mesenchymal stem cells (MSCs). Activation of RhoA-ROCK signaling in cultured MSCs *in vitro* induces their osteogenesis but inhibits the potential of adipogenesis, while the application of Y-27632, a specific inhibitor of ROCK, reversed the process. Inflammation has been shown to be one of main contributors to HO, while the role of RhoA signaling in inflammation reaction has been demonstrated. The objective of the current study is to investigate the potential role of RhoA signaling in regulating HO and fatty infiltration in dystrophic skeletal muscle.

Methods: 1.Mice models: Animal experiments were approved by IACUC of University of Pittsburgh. mdx mice (dystrophin-deficient) and dKO (Dystrophin/Utrophin double knockout) mice are both important mouse models of DMD; however, in contrast to the mild phenotype of mdx mice, dKO mice display a far more severe phenotype as is observed in human DMD patients, including a much shorter life span (~ 8 weeks compared to 2 years), more necrosis and fibrosis in the skeletal muscle, etc. 2. Tissue histological analysis: The gastrocnemius muscles (GM) of the mice were used for histological analysis. Alizarin red stain shows calcium deposition caused by HO or during osteogenic differentiation, Oil Red O stain shows fatty infiltration in muscle or fat cells, and Trichrome stain shows fibrosis. 3. Statistics: N >=6 for each group in animal study. Student's T-test was used to evaluate the significance.

Results: 1. Skeletal muscle of dKO mice features more HO but less fatty infiltration than mdx mice (Fig. 1). Both µ-CT scan of animals (**Fig. 1A**) and Alizarn Red stain (**Fig. 1B**) of the muscle tissues revealed greatly enriched HO in the dystrophic muscles of the dKO mice. While, Oil Red O stain (**Fig. 1C**) and Trichrome stain **(Fig. 1D)** of the muscle tissues revealed reduced fatty infiltration and a number of normal muscle fibers in the muscle of dKO mice.

2. RhoA signaling is more activated in both skeletal muscle and muscle-derived stem cells (MDSCs) from dKO mice. Both semi-quantitative PCR and immunohistochemistry study demonstrated that RhoA signaling is more activated in the muscles of dKO mice, as well as dKO MDSCs.

3. *In vitro* RhoA inactivation of cultured MDSCs from dKO mice decreases the osteogenesis potential and increases adipogenesis and myogenesis potential (Fig. 2). Semi-quantitative PCR study showed that Y27632 treatment *(*10 µM) of dKO-MDSCs down-regulated the expression of RhoA, BMP2 and 4, and inflammatory factors such as TNF-α and IL-6 (**Fig. 2A**). Osteogenesis potential was repressed while the adipogenesis and myogenesis potential of the dKO-MDSCs were increased by Y27632 (**Fig. 2B**).

4. RhoA inactivation in the skeletal muscle of dKO mice decreased HO and increased both fatty infiltration and muscle regeneration. GM muscles of 6 dKO mice were injected with Y27632 (5mM in 20µL of DMSO) (left limb) or control (20µL of DMSO) DMSO (right limb). Injections were conducted 3 times a week for 3 weeks. The skeletal muscles that received Y27632 injection demonstrated much slower development of HO and improved muscle regeneration, as well as reduced fibrosis formation.

Discussion: Our current results revealed that DMD mouse models featuring different severity of muscular dystrophy may have varied potentials for developing HO or fatty infiltration in the dystrophic muscle, and RhoA signaling might be a critical mediator of the determining these differential fates, including the progression towards HO, fatty infiltration, or normal muscle regeneration. RhoA inactivation is shown to have a great potential to repress HO and improve the phenotypes of dystrophic muscle. The status of RhoA activation in the skeletal muscle of human DMD patients and the potential effect of RhoA inactivation in human dystrophic muscle requires further investigation.

Significance: Our data reveals the involvement of RhoA signaling in regulating the process of heterotopic ossification, and indicates that RhoA may serve as a potential target for repressing injury-induced and congenital heterotopic ossification in humans.
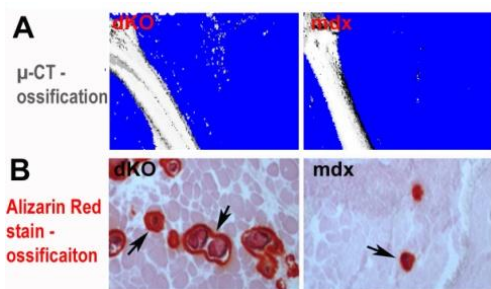
Fig 1   Fig 2
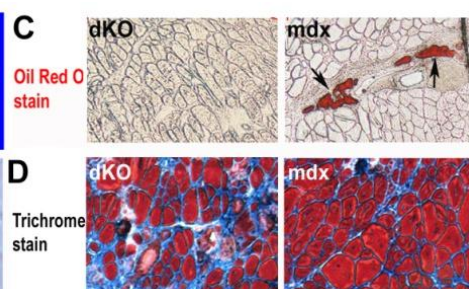
RhoA inactivation represses BMP-induced heterotopic ossification (HO) in skeletal muscle and potential for HO treatment

Xiaodong Mu, Kurt Weiss, and Johnny Huard
Stem Cell Research Center, Department of Orthopaedic Surgery, University of Pittsburgh

Introduction: HO is a process where bone tissue forms in soft tissues which can be caused by trauma, neurologic injury *and* genetic abnormalities; however, little is known about the molecular regulatory mechanisms that cause HO. The RhoA-Rho kinase (ROCK) signaling pathway has been shown to function as a commitment switch of the osteogenesis and adipogenesis differentiation of mesenchymal stem cells (MSCs), and is involved in regulating myogenesis differentiation of muscle cells. Activation of RhoA-ROCK signaling in cultured MSCs *in vitro* induces their osteogenic differentiation but inhibits their potential for adipogenic differentiation, while the application of Y-27632, a specific inhibitor of ROCK, can reverse the process. An important role of RhoA in myogenic differentiation has also been demonstrated and the activation of the RhoA pathway can block muscle differentiation by inhibiting myoblast fusion. Inflammation has been shown to be one of main contributors to HO, while the role of RhoA signaling in inflammation has also been demonstrated. The objective of the current study was to discern whether the inactivation of RhoA signaling can improve muscle regeneration by repressing BMP-induced HO in injured skeletal muscle.

Methods: 1. Induction of HO and RhoA inactivation: The gastrocnemius muscles (GM) of C57BL/6J mice were injected with cardiotoxin. Two days later the muscles were co-injected with BMP2 and Y27632 (RhoA inhibitor) (left limb) or with BMP2 only. Four days later, the muscle tissues were harvested for histological analysis. 2. Tissue histological analysis and *in vitro* differentiation assay. Alizarin red stain was conducted to stain calcium deposition caused by HO, and immunostaining of dystrophin was conducted to show myofibers. Alkaline phosphatase *(ALP)* and Alizarin red stain was used for in vitro osteogenesis assay in osteogenic medium, and the progression of myotube formation in the myogenic medium was tracked by counting the number of myotubes. 3. Statistics: N >=6 for each group of animal study. Student's T-test was used to evaluate the significance.

Results: 1. *In vitro* inactivation of RhoA decreases osteogenic potential and increases the myogenic potential of muscle-derived stem cells (MDSCs) (Fig. 1). *In vitro* osteogenesis and myogenesis assays showed that, Y27632 treatment *(*10 µM) of MDSCs isolated from skeletal muscle greatly repressed their osteogenic differentiation **(Fig. 1A, B)** in osteogenic medium, but promoted their myogenic differentiation in myogenic medium **(Fig. 1C).**

2. *In vivo* inactivation of RhoA in the skeletal muscle of mice decreased BMP-induced HO and improved muscle regeneration (Fig. 2). The GM muscles of 6 C57BL/6J mice were injured by cardiotoxin 2 days before being injected with BMP2 +Y27632 (left limb) or BMP2 only (right limb). 4 days after Y27632 administration, skeletal muscles that received Y27632 injection demonstrated a much slower development of HO **(Fig. 2A)**, and improved muscle regeneration **(Fig. 2B)**.

Discussion: Our current results revealed that the RhoA signaling pathway may mediate BMP-induced HO in skeletal muscle. RhoA activity appears to be elevated by BMPs and mediates BMP-induced osteogenesis, and RhoA inactivation could therefore repress BMP-induced HO in injured skeletal muscle. RhoA activity was shown to be positive for osteogenesis of muscle stem cells and negative for myogenesis, therefore, inactivation of RhoA could serve to repress HO formation while promoting myofiber development in the injured muscle. The detailed mechanisms of RhoA signaling in regulating HO require further investigation.

Significance: Our data revealed that RhoA signaling is involved in regulating the process of heterotopic ossification and indicated that RhoA may serve as a potential target for repressing injury-induced and congenital heterotopic ossification in humans.
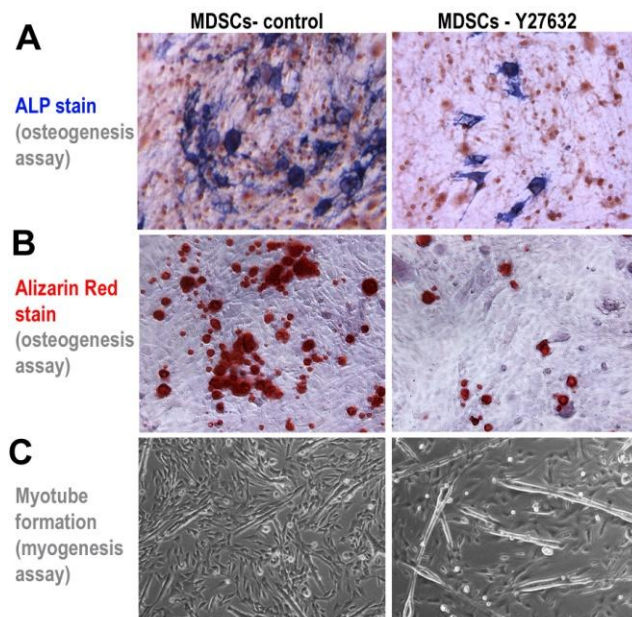
Fig 1   Fig 2
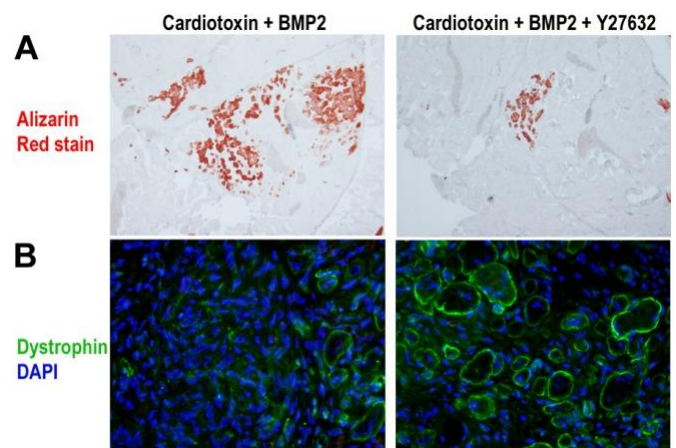
Human Pericytes for Ischemic Heart Repair

Chien-Wen Chen, MD, PhD[1,2,7], Masaho Okada, MD, PhD[2,7], Jonathan D. Proto, BS[2,6,7,*], Xueqin Gao, MD, PhD[2,7,*], Naosumi Sekiya, MD, PhD[2,5,7,*], Sarah A. Beckman, BS[2,6,7], Mirko Corselli, PhD[9], Mihaela Crisan, PhD[10], Arman Saparov, MD, PhD[11], Kimimasa Tobita, MD[3,4,8], Bruno Péault, PhD[9,12], Johnny Huard, PhD[2,7,8]

Department of [1]Bioengineering, [2]Orthopedic Surgery, [3]Pediatrics, [4]Developmental Biology, [5]Surgery, [6]Pathology, [7]Stem Cell Research Center, [8]McGowan Institute for Regenerative Medicine, University of Pittsburgh, [9]UCLA Orthopaedic Hospital, Department of Orthopaedic Surgery, and the Orthopaedic Hospital Research Center, University of California at Los Angeles, USA, [10]Erasmus MC Stem Cell Institute, Department of Cell Biology, Rotterdam, The Netherlands, [11]Center for Energy Research, Nazarbayev University, Kazakhstan, and [12]Centre for Cardiovascular Science and Centre for Regenerative Medicine, University of Edinburgh, UK
*These authors contributed equally

Correspondence to:
Johnny Huard, Ph.D.
Stem Cell Research Center
Department of Orthopaedic Surgery,
University of Pittsburgh School of Medicine
206 Bridgeside Point II, 450 Technology Drive,
Pittsburgh, PA15219, USA
Tel: (412) 648-2798
Fax: (412) 648-4066
Email: jhuard@pitt.edu

Authorship Contributions:
C.W.C. designed and performed research, analyzed data, and wrote the manuscript. M.O. performed research and analyzed data. J.D.P. performed research and analyzed data. X.G. performed research and analyzed data. N.S. performed research. S.A.B. performed research and analyzed data. M.Corselli performed research. M.Crisan performed research. A.S. participated in experimental design and provided funding. K.T. designed and performed research. B.P. designed research, provided funding, and edited the manuscript. J.H. designed research, provided funding, edited and approved the manuscript.

Abstract

Human microvascular pericytes (CD146^{+}/34^{-}/45^{-}/56^{-}) contain multipotent precursors and repair/regenerate defective tissues, notably skeletal muscle. However, their ability to repair the ischemic heart remains unknown. We investigated the therapeutic potential of human pericytes, purified from skeletal muscle, for treating ischemic heart disease and mediating associated repair mechanisms in mice. Echocardiography revealed that pericyte transplantation attenuated left ventricular dilatation and significantly improved cardiac contractility, superior to CD56+ myogenic progenitor transplantation, in acutely infarcted mouse hearts. Pericyte treatment substantially reduced myocardial fibrosis and significantly diminished infiltration of host inflammatory cells at the infarct site. Hypoxic pericyte-conditioned medium suppressed murine fibroblast proliferation and inhibited macrophage proliferation *in vitro.* High expression by pericytes of immunoregulatory molecules, including IL-6, LIF, COX-2 and HMOX-1, was sustained under hypoxia, except for MCP-1. Host angiogenesis was significantly increased. Pericytes supported microvascular structures *in vivo* and formed capillary-like networks with/without endothelial cells in three-dimensional co-cultures. Under hypoxia, pericytes dramatically increased expression of VEGF-A, PDGF-β, TGF-β1 and corresponding receptors while expression of bFGF, HGF, EGF, and Ang-1 was repressed. The capacity of pericytes to differentiate into and/or fuse with cardiac cells was revealed by GFP-labeling, though to a minor extent. In conclusion, intramyocardial transplantation of purified human pericytes promotes functional and structural recovery, attributable to multiple mechanisms involving paracrine effects and cellular interactions.

Keyword: pericytes, angiogenesis, immunomodulation, myocardial infarction, stem cell therapy

Introduction

Coronary heart disease (CHD) is the leading cause of death in the United States, affecting 16.3 million people and accounting for 1 of every 3 deaths in 2007.[1] Prolonged pathological interference with the coronary blood supply, such as atherosclerosis and thromboemboli, results in ischemic cardiomyopathy and/or myocardial infarction (MI).[2] MI often leads to heart failure (HF) due to the limited capacity of the human heart to repair/regenerate its damaged myocardium.[2,3] As an alternative to heart transplantation, stem/progenitor cell therapy (SCT) is deemed promising for restoration of cardiac function and prevention of progressive HF.[3,4] In particular, human bone marrow precursor cells, endothelial progenitor cells, skeletal myoblasts, and endogenous cardiac progenitor cells, have been intensively investigated with uneven success in pre-clinical and clinical trials.[3-6] Given the vascular origin of CHD pathology, stem/progenitor cells capable of reconstituting host vascular networks, in addition to other merits, will be ideal cell sources for SCT.

Microvascular pericytes (aka mural cells or Rouget cells) that tightly encircle capillaries and microvessels (arterioles and venules) and regulate microvascular physiology have recently been shown to contain precursor cells endowed with mesodermal differentiation potential.[7] Pericytes ($CD146^+/34^-/45^-/56^-$) purified by cell sorting from human skeletal muscle, adipose, placenta, pancreas and other organs repair and regenerate damaged/defective tissues[8-12] and represent the CD146-positive developmental origin of the heterogeneous mesenchymal stem/stromal cells (MSCs).[12-16] Owing to their wide distribution in the microvasculature, pericytes are regarded as a promising and attractive source of precursor cells for regenerative medicine.[17-19] We hypothesize SCT with purified pericytes to be a suitable approach for the treatment of ischemic heart disease (IHD).[20]

Besides cardiomyogenesis, cardioprotective mechanisms, including anti-fibrosis, anti-inflammation, and neovascularization, play critical roles in SCT-mediated cardiac repair following ischemic insults.[21-23] SCT reduces myocardial fibrosis and induces favorable tissue remodeling in the ischemic heart, which in turn increases myocardial compliance/strength and prevents the progressive, pathological decline toward HF.[24,25] This anti-fibrotic feature was attributed in part to increased collagen degradation by matrix metalloproteinases (MMPs) and inhibition of fibroblast activation, possibly through a paracrine mechanism.[26,27] Additionally, the immunosuppressive/anti-inflammatory capacity of MSCs through secretion of immunoregulatory molecules has recently attracted clinical attention in organ transplantation and immune regulation.[28,29] Whether pericytes possess similar anti-fibrotic and immunoregulatory capacities within the ischemic microenvironment remains to be addressed.

To relieve the underlying cause of IHD, SCT-based approaches toward myocardial revascularization have been extensively pursued.[30,31] Due to their native vascular localization

and secretion of trophic factors that are associated with tissue repair and vascular growth/remodeling, pericytes may restore injured vascular networks more efficiently.[18] Pro-angiogenic signaling molecules released by stem/progenitor cells stimulate neovascularization in ischemic tissues.[31] Additionally, cell-cell interaction between vascular mural cells and endothelial cells was lately suggested to play essential roles in blood vessel remodeling and maturation.[32,33] Whether pericytes mediate revascularization of the ischemic myocardium through any of these two mechanisms has yet to be tested

In the present study, we investigated the therapeutic potential of purified human skeletal muscle pericytes in IHD, using an acute MI (AMI) model in immunodeficient mice. Transplantation of pericytes not only reversed cardiac dilatation but also improved cardiac contractility. Major repair mechanisms were investigated, including reduction of fibrosis, inhibition of chronic inflammation, promotion of angiogenesis, and regeneration of the myocardium. We further describe putative mediators employed by pericytes. GFP-labeling was used to track perivascular homing and lineage fate of transplanted pericytes. Our results demonstrate that the overall benefit of pericyte treatment is collectively attributed to multiple cardioprotective mechanisms that involve paracrine and direct cell-cell interactions.

Material and Methods

Human Tissue Biopsies and Cell Isolation

In total, 3 independent human skeletal muscle specimens (1 adult and 2 fetal) were used for cell isolation. The procurement of adult muscle biopsies from the National Disease Research Interchange was approved by the Institutional Review Board (IRB) at the University of Pittsburgh. Muscle biopsies (male subject, 57 years old) were preserved in DMEM containing 1% antibiotics and transported to the laboratory on ice. Human fetal tissues (21 and 23 weeks of gestation) were obtained following voluntary pregnancy interruptions performed at Magee Womens Hospital, Pittsburgh, in compliance with IRB protocol 0506176. Informed consents for the use of fetal tissues were obtained from all patients. Cells were mechanically and enzymatically dissociated from muscle biopsies following the reported protocol.[12] Details are described in supplemental material.

Fluorescence-activated Cell Sorting (FACS) and Flow Cytometry Analysis

FACS and flow cytometry were used to purify microvascular pericytes (CD146$^+$/34$^-$/45$^-$/56$^-$) and examine cell lineage marker expression respectively, as we previously reported.[12] Details are documented in supplemental material.

Cell Culture and Cell Labeling

Sorted pericytes were expanded in reported culture conditions.[12] Single donor-derived human umbilical cord vein endothelial cells (HUVECs, Lonza) were cultured in endothelial cell growth medium-2 (EGM-2, Lonza). Cultured pericytes were labelled with green fluorescence protein (GFP) following a published protocol,[12] using a lentivirus-based CMV-driven eGFP-expression vector. For short-term experiments, cells were labelled with cell membrane dyes, PKH26 (red) and PKH67 (green) (both from Sigma-Aldrich), and used immediately without further expansion.

Cell Transplantation in an Acute Myocardial Infarction Model

The Institutional Animal Care and Use Committee at Children's Hospital of Pittsburgh and University of Pittsburgh approved the animal usage and surgical procedures (Protocol#37-04, 55-07, 0901681A-5). A total of 78 male NOD/SCID mice (Jackson Laboratory) were used. MI induction (by ligation of left anterior descending coronary artery) and intramyocardial cell injection (3×10^5 cells/heart) were performed by a blinded surgeon as previously reported.[34] Control mice received injections of 30 µl phosphate-buffered saline (PBS).

Evaluation of Cardiac Function by Echocardiography

Mice were anesthetized with isoflurane and transthoracic echocardiography was performed by a blinded investigator repeatedly before and after surgery (at 2 and 8 weeks), using a high resolution ultrasound system (Vevo 770, Visual Sonics), as described previously.[34] Mice which died prior to 8 weeks post-injection were excluded. Echocardiographic measurements are listed in supplemental material.

Histological and Immunohistochemical Analyses

At 1, 2, and 8 weeks post-surgery, hearts were harvested and processed as previously described.[34] Cryosections at 6-8 µm thickness were used for histological and immunohistochemical analyses following published protocols.[34] Anti-GFP immunofluorescent staining was performed on 4% paraformaldehyde-fixed sections. Donor cell engraftment and perivascular homing were quantified on serial sections stained with anti-GFP antibody (Abcam) and dual-stained with anti-GFP/anti-mouse CD31 (BD Biosciences) antibodies respectively, using Image J. The engraftment ratio was defined as the extrapolated total number of engrafted GFP-positive cells to the initial 3×10^5 cells injected. Perivascular homing ratio was defined as the extrapolated number of GFP-positive cells juxtaposing CD31-positive mouse endothelial cells to the extrapolated total number of engrafted cells.

Using Masson's trichrome staining (San Marcos), fibrotic area fraction and infarct wall thickness were estimated from 6 randomly selected sections at comparable infarct levels per heart as previously described.[34] Quantification of host angiogenesis and chronic inflammation was computed from 6-10 randomly selected images taken from the designated area in sections stained with anti-mouse CD31 and anti-mouse CD68 (Abcam) at the mid-infarct level respectively. Experimental details are documented in supplemental material.

Hypoxia Assay and ELISA

To simulate the lower oxygen tension at the tissue level, physiologically or pathologically, pericytes were cultured under 2.5% O_2 hypoxic conditions (with 5% CO_2 and 92.5% N_2) as formerly described.[34] Cells were washed twice before defined, serum-free DMEM medium was added upon the transition to low O_2 conditions. Culture supernatant and cell lysates were collected 24 hours later. Cells cultured under 21% O_2 (normoxia) served as controls. The secretion of vascular endothelial growth factor (VEGF), angiopoietin-1 (Ang-1), angiopoietin-2 (Ang-2), and transforming growth factor (TGF)-β1 in the culture supernatant was measured by respective enzyme-linked immunosorbent assay (ELISA) with human VEGF (Invitrogen), Ang-1, Ang-2, and TGF-β1 (all from R&D Systems) ELISA Kits.

Real-time Quantitative PCR and Semi-quantitative RT-PCR

Real-time quantitative PCR (rt-qPCR) was performed as previously reported.[9] Total RNA (N=6) was extracted for cDNA synthesis. The quantitative analyses were performed in the core facility at the University of Pittsburgh. All data are presented as expression level normalized to human cyclophilin (in arbitrary fluorescence units). For semi-quantitative RT-PCR (sqRT-PCR), total RNA (N=3) were extracted using RNeasy plus-mini-kits (Qiagen). From each sample, 500ng of total RNA were reverse transcribed, followed by PCR. The intensity of the product bands were calculated using Quantify-One software and normalized to β-actin. The primer sequences are listed in supplemental table T1 and T2.

In vitro Vascular Network Formation

Cell culture/co-culture experiments using 2D and 3D Matrigel systems were performed to observe the capillary-like network formation. For 2D culture, 5×10^4 pericytes or HUVECs were seeded onto Matrigel-coated well and incubated for 24 hours. For 3D culture, 25×10^4 pericytes or HUVECs were re-suspended in EGM-2 medium and mixed with Matrigel in a 3:1 ratio. The Matrigel plug was subsequently incubated for 72 hours. Equal numbers of dye-labeled pericytes and HUVECs were well mixed in 2D or 3D co-culture for 72 hours to observe pericyte-HUVEC interactions.

Measurement of Cell Proliferation

Murine RAW264.7 monocyte/macrophage cells (ATCC) or primary murine skeletal myoblasts, muscle fibroblasts, and cardiac fibroblasts were cultured with normoxic or hypoxic pericyte-culture conditioned medium, or with serum-free control medium, for 72 hours. Cell proliferation was measured by the absorbance at 490nm after incubation with CellTiter Proliferation Assay Reagent (Promega) for 3 hours. Experiments were performed in quadruplicates and repeated 3 times independently.

Statistical Analysis

All measured data are presented as mean ± standard error (SE). Kaplan-Meier survival curve estimation with log-rank test was performed to compare the animal survival rate between treatment groups. Statistical differences were analyzed by Student's *t*-test (two groups), one-way ANOVA (multiple groups), or two-way repeated ANOVA (repeated echocardiographic measurements) with 95% confidence interval. Statistical significance was set at $p < 0.05$. Student-Newman-Keuls multiple comparison test (or Bonferroni test if specified) was performed for ANOVA post-hoc analysis. Statistical analyses were performed with SigmaStat 3.5 (Systat Software) and SPSS19 (IBM) statistics software.

Results

Isolation and Transplantation of Human Pericytes

As reported in our previous studies,[12] FACS was used to purify human microvascular pericytes (CD146$^+$/34$^-$/45$^-$/56$^-$) to homogeneity from skeletal muscle biopsies of three donors (one adult and two fetal, designated as AP, FP1, and FP2 respectively), by their differential expression of cell lineage markers, including CD34 (endothelial/stem cells), CD45 (hematolymphoid cells), CD56 (myogenic cells), and CD146 (pericyte/endothelial cells) (Supplemental Figure S1). No phenotypical difference between adult and fetal pericytes was noted, consistent with our previous observations.[12] After *in vitro* expansion (25-35 cell doublings) and prior to transplantation, in all three pericyte populations, we have observed no alteration to their distinctive morphology as well as classic antigenic profile, including robust expression of CD146, alkaline phosphatase (ALP), and typical MSC markers: CD44, CD73, CD90, CD105 with the absence of CD34, CD45, and CD56 (Supplemental Figure S2A and S2B). Additionally, cell labeling (in subsequent experiments) did not alter pericyte phenotype (data not shown). Cells (3.0×10^5 cells/heart) resuspended in 30μl PBS were injected into the acutely infarcted myocardium of immunodeficient mice. The control group received injections of 30μl PBS following the induction of MI.

Human Pericyte Transplantation Improves Cardiac Function

The survival of animals receiving pericyte treatment or PBS injection was monitored over the course of 8 weeks (Kaplan-Meier survival curve, log-rank test $p=0.529$, Figure1A). Cardiac function was assessed by echocardiography performed repeatedly before (healthy) and at 2 and 8 weeks after surgery (Supplemental Figure S3). Ischemic hearts injected with either of the three pericyte populations (N=8 per donor) had significantly smaller left ventricular (LV) chamber size, as measured by LV end-diastolic area (LVEDA, Figure 1B) and end-systolic area (LVESA, Figure 1C), than the control group (N=8) (all $p<0.05$), suggesting the reversal of progressive heart dilatation. Moreover, all pericyte-transplantation groups displayed significantly better LV contraction, evaluated by LV fraction shortening (LVFS, Figure 1D), LV fractional area change (LVFAC, Figure 1E), and LV ejection fraction (LVEF, Figure 1F), than the control group (all $p<0.05$). Collectively, when compared to vehicle treatment, pericyte treatment not only resulted in considerably smaller LV chamber dimension ($p<0.001$, two-way repeated ANOVA) but also notably improved LV contractility ($p<0.001$, two-way repeated ANOVA) for up to 2 months. Dimensional and functional echocardiographic parameters are documented in Supplemental Table T3. In a separate experiment, we compared cardiac function of acutely infarcted hearts injected with either APs or CD56+ myogenic progenitors, sorted from a single adult muscle biopsy. The echocardiographic results at 2 weeks post-infarction showed that pericyte-treated hearts (N=6) have significantly better LV function than CD56+ progenitor-treated ones (N=6) in five parameters examined, including LVEDA ($p=0.004$), LVESA ($p=0.002$), LVFS ($p=0.003$), LVFAC ($p=0.003$), and LVEF ($p\leq0.001$) (Supplemental Figure S4).

Transplantation of Pericytes Reduces Cardiac Fibrosis

To understand the influence of pericyte treatment on cardiac fibrosis, we evaluated scar tissue formation using Masson's trichrome histological staining. At 2 weeks post-infarction, pericyte-treated hearts displayed less collagen deposition (stained in blue/purple) at the ischemic area (Figure 2A). Estimation of the total fibrotic tissue ratio unveiled a 45.3% reduction of cardiac fibrosis in the pericyte-injected myocardium (N=5, 22.03±1.81%) when comparing to saline-injected controls (N=5, 40.28±2.15%) (Figure 2B, $p\leq0.001$), suggesting the anti-fibrotic efficacy of pericytes. Measurement of LV wall thickness at the center of the infarct indicated no significant difference ($p>0.05$) between the pericyte group (0.255±0.026 mm) and the PBS group (0.202±0.040 mm), suggesting that pericytes had limited beneficial effects to reduce transmural infarct thinning following MI (Figure 2C).

Paracrine Anti-fibrotic Effects of Pericytes under Hypoxia

Oxygen tension within tissues, physiologically or pathologically, is considerably lower than the ambient oxygen concentration *in vitro*. To elucidate the mechanism involved in pericyte-mediated reduction of fibrosis, we mimicked, at least in part, the hostile hypoxic microenvironment that donor cells encounter within the ischemic myocardium by culturing pericytes under 2.5% oxygen for 24 hours in defined, serum-free medium. Pericytes cultured under 21% oxygen (normoxia) served as controls. We then performed a cell proliferation assay using primary murine skeletal muscle and cardiac fibroblasts as well as skeletal myoblasts cultured with pericyte-conditioned medium (P-CM). Cardiac fibroblast proliferation was significantly reduced when cultured in hypoxic P-CM, compared to normoxic P-CM (p=0.019) (Figure 2D). Muscle fibroblast proliferation exhibited the same inhibitory pattern (p<0.001, hypoxic versus normoxic P-CM) with normoxic P-CM showing a pro-proliferative effect over control serum-free medium (p<0.05) (Figure 2D). Neither of the two P-CMs had significant influence over skeletal myoblast proliferation (p=0.76). One-way ANOVA with Bonferroni multiple comparisons was performed for statistical analysis. This suggests a paracrine anti-fibrotic effect by pericytes in hypoxia. We further proposed a fibrolytic role of pericyte-derived matrix metalloproteinases (MMPs) and examined gene expression of MMP-2 and MMP-9 by real-time qPCR. Cultured pericytes expressed more MMP-2 but nearly 10 times less MMP-9 than total skeletal muscle lysates (tissue origin control) (Figure 2E). We then explored MMP expression in hypoxia-cultured pericytes and demonstrated that MMP-2 expression in pericytes was well sustained under 2.5% oxygen, compared to normoxic culture (Figure 2F, p>0.05), while MMP-9 expression remained extremely low without significant change (Figure 2F, p>0.05). Immunohistochemical study revealed that some of the transplanted pericytes within the infarct region expressed MMP-2 (Figure 2G, a-d).

Transplantation of Pericytes Inhibits Chronic Inflammation

Histological analysis of pericyte- and PBS-injected hearts after hematoxylin and eosin (H&E) staining indicated an increased focal infiltration of inflammatory cells (cluster of cells with dark blue-stained nuclei) within the infarct region in the latter (Figure 3A). To more precisely evaluate the immunomodulatory effect of pericyte transplantation, we detected host CD68-positive monocytes/macrophages by immunohistochemistry. Pericyte-injected hearts exhibited diminished infiltration of host phagocytic cells within the infarct region at 2 weeks post-infarction (Figure 3B). Districts of the myocardium unaffected by the ischemic insult (posterior and septal walls) contained few CD68-positive cells in either group, similar to healthy hearts (Figure 3C). Quantitatively, injection of pericytes (N=5) resulted in a 34% reduction in infiltration of CD68-positive cells at 2 weeks post-infarction when compared to PBS controls (N=5) (Figure 3D, p<0.001).

Paracrine Immunomodulation by Pericytes

To understand the underlying mechanism of pericyte-induced inhibition of phagocytic cell infiltration, we analyzed the proliferation of murine macrophages cultured with pericyte-conditioned medium. Murine macrophage proliferation was significantly inhibited when culturing with both normoxic (p=0.018) and hypoxic (p<0.001) pericyte-conditioned media, compared to control medium (Figure 3E). Furthermore, hypoxic pericyte-conditioned medium exhibited a more prominent immunomodulatory effect than the normoxic counterpart (Figure 3E, p=0.002). We then investigated by sqRT-PCR the differential expression of genes encoding immunoregulatory molecules that are potentially accountable for this paracrine immunomodulation by pericytes. Under either normoxia or hypoxia, pericytes indeed expressed a considerable array of anti-inflammatory cytokines: interleukin-6 (IL-6), leukemia inhibitory factor (LIF), cyclooxygenase-2 (COX-2/PTGS-2, prostaglandin endoperoxide synthase-2) and heme oxygenase-1 (HMOX-1) (Figure 3F). Similarly, monocyte chemotactic protein-1 (MCP-1) and hypoxia-inducible factor-1α (HIF-1α) were highly expressed by pericytes (Figure 3F). Conversely, we detected very low to no expression of pro-inflammatory cytokines including interleukin-1α (IL-1α), tumor necrosis factor-α (TNF-α), and interferon-γ (IFNγ) (Figure 3F). No expression of interleukin-4 (IL-4), interleukin-10 (IL-10), inducible nitric oxide synthase (iNOS), and indoleamine 2,3-dioxygenase (2,3-IDO) was observed (Figure 3F). Quantitatively, there was no significant alteration of expression under hypoxia of immunoregulatory genes investigated, except MCP-1, whose expression was notably decreased in hypoxia-cultured pericytes (Figure 3G, all p>0.05; MCP-1, p=0.027).

Transplanted Pericytes Promote Host Angiogenesis

We examined whether intramyocardial transplantation of pericytes restores the host vascular network post-infarction. Capillaries in the peri-infarct areas (Figure 4A) and within the infarct region (Figure 4B) were revealed by anti-mouse CD31 (platelet endothelial cell adhesion molecule, PECAM-1) immunofluorescent staining and subsequently quantified. Capillary structure density in the peri-infarct areas of pericyte-injected hearts (N=5) was increased by 45.4% when compared to PBS-injected controls (N=5) (Figure 4C, p=0.01). Higher microvascular density was also observed within the infarct region, with 34.8% more capillaries in the pericyte-treated hearts (Figure 4C, p=0.002). Detection of the proliferating host ECs by Ki-67, a cell proliferation marker, and CD31 showed that pericyte-injected hearts (N=3) had significantly more proliferating ECs than PBS-injected controls (N=3) in both the infarct region (p=0.034) and peri-infarct areas (p=0.025) (Supplemental Figure S5A-C). These findings suggest that transplanted pericytes promote host angiogenesis not only in the peri-infarct areas, where blood vessels were generally better preserved after the ischemic

injury, but also within the blood vessel-deprived infarct region.

Pericytes Support Microvascular Structures

To demonstrate that pericytes benefit host vascular networks through their support of microvascular structures, we developed 2D and 3D Matrigel cultures/co-cultures using pericytes and HUVECs. HUVECs seeded onto Matrigel-coated wells formed typical capillary-like networks after 24 hours (Figure 5A). Pericytes, however, formed similar structures within 6-12 hours of seeding (Figure 5B). To illustrate the reciprocal influence between pericytes and endothelial cells (ECs), dye-labeled pericytes (PKH67, green) and HUVECs (PKH26, red) were mixed and co-cultured in 2D Matrigel, which resulted in the formation within 6-12 hours of capillary-like structures that included both cell types (Figure 5C). Pericytes (green) were observed to collocate with HUVECs (red) in the co-formed three-dimensional structures after incubation for 24 hours (Figure 5C, inset). Additionally, HUVECs (red) appeared to morphologically align with pericytes (green) (Figure 5D). To further unveil the vascular supportive role of pericytes, an *in vitro* 3D Matrigel system designed to simulate native capillary formation was used. HUVECs evenly distributed within the 3D Matrigel plug were unable to form organized structures after 72 hours (Figure 5E). To the contrary, pericytes started to form capillary-like networks 24 hours after gel-casting, with structural remodeling over time (Figure 5F). The dynamic interaction between pericytes and ECs was best depicted by encapsulating dye-labeled pericytes (green) and HUVECs (red) in a 3D Matrigel plug. Together these two types of cells formed capillary-like structures after incubation for 72 hours (Figure 5G) with pericytes surrounding HUVECs (Figure 5H). These data suggest that pericytes retained vascular cell features and formed structures supportive of microvascular networks even after purification and long-term culture, while pericyte-EC association may play a role in the pericyte-facilitated angiogenic process.

Differential Expression of Pro-angiogenic Factors and Associated Receptors by Pericytes under Hypoxia

The paracrine angiogenic potential of pericytes in the ischemic heart was investigated using the simulated hypoxic environment *in vitro*. Expression of genes encoding pro-angiogenic factors and corresponding receptors was assessed by real-time qPCR. Vascular endothelial growth factor-A (VEGF-A), platelet-derived growth factor-β (PDGF-β), and transforming growth factor (TGF)-β1 were notably up-regulated by 307% ($p \leq 0.001$), 437% ($p = 0.067$), and 178% ($p = 0.037$) respectively in pericytes cultured under hypoxic conditions (Figure 6A). Expression of other pro-angiogenic factors, including basic fibroblast growth factor (bFGF), hepatocyte growth factor (HGF), and epidermal growth factor (EGF), was down-regulated to 44% ($p < 0.05$), 23% ($p \leq 0.001$), and 60% ($p > 0.05$) of their expression

levels in normoxia (Figure 6A). On the other hand, VEGF receptor-1 (VEGFR-1/Flt-1) and -2 (VEGFR-2/KDR/Flk-1) were substantially up-regulated by 458% (p=0.004) and 572% ($p \leq 0.001$) respectively under 2.5% oxygen (Figure 6B). PDGF receptor-β (PDGF-Rβ) expression was not significantly changed (161%, p>0.05) (Figure 6B). VEGF secretion by pericytes, measured by ELISA, significantly increased over 3-fold ($p \leq 0.001$) under hypoxic culture conditions while angiopoietin-1 (Ang-1) secretion reduced by 35% (p>0.05) (Figure 6C). Very little secretion of angiopoietin-2 (Ang-2) by pericytes was detected under both conditions (p>0.05) (Figure 6C). Additionally, TGF-β1 secretion increased by 30.1% under hypoxia (p=0.028) (Figure 6C), consistent with its up-regulated gene expression. The expression of human VEGF$_{165}$ by engrafted pericytes within the infarct region was confirmed by immunohistochemistry (Figure 6D, a-c).

Transplanted Pericytes Home to Perivascular Locations

It is not known whether purified pericytes home back to perivascular areas *in vivo*. To reveal their engraftment and homing pattern, cultured pericytes were transduced with a GFP reporter gene at near 95% efficiency (Figure 7A) and injected (3.0×10^5 cells) into acutely infarcted hearts. GFP-labeled pericytes engrafted throughout the ventricular myocardium (Figure 7B), particularly in the peri-infarct area (Supplemental Figure S6). Many donor pericytes retained expression of NG2, a pericyte marker (Supplemental Figure S7). Confocal microscopy showed that a fraction of pericytes were identified in perivascular positions, adjacent to host CD31-positive endothelial cells (Figure 7C). Indeed, pericytes were aligned with (Figure 7C, main) or surrounding (Figure 7C, inset) CD31-positive microvessels, suggestive of perivascular homing. The number of engrafted GFP-positive pericytes was approximately 9.1±1.3% of total injected cells at the first week and declined over time to 3.4±0.5% at 8 weeks post-infarction (N=3 per time point) (Figure 7D, dash-dot line). The perivascular homing rate instead increased from 28.6% to 40.1% over the course of 8 weeks, implicating the merit of niche-homing for long-term donor cell survival (Figure 7D, solid line). To demonstrate cellular interactions between donor pericytes and host ECs, we performed immunohistochemical studies for ephrin type-B receptor 2 (EphB2) and connexin43, a gap junction protein. Confocal images revealed that some GFP-positive pericytes juxtaposing host ECs expressed human-specific EphB2 (Figure 7E) or formed gap junctions with ECs (Figure 7F). These results suggest cellular interactions between host ECs and donor pericytes homed to perivascular locations.

Cell Lineage Fate of Transplanted Pericytes

GFP-labeled pericytes were employed to track cell lineages developed from donor pericytes and investigate the capacity of human muscle pericytes to reconstitute major

cardiac cell types after injury. Immunohistochemistry was performed to simultaneously detect GFP and cell lineage markers: the cardiomyocyte marker, cardiac troponin-I (cTn-I); the smooth muscle cell (SMC) marker, smooth muscle myosin heavy chain (SM-MHC); the endothelial cell (EC) marker, CD31. Confocal microscopy revealed that in the peri-infarct area, a minor fraction of transplanted pericytes co-express GFP and cTn-I (Supplemental Figure S8A-C, main), a few of which appear single-nucleated (Supplemental Figure S8A-C, inset). Some GFP-positive cardiomyocytes were identified within the remaining myocardium (Supplemental Figure S8D-F) with organized sarcomeric patterns (Supplemental Figure S8G-I). A very small number of donor pericytes co-expressed GFP and human-specific CD31 (<1%) (Supplemental Figure S8J-L). Similarly, co-expression of GFP and human-specific SM-MHC was detected in very few transplanted cells (<0.5%) (Supplemental Figure S8M-O). Negative control images were stained only with matching fluorescence-conjugated secondary antibodies (Supplemental Figure S8P-R).

Discussion

Pericytes constitute a major structural component of small blood vessels, regulating vascular development, integrity and physiology. The recent identification of microvascular pericytes as one of the native sources of MSC ancestors raised the possibility that these cells participate in the repair of injured/ageing organs.[11-16,35] The therapeutic potential of microvascular pericytes was indicated by structural and functional regeneration of skeletal muscle involving direct pericyte differentiation into regenerative units as well as applications in lung repair and vascular tissue engineering.[8,11,12,35,36] Pericytes can also repair tissue via secretion of trophic factors, implying broad usage in clinical settings.[8,18]

Recent studies indicated a possible developmental hierarchy among different stem/progenitor cell populations residing in the blood vessel walls.[15,37] Katare et al. reported that transplantation of adventitial progenitor cells repairs infarcted hearts through angiogenesis involving microRNA-132.[38] Herein we demonstrate that transplantation of human FACS-purified microvascular pericytes contributes to the functional and structural repair of the ischemic heart, albeit unequally, through both paracrine effects and cellular interactions. A major goal of SCT, the prevention of progressive LV dilatation and consequent heart failure, was largely achieved by pericyte treatment, implicating the attenuation of deleterious remodeling. We also observed significant improvement of cardiac contractility in an acute infarction milieu, with up to 70% of healthy contractile function consistently maintained for at least two months. No significant difference was observed between adult and fetal pericytes in terms of heart repair. The therapeutic benefits observed could be explained, at least in part, by anti-fibrotic, anti-inflammatory, angiogenic, and to a lesser extent, cardiomyogenic properties of pericytes.

The anti-fibrotic action of mesodermal stem/progenitor cells in the injured heart has been reported.[25-27] MSC-conditioned medium diminished viability, proliferation, collagen synthesis, and α-SMA expression in cardiac fibroblasts but stimulated MMP2/9 activities, indicating a paracrine anti-fibrotic property of MSCs.[26,27] Our results demonstrated a near 50% reduction of myocardial fibrosis following pericyte injection. Along with the attenuation of progressive LV dilatation, pericyte treatment appears to result in propitious remodeling, leading to improved myocardial compliance and strengthening of the ischemic cardiac tissue.

We speculated that decreased fibrosis/scar formation is, at least partially, associated with a reduced number of fibrotic cells resulting from the administration of pericytes. Interestingly, pericyte-treated hearts contained significantly less cells within the infarct area than PBS-injected controls ($p<0.05$, Supplemental Figure S9A) with no statistical difference in Ki-67(+) proliferating cell density ($p=0.808$, Supplemental Figure S9B). Additionally, TUNEL staining revealed no significant difference between pericyte- and PBS-injected hearts in the number of apoptotic cells within the infarct region ($p=0.296$, Supplemental Figure S10A-B). Due to the highly fibrotic nature of MI, we were unable to quantitate fibrotic cells *in vivo*. Nevertheless, murine fibroblast proliferation was notably inhibited when cultured in hypoxic pericyte-conditioned medium *in vitro*, indicating the paracrine fibrosuppressive effect of pericytes under hypoxia. MMPs were suggested to play important roles in post-injury scar remodeling, angiogenesis, and vascular cell proliferation/migration.[27,39] In particular, a preponderant role of MMP-2 in preventing collagen accumulation by cardiac fibroblasts was proposed.[27] Consequently, we postulated the existence of a fibrolytic activity from donor pericytes, involving MMPs, which contributes to the attenuation of cardiac fibrosis. Indeed, high expression of MMP-2, but not MMP-9, by pericytes, even under hypoxic conditions, was observed. The expression of MMP-2 was confirmed in some, but not all, transplanted pericytes, implying a minor role of pericyte-mediated fibrolysis. Overall, our data suggest that the gross amelioration of fibrosis presumably involves decreased collagen deposition, reduced proliferation of fibroblasts, and altered remodeling of the extracellular matrix (ECM). Yet whether there exists one or more determining mechanism(s) remains to be investigated.

The immunosuppressive potential of MSCs, demonstrated by inhibiting T-lymphocyte proliferation in culture and counteracting graft-versus-host reaction in recipients of allogeneic blood stem cells, is currently exploited in clinical trials.[28,29] In the cardiac milieu, MSC transplantation in a rat model of acute myocarditis mitigated the increase in CD68+ phagocytic cells.[40] In the present study, pericyte treatment significantly diminished host monocyte/macrophage infiltration in the infarcted myocardium, suggesting an anti-inflammatory potential which contributed to the reduction of fibrosis, amelioration of adverse remodeling, and improvement of cardiac function. Nevertheless, whether pericytes inhibit the acute-phase inflammation occurring soon after the incidence of MI is unknown. Inhibition of murine macrophage proliferation in culture by pericyte-conditioned medium

suggests a paracrine mechanism of their immunomodulatory capacity.

The immunosuppressive and anti-inflammatory capacities of MSCs are primarily attributed to soluble factors/molecules, as IL-6, LIF, and HMOX-1 were shown to exercise beneficial immunosuppressive effects.[28,29] The attenuation of intense inflammation and mitigation of multi-organ damage by MSCs during sepsis are dependent on monocyte/macrophage-derived cytokines and regulated via PGE$_2$ signaling.[41] The immunoregulatory and cardioprotective functions of these molecules appear to be similar in the cardiac milieu.[22,42] Our data demonstrate that pericytes express high levels of IL-6, LIF, COX-2, HMOX-1, and HIF-1α, which are sustained under hypoxic conditions. MCP-1 expression, however, notably decreased under hypoxia, corresponding with the reduced CD68+ cell infiltration in vivo. Little to no expression of pro-inflammatory cytokines including IL-1α, TNF-α and IFNγ was detected. Virtually no expression of IL-4, IL-10, iNOS, and 2,3-IDO was observed in pericytes, suggestive of an immunoregulatory cytokine secretome that is unique to human microvascular pericytes.[29,43] Intriguingly, TGF-β1, also an anti-inflammatory yet fibrogenic cytokine, was strongly expressed by pericytes.[22,44] Our data suggested increased TGF-β1 expression/secretion by pericytes under hypoxic conditions (Figure 6A and 6C). Given the multiple functions each proposed growth factor/cytokine possesses, it is likely that a dynamic, interactive, and intricately orchestrated balance of trophic factors between donor and host cells holds the key to a successful ischemic tissue remodeling and regeneration.

A linear correlation between secretion of pro-angiogenic factors, angiogenesis and cardiac restoration was illustrated by blocking the bioactivity of VEGF secreted from transplanted murine muscle-derived stem cells in a mouse MI model, which not only abolished their stimulation of neovascularization but in turn negatively influenced LV contractility and infarct size.[45] Okada et al. further delineated the superior angiogenic properties of human myoendothelial progenitor cells and increased secretion of VEGF in response to hypoxia.[34] Given the indigenous vascular association of pericytes, we hypothesized that pericytes are able to repair the damaged host vasculature. Indeed, upon pericyte treatment, we observed a significantly larger host microvascular network not only in the peri-infarct collateral circulation but within the infarct region. Cultured pericytes secrete growth factors/cytokines/chemokines related to vascular physiology and remodeling[18]; among which, only VEGF-A, PDGF-β, and TGF-β1 were substantially up-regulated under hypoxia, suggesting their role in pericyte-enhanced angiogenesis.[39,46]

Angiogenesis may follow cell-cell contact between donor pericytes and host ECs, in addition to stimulation by angiogenic factors. Recent studies reported that MSCs and vascular mural/adventitial cells support ECs in small blood vessel formation and maturation in culture and in vivo.[33,47] We did observe the perivascular homing of donor pericytes in the

ischemic heart. Some donor pericytes juxtaposing host ECs expressed interactive molecules including EphB2 and connexin43, suggestive of cellular interactions.[48,49] Planar Matrigel culture confirmed the vascular cell characteristics of pericytes and their capability to enhance the angiogenic behavior of ECs. We further demonstrated microvessel formation and vascular support by pericytes in three-dimensional cultures, indicating that associations between pericytes and ECs may contribute to revascularization. Nevertheless, the vibrant angiogenic response of pericytes observed *in vitro* may be reduced *in vivo* because of the harsh microenvironment caused by post-MI ischemia and inflammation. Altogether, these results demonstrate that the angiogenic properties of pericytes may result from indirect paracrine effects and, albeit minor, direct cellular interactions.

Compared to other types of stem/progenitor cells, pericytes appear to engraft well in the infarcted heart initially, presumably attributable to several factors.[50] We did not observe apparent cell death of pericytes cultured under 2.5% O_2 for up to 48 hours, implying their resistance to hypoxia (data not shown). The increased proliferation and migration of pericytes in response to low oxygen concentration and ECM degradation products have important implications for ischemic injury repair.[10] The perivascular niche-homing capacity may further benefit the long-term survival of pericytes. Nonetheless, it remains unclear whether pericytes actively migrated to perivascular locations or served as a re-vascularizing center inducing/recruiting angiogenic proliferation/migration of host ECs. Future studies are needed to reveal the kinetics of pericyte-EC interaction and migration *in vivo*.

The potential of human muscle pericytes to reconstitute major cell types in the injured myocardium, though to a small extent, was hereby demonstrated. Cell fate tracking suggests that a minor fraction of donor pericytes differentiated into and/or fused with cardiomyocytes. Given the small number of GFP-cTnI dual-positive cells present, it is unlikely that these cells contributed significantly to functional recovery.[21] Pericytes, all of which were α-SMA-positive during culture expansion, lost α-SMA expression once homing to host microvasculature (data not shown), consistent with our finding that a subset of native microvascular pericytes do not express α-SMA *in situ*.[12]

In summary, FACS-purified human microvascular pericytes contribute to anatomic and functional cardiac improvement post-infarction through multiple cardioprotective mechanisms: reverse of ventricular remodeling, reduction of cardiac fibrosis, diminution of chronic inflammation, and promotion of host angiogenesis. Vessel-homing and small-scale regenerative events by pericytes partially reconstitute lost cardiac cells and contribute to the structural recovery. These cardioprotective and cardioregenerative activities of a novel stem cell population that can be purified to homogeneity and expanded *in vitro* await further research and exploitation in ischemic cardiovascular diseases.

Disclosure of Conflicts of Interest

J.H. received remuneration from Cook MyoSite, Inc. for consulting services and for royalties received from technology licensing during the period that the above research was performed. All other authors have no conflict of interest to disclose.

References

1.   **American Heart Association. Heart Disease and Stroke Statistics--2011 Update: A Report From the American Heart Association.** *Circulation.* **February 1, 2011 2011;123(4):e18-209.**

2.   **Kumar V, Fausto N, Abbas A.** *Robbins & Cotran Pathologic Basis of Disease***. 7th ed. Philadelphia, PA: Saunders; 2004.**

3.   **Hansson EM, Lindsay ME, Chien KR. Regeneration Next: Toward Heart Stem Cell Therapeutics.** *Cell Stem Cell.* **2009;5(4):364-377.**

4.   **Segers VFM, Lee RT. Stem-cell therapy for cardiac disease.** *Nature.* **2008;451(7181):937-942.**

5.   **Janssens S. Stem Cells in the Treatment of Heart Disease.** *Annual Review of Medicine.* **2010;61(1):287-300.**

6.   **Menasche P. Cardiac cell therapy: Lessons from clinical trials.** *Journal of Molecular and Cellular Cardiology.* **2011;50(2):258-265.**

7.   **Armulik A, Abramsson A, Betsholtz C. Endothelial/pericyte interactions.** *Circ. Res.* **2005;97(6):512-523.**

8.   **Montemurro T, Andriolo G, Montelatici E, et al. Differentiation and migration properties of human foetal umbilical cord perivascular cells: potential for lung**

repair. *Journal of Cellular and Molecular Medicine.* 2011;15(4):796-808.

9. Park TS, Gavina M, Chen C-W, et al. Placental Perivascular Cells for Human Muscle Regeneration. *Stem Cells and Development.* 2011;20(3):451-463.

10. Tottey S, Corselli M, Jeffries EM, Londono R, Peault B, Badylak SF. Extracellular Matrix Degradation Products and Low-Oxygen Conditions Enhance the Regenerative Potential of Perivascular Stem Cells. *Tissue Engineering Part A.* 2011;17(1-2):37-44.

11. Dellavalle A, Sampaolesi M, Tonlorenzi R, et al. Pericytes of human skeletal muscle are myogenic precursors distinct from satellite cells. *Nat Cell Biol.* 2007;9(3):255-267.

12. Crisan M, Yap S, Casteilla L, et al. A Perivascular Origin for Mesenchymal Stem Cells in Multiple Human Organs. *Cell Stem Cell.* 2008;3(3):301-313.

13. Sacchetti B, Funari A, Michienzi S, et al. Self-Renewing Osteoprogenitors in Bone Marrow Sinusoids Can Organize a Hematopoietic Microenvironment. *Cell.* 2007;131(2):324-336.

14. Feng J, Mantesso A, De Bari C, Nishiyama A, Sharpe PT. Dual origin of mesenchymal stem cells contributing to organ growth and repair. *Proceedings of the National Academy of Sciences.* April 19, 2011 2011;108(16):6503-6508.

15. Corselli M, Chen C-W, Sun B, Yap S, Rubin PJ, Peault B. The tunica adventitia of human arteries and veins as a source of mesenchymal stem cells. *Stem Cells and Development.* 2011;21(8):1299-1308.

16. Tormin A, Li O, Brune JC, et al. CD146 expression on primary nonhematopoietic bone marrow stem cells is correlated with in situ localization. *Blood.* May 12, 2011 2011;117(19):5067-5077.

17. Corselli M, Chen CW, Crisan M, Lazzari L, Peault B. Perivascular ancestors of adult multipotent stem cells. *Arterioscler Thromb Vasc Biol.* Jun 2010;30(6):1104-1109.

18. Chen CW, Montelatici E, Crisan M, Corselli M, Huard J, Lazzari L, Péault B. Perivascular multi-lineage progenitor cells in human organs: regenerative units, cytokine sources or both? *Cytokine Growth Factor Rev.* 2009;20(5-6):429-434.

19. James A, Zara J, Zhang X, et al. Perivascular Stem Cells: A Prospectively Purified Mesenchymal Stem Cell Population for Bone Tissue Engineering. *Stem Cells.* 2012;In press.

20. Chen CW, Okada M, Tobita K, Peault B, Huard J. Purified Human Muscle-derived Pericytes Support Formation of Vascular Structures and Promote Angiogenesis After Myocardial Infarction. *Circulation.* 2009;120:S1053.

21. Gnecchi M, Zhang Z, Ni A, Dzau VJ. Paracrine Mechanisms in Adult Stem Cell Signaling and Therapy. *Circ Res.* November 21, 2008 2008;103(11):1204-1219.

22.   Frangogiannis NG. The immune system and cardiac repair. *Pharmacological Research.* 2008;58(2):88-111.

23.   Caplan AI, Dennis JE. Mesenchymal stem cells as trophic mediators. *Journal of Cellular Biochemistry.* 2006;98(5):1076-1084.

24.   Berry MF, Engler AJ, Woo YJ, et al. Mesenchymal stem cell injection after myocardial infarction improves myocardial compliance. *Am J Physiol Heart Circ Physiol.* June 1, 2006 2006;290(6):H2196-2203.

25.   Pittenger MF, Martin BJ. Mesenchymal Stem Cells and Their Potential as Cardiac Therapeutics. *Circ Res.* July 9, 2004 2004;95(1):9-20.

26.   Ohnishi S, Sumiyoshi H, Kitamura S, Nagaya N. Mesenchymal stem cells attenuate cardiac fibroblast proliferation and collagen synthesis through paracrine actions. *FEBS Letters.* 2007;581(21):3961-3966.

27.   Mias C, Lairez O, Trouche E, et al. Mesenchymal stem cells promote matrix metalloproteinase secretion by cardiac fibroblasts and reduce cardiac ventricular fibrosis after myocardial infarction. *Stem Cells.* Nov 2009;27(11):2734-2743.

28.   Ghannam S, Bouffi C, Djouad F, Jorgensen C, Noel D. Immunosuppression by mesenchymal stem cells: mechanisms and clinical applications. *Stem Cell Res Ther.* 2010;1(1):2.

29.   Shi Y, Hu G, Su J, et al. Mesenchymal stem cells: a new strategy for immunosuppression and tissue repair. *Cell Res.* May 2010;20(5):510-518.

30.   Renault MA, Losordo DW. Therapeutic myocardial angiogenesis. *Microvasc Res.* 2007 74(2-3):159-171. .

31.   Sieveking DP, Ng MKC. Cell therapies for therapeutic angiogenesis: back to the bench. *Vasc. Med.* 2009;14(2):153-166.

32.   Saunders WB, Bohnsack BL, Faske JB, et al. Coregulation of vascular tube stabilization by endothelial cell TIMP-2 and pericyte TIMP-3. *The Journal of Cell Biology.* October 9, 2006 2006;175(1):179-191.

33.   Au P, Tam J, Fukumura D, Jain RK. Bone marrow-derived mesenchymal stem cells facilitate engineering of long-lasting functional vasculature. *Blood.* 2008;111(9):4551-4558.

34.   Okada M, Payne TR, Zheng B, et al. Myogenic Endothelial Cells Purified From Human Skeletal Muscle Improve Cardiac Function After Transplantation Into Infarcted Myocardium. *Journal of the American College of Cardiology.* 2008;52(23):1869-1880.

35.   Dellavalle A, Maroli G, Covarello D, et al. Pericytes resident in postnatal skeletal muscle differentiate into muscle fibres and generate satellite cells. *Nat Commun.* 2011;2:499.

36.   He W, Nieponice A, Soletti L, et al. Pericyte-based human tissue engineered

vascular grafts. *Biomaterials.* 2010;31(32):8235-8244.

37. Zimmerlin L, Donnenberg VS, Pfeifer ME, et al. Stromal vascular progenitors in adult human adipose tissue. *Cytometry A.* Jan 2010;77(1):22-30.

38. Katare R, Riu F, Mitchell K, et al. Transplantation of Human Pericyte Progenitor Cells Improves the Repair of Infarcted Heart Through Activation of an Angiogenic Program Involving Micro-RNA-132 / Novelty and Significance. *Circulation Research.* September 30, 2011 2011;109(8):894-906.

39. Enciso JM, Hirschi KK. Understanding Abnormalities in Vascular Specification and Remodeling. *Pediatrics.* July 1, 2005 2005;116(1):228-230.

40. Ohnishi S, Yanagawa B, Tanaka K, et al. Transplantation of mesenchymal stem cells attenuates myocardial injury and dysfunction in a rat model of acute myocarditis. *Journal of Molecular and Cellular Cardiology.* 2007;42(1):88-97.

41. Nemeth K, Leelahavanichkul A, Yuen PS, et al. Bone marrow stromal cells attenuate sepsis via prostaglandin E(2)-dependent reprogramming of host macrophages to increase their interleukin-10 production. *Nat Med.* Jan 2009;15(1):42-49.

42. Liu X, Pachori AS, Ward CA, et al. Heme oxygenase-1 (HO-1) inhibits postmyocardial infarct remodeling and restores ventricular function. *Faseb J.* Feb 2006;20(2):207-216.

43. Ren G, Su J, Zhang L, et al. Species variation in the mechanisms of mesenchymal stem cell-mediated immunosuppression. *Stem Cells.* Aug 2009;27(8):1954-1962.

44. Abarbanell AM, Coffey AC, Fehrenbacher JW, et al. Proinflammatory cytokine effects on mesenchymal stem cell therapy for the ischemic heart. *Ann Thorac Surg.* Sep 2009;88(3):1036-1043.

45. Payne TR, Oshima H, Okada M, Momoi N, Tobita K, Keller BB, Peng H, Huard J. A relationship between vascular endothelial growth factor, angiogenesis, and cardiac repair after muscle stem cell transplantation into ischemic hearts. *J Am Coll Cardiol.* 2007;50(17):1677-1684.

46. Ohnishi S, Yasuda T, Kitamura S, Nagaya N. Effect of Hypoxia on Gene Expression of Bone Marrow-Derived Mesenchymal Stem Cells and Mononuclear Cells. *Stem Cells.* 2007;25(5):1166-1177.

47. Campagnolo P, Cesselli D, Al Haj Zen A, et al. Human Adult Vena Saphena Contains Perivascular Progenitor Cells Endowed With Clonogenic and Proangiogenic Potential. *Circulation.* April 20, 2010 2010;121(15):1735-1745.

48. Salvucci O, de la Luz Sierra M, Martina JA, McCormick PJ, Tosato G. EphB2 and EphB4 receptors forward signaling promotes SDF-1–induced endothelial cell chemotaxis and branching remodeling. *Blood.* November 1, 2006 2006;108(9):2914-2922.

49. **Hirschi KK, Burt JM, Hirschi KD, Dai C. Gap Junction Communication Mediates Transforming Growth Factor-β Activation and Endothelial-Induced Mural Cell Differentiation.** *Circulation Research.* September 5, 2003 2003;93(5):429-437.

50. **Wu KH, Mo XM, Han ZC, Zhou B. Stem Cell Engraftment and Survival in the Ischemic Heart.** *The Annals of Thoracic Surgery.* 2011;92(5):1917-1925.

Figure Legends

Figure 1. Survival rate and cardiac functional assessment

(A) Cumulative survival rate of the animals over 8 weeks post-surgery (Kaplan-Meier Survival Curve, log-rank test p=0.529). Echocardiographic analyses revealed a significant reduction of LV dilatation by transplantation of all three pericyte populations (AP, FP1, and FP2), as shown by the smaller LV area in end-diastole (B) and end-systole (C) of hearts at both time points. Injection of pericytes also resulted in substantial improvement in LV contractility, as indicated by greater fractional shortening (D), fractional area change (E), and ejection fraction (F), at both time points. ([†]p≤0.001; [§]p≤0.005; [#]p≤0.01; [*]p≤0.05; versus PBS control group at each time point)

Figure 2. Attenuation of myocardial fibrosis by pericyte treatment

(A) Masson's trichrome-stained transverse sections of hearts injected with pericytes or PBS (collagen in blue/purple, cardiac muscle in red; scale bars=1 mm). (B) The fibrotic area fraction was dramatically decreased in pericyte-injected hearts (p≤0.001). (C) Pericyte group had no significant increase in the infarct wall thickness. (D) When culturing with hypoxic pericyte-conditioned medium (P-CM), the proliferation of murine cardiac fibroblasts was significantly reduced ([†]p=0.019, versus normoxic P-CM) while muscle fibroblast proliferation exhibited the same pattern ([*]p<0.001). Normoxic P-CM had a pro-proliferative effect over control medium in muscle fibroblasts, but not in cardiac fibroblasts ([#]p<0.05). Skeletal myoblast proliferation was not significantly affected by either of the P-CMs. (E) Expression of MMP-2 in cultured pericytes was higher than that in skeletal muscle lysates. Conversely, MMP-9 expression in pericytes was nearly 10 times less (logarithmic scale of 10 in arbitrary fluorescence units). (F) Expression of both MMP-2 and -9 in pericytes did not change significantly under hypoxia (p>0.05, logarithmic scale of 10 in arbitrary fluorescence units). (G) Immunohistochemistry revealed MMP-2 expression (red arrows) by some of the GFP-labeled donor pericytes (green arrows) within the infarct area at 2 weeks post-infarction (a) merge (b) anti-GFP in green (c) MMP-2 in red (d) DAPI nuclei staining in blue (scale bar=20μm).

Figure 3. Reduction of host phagocytic cell infiltration by pericyte transplantation

(A) H&E staining revealed a greater focal infiltration of leukocytes (dark blue-stained nuclei) within the infarct region in PBS-injected controls at 2 weeks post-infarction (scale bars=100μm). (B) Anti-mouse CD68 immunostaining showed that the infarct region of pericyte-injected hearts contains less host phagocytic cells (scale bars=50μm). (C) Host CD68-positive cells were locally attracted to the infarct region but not to the unaffected myocardium (posterior ventricular wall) in both groups (scale bars=50μm). (D) Host monocytes/macrophage infiltration at the infarct site was significantly reduced ($p<0.001$). (E) The proliferation of murine macrophages was significantly inhibited when culturing with pericyte-conditioned media ($^*p=0.018$, $^\#p<0.001$, versus control medium), an effect more prominent with hypoxic pericyte-conditioned medium ($^\dagger p=0.002$, hypoxia versus normoxia). (F) Cultured pericytes exhibited sustained, high expression of genes regulating the inflammatory responses, even under 2.5% O_2 (N: normoxia; H: hypoxia). Little expression of IL-1α and no expression of IL-4, IL-10, iNOS, 2,3-IDO, TNF-α, and IFNγ were detected. (G) No statistically significant difference in expression of genes of immunoregulatory molecules between normoxic- and hypoxic-cultured pericytes except MCP-1, which notably decreased in hypoxic cultures (sqRT-PCR analysis, $p=0.027$).

Figure 4. Promotion of host angiogenesis by pericyte treatment

Representative images of anti-mouse CD31 immunostaining (A) in the peri-infarct area and (B) within the infarct region of hearts injected with pericytes or PBS (scale bars=50μm). (C) Pericyte-treated hearts displayed significantly higher capillary densities in the peri-infarct area ($p<0.05$) and within the infarct region ($p<0.001$).

Figure 5. Pericytes support microvascular structures

(A) While HUVECs seeded onto Matrigel-coated wells formed typical capillary-like networks after 24 hours, (B) pericytes formed similar structures within 6-12 hours (scale bars=1mm). (C) When co-cultured on Matrigel, dye-labeled pericytes (green) and HUVECs (red) co-formed capillary-like networks within 6-12 hours, ([C], inset) with collocations of pericytes and HUVECs in three-dimensional structures formed 24 hours after seeding (scale bars: main=200μm; inset=100μm). (D) HUVECs (red) appear to line and spread out on top of the pericyte-formed structures (green) (scale bar=100μm). (E) To simulate native capillary formation, HUVECs were evenly encapsulated into 3D Matrigel plug for 72 hours but unable to form any organized structure (scale bars=1mm). (F) Pericytes instead formed capillary-like networks in Matrigel plug with structural organization and maturation over time (scale bars=1mm). (G) When dye-labeled pericytes (green) and HUVECs (red) were co-casted into the 3D-gel plug, the two types of cells formed microvessel-like networks within 72 hours, (H) with pericytes surrounding HUVECs (scale bars: G=200μm; H=50μm).

Figure 6. Expression of pro-angiogenic factors and associated receptors under hypoxia

(A) Pericytes dramatically up-regulated VEGF-A, PDGF-β, TGF-β1 gene expression under hypoxic conditions (2.5% O_2) while expression of other pro-angiogenic factors, including bFGF, HGF and EGF were distinctively repressed. (B) Simultaneously, VEGFR-1 (Flt-1) and -2 (Flk-1) were substantially up-regulated, and PDGF-Rβ expression was moderately increased. All expression levels are normalized to human cyclophilin and presented in arbitrary fluorescence units on an expanded logarithmic scale (#$p<0.05$, *$p≤0.001$, †$p<0.01$, hypoxia versus normoxia). (C) Significantly increased secretion of VEGF ($p≤0.001$) and TGF-β1 ($p=0.028$) by pericytes under hypoxic culture conditions was detected by ELISA while secretion of Ang-1 was reduced by 35% ($p>0.05$). Very little secretion of Ang-2 was detected under both conditions ($p>0.05$). (D) Immunohistochemistry revealed human VEGF$_{165}$ expression by GFP-labeled donor pericytes within the infarct area at 2 weeks post-infarction (a) merge (b) hVEGF$_{165}$ in red (c) anti-GFP in green (scale bar=50μm).

Figure 7. Transplanted pericytes home to perivascular locations

(A) Pericytes were transduced with GFP reporter at nearly 95% efficiency. Fluorescence ([A], main) and bright-field ([A], inset) images were taken from the same low-power field (scale bars=200μm). (B) Engraftment of GFP-labeled pericytes within host myocardium was revealed by anti-GFP immunostaining at 1 week post-injection (scale bar=500μm, infarct site encircled by dotted lines). (C) Pericytes were lining with ([C], main) or surrounding ([C], inset) host CD31-positive microvasculature (scale bars=20μm). (D) The engraftment efficiency of pericytes at 1 week (9.1±1.3%) and 8 weeks (3.4±0.5%) post-infarction was depicted (dash-dot line). The perivascular homing ratio instead increased from 28.6% to 40.1% and was delineated separately (solid line). Some GFP-positive pericytes juxtaposing host ECs (E) expressed human-specific EphB2 (green/white arrows) or (F) formed connexin43-positive gap junctions with ECs (red arrow heads) (scale bars=10μm).
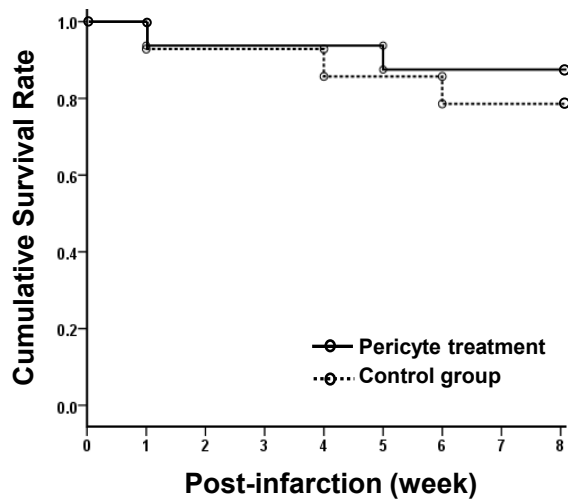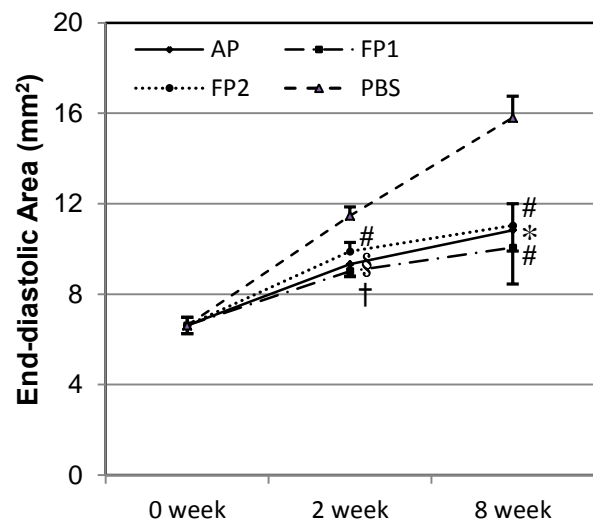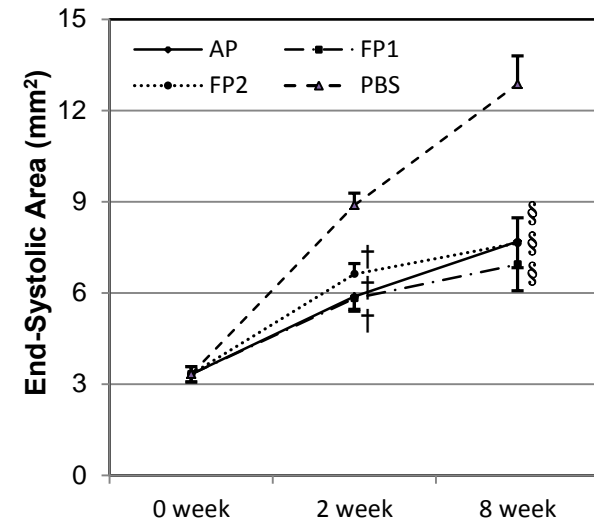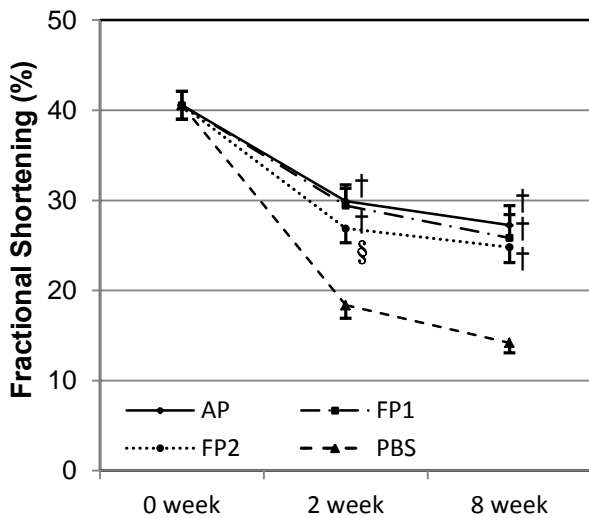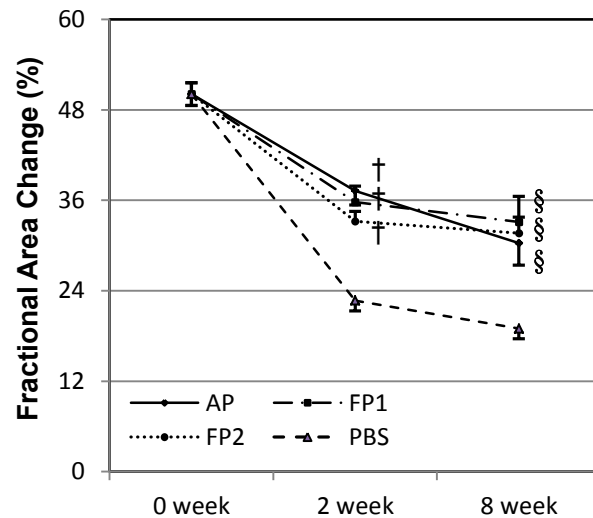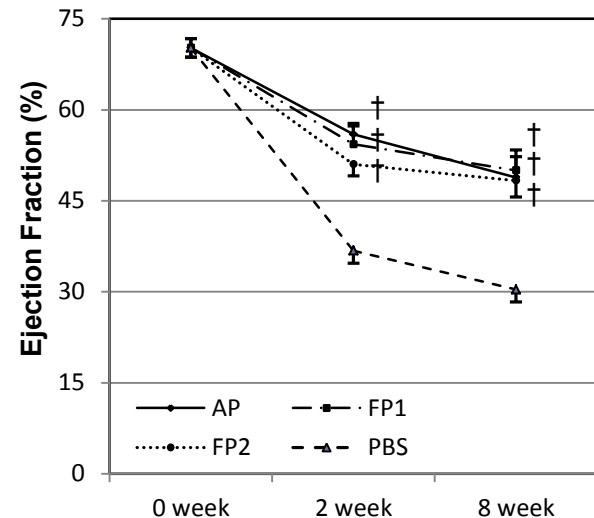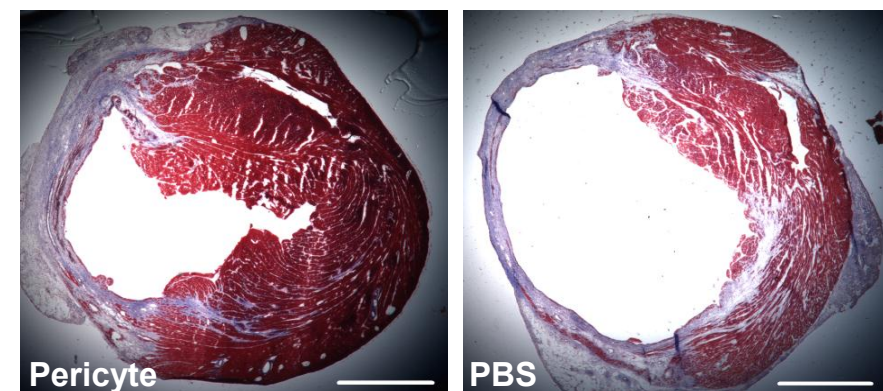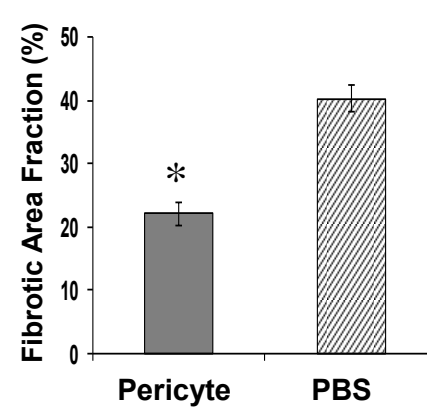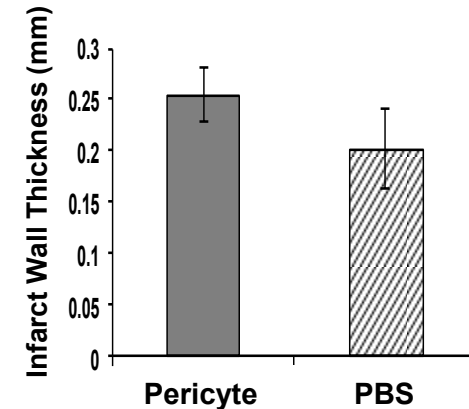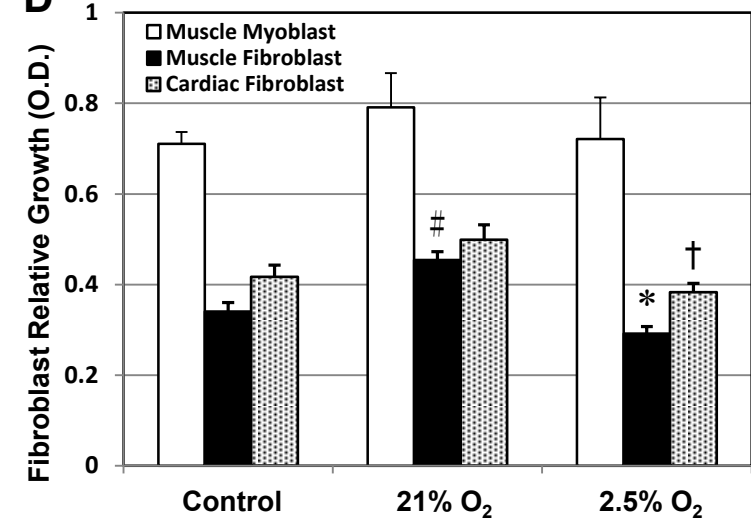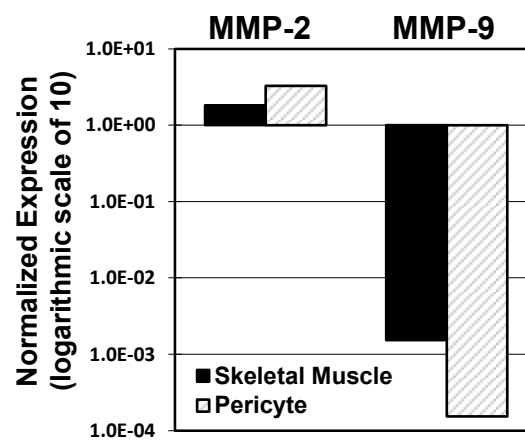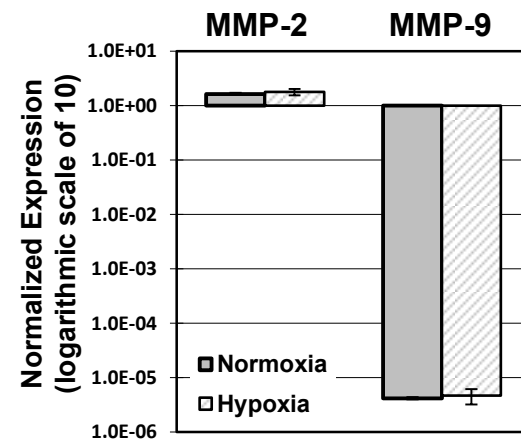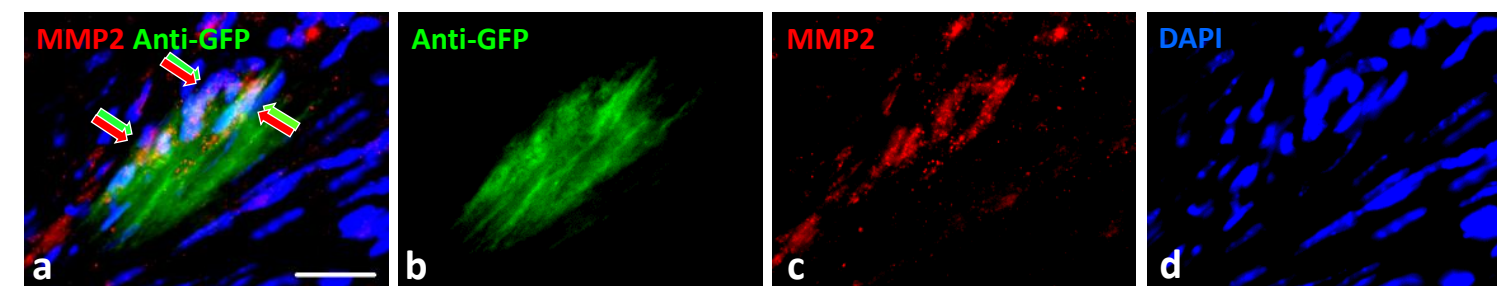
Figure 1
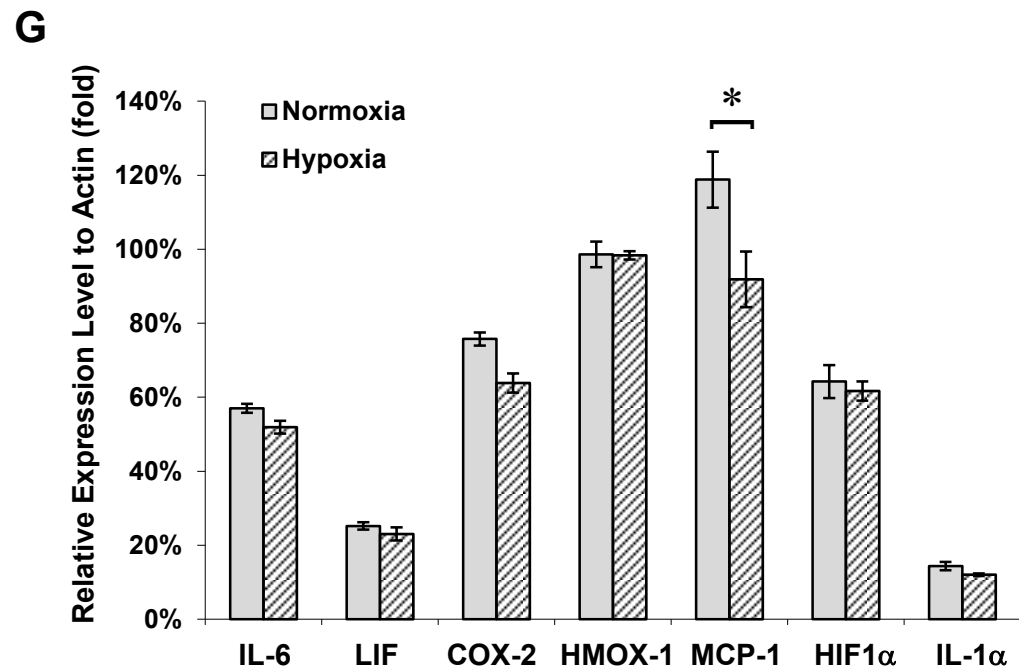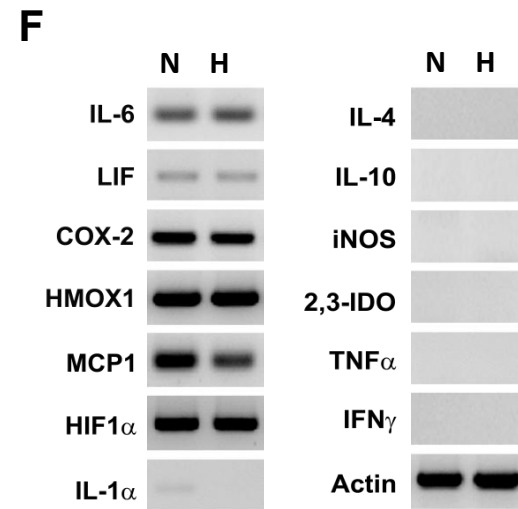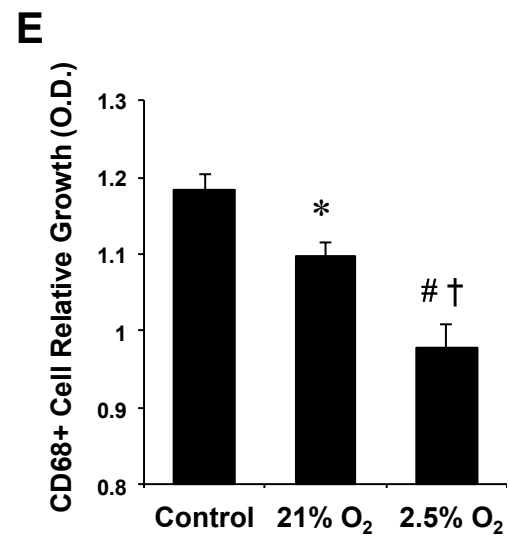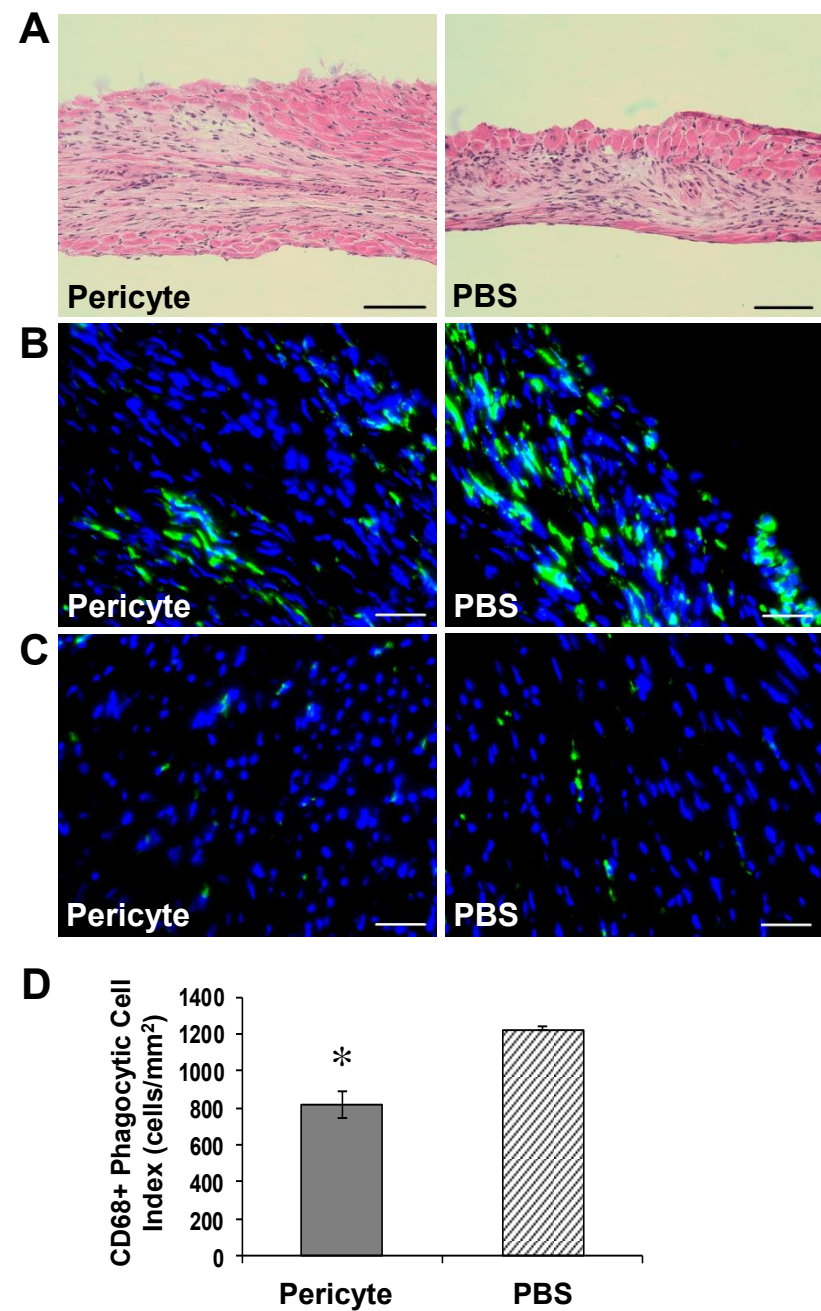
Figure 2

Figure 3

Figure 4

A Peri-infarct Area
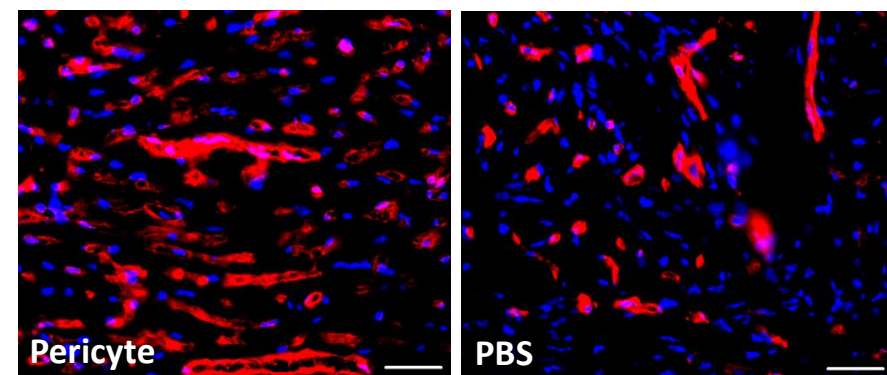
B Infarct Region
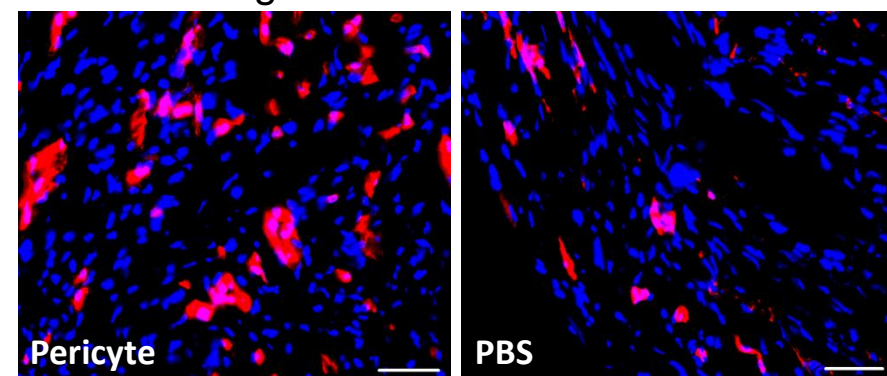
C
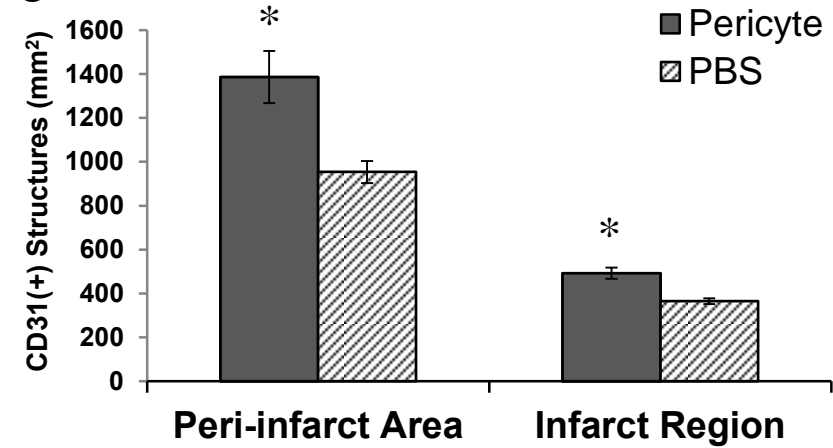
Figure 5

Figure 6

Figure 7

A — GFP

B — Anti-GFP

C — Anti-GFP mCD31

Inset: Anti-GFP CD31

D — Engraftment Ratio / Perivascular Homing Ratio; 50%, 40%, 30%, 20%, 10%, 0%; 1 week, 8 week

E — Anti-GFP mCD31 hEphB2

F — Anti-GFP Connexin43 mCD31
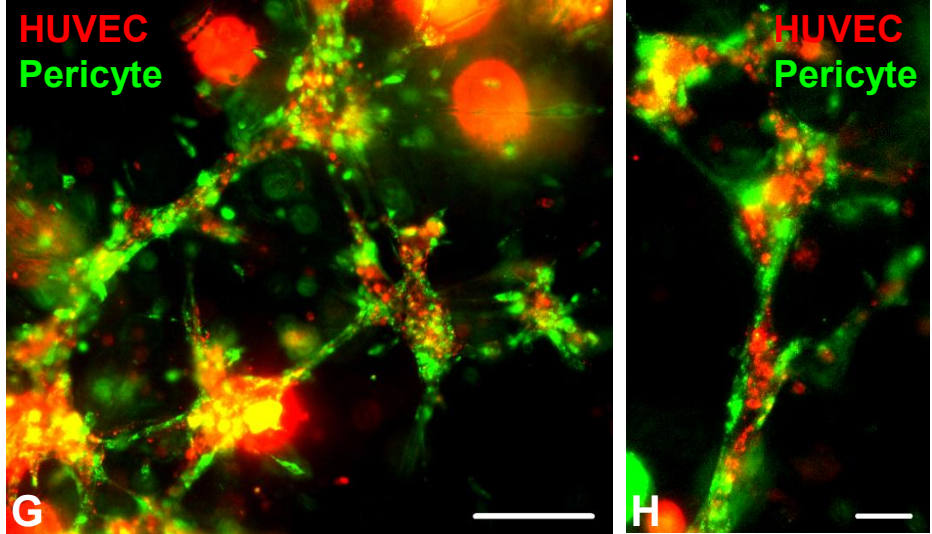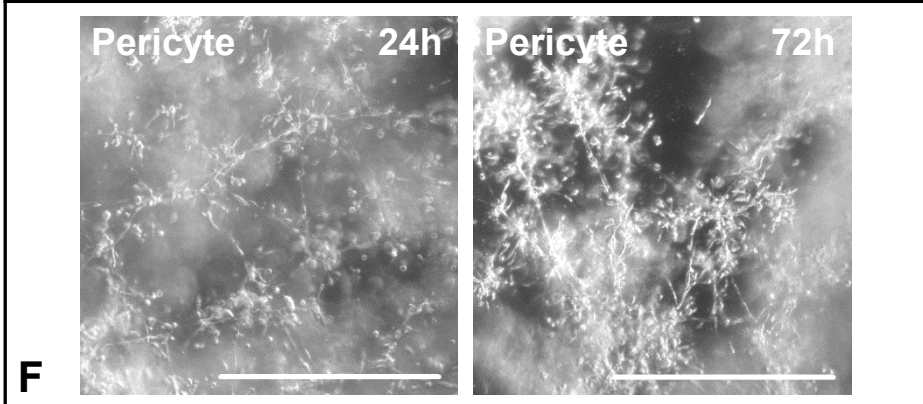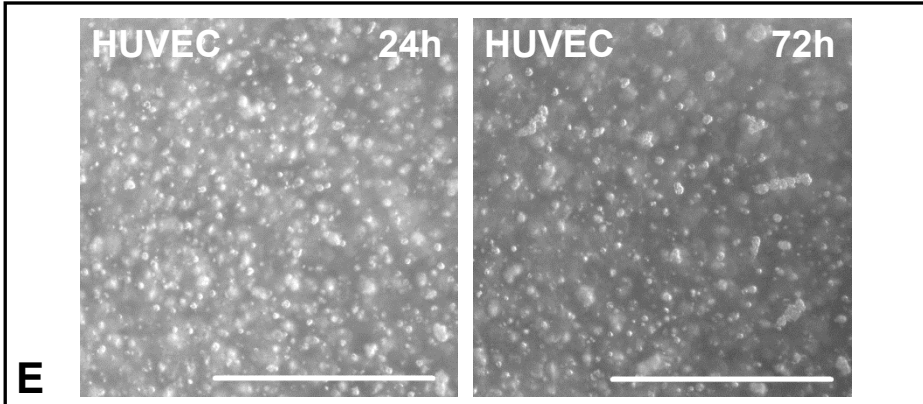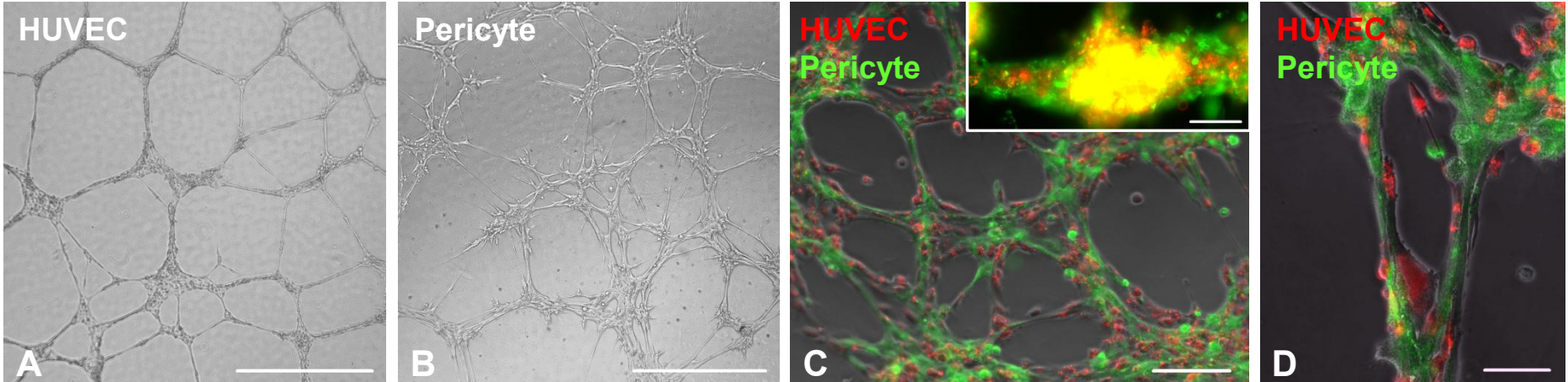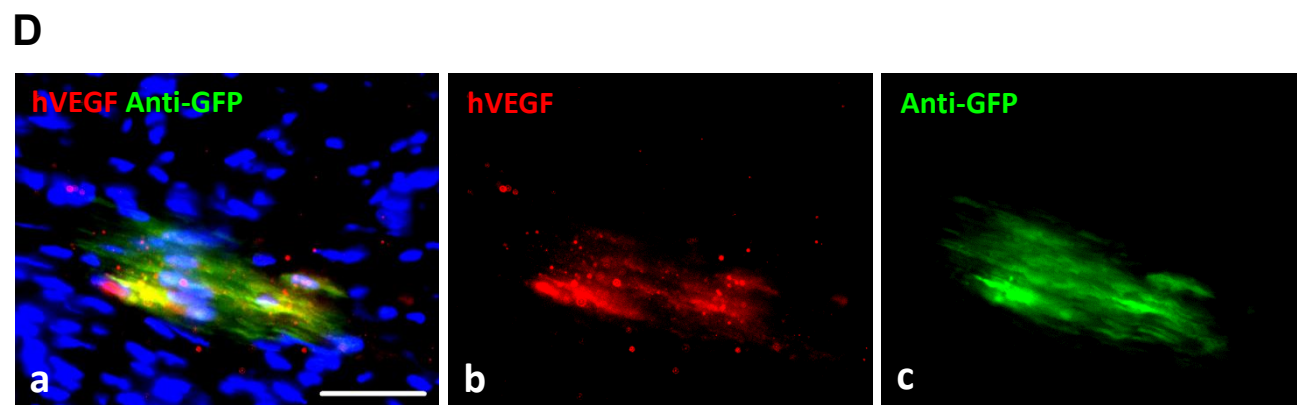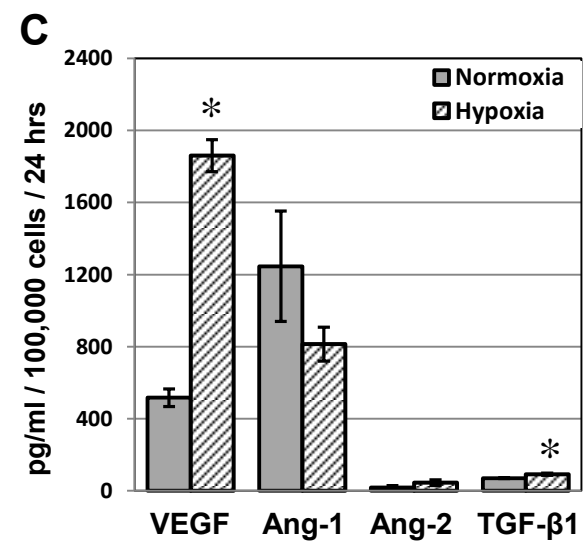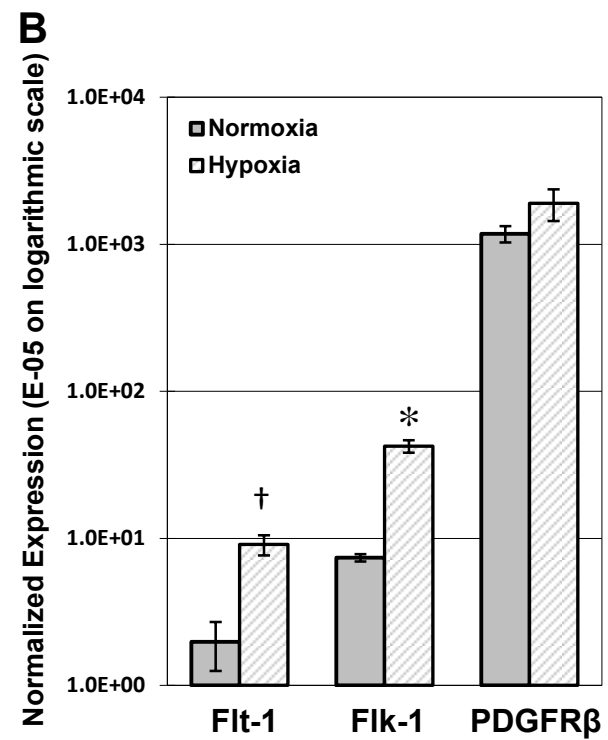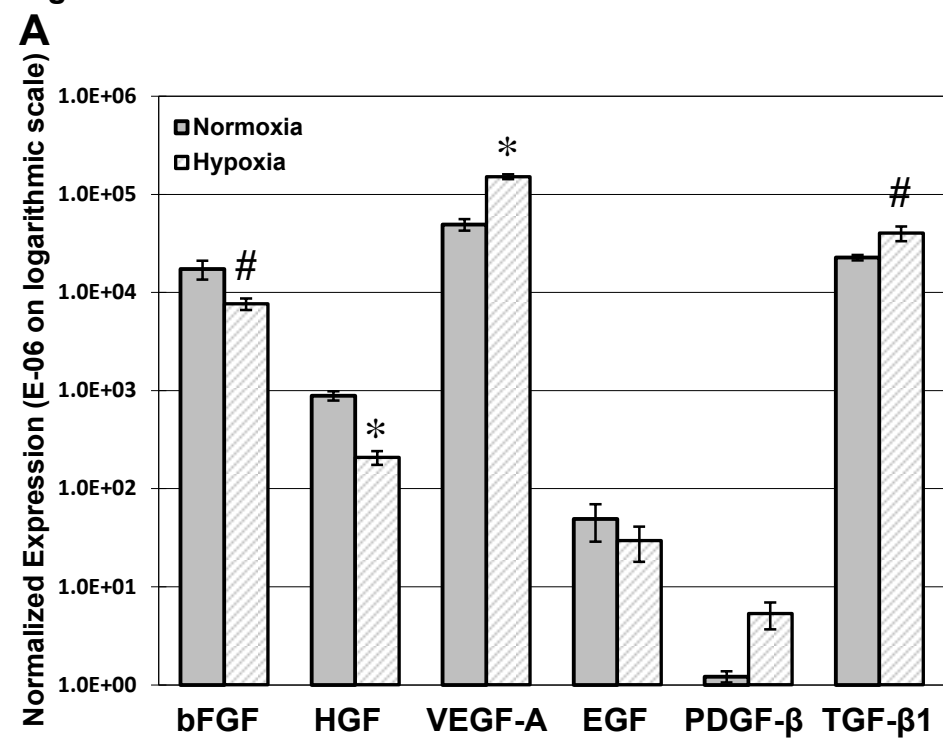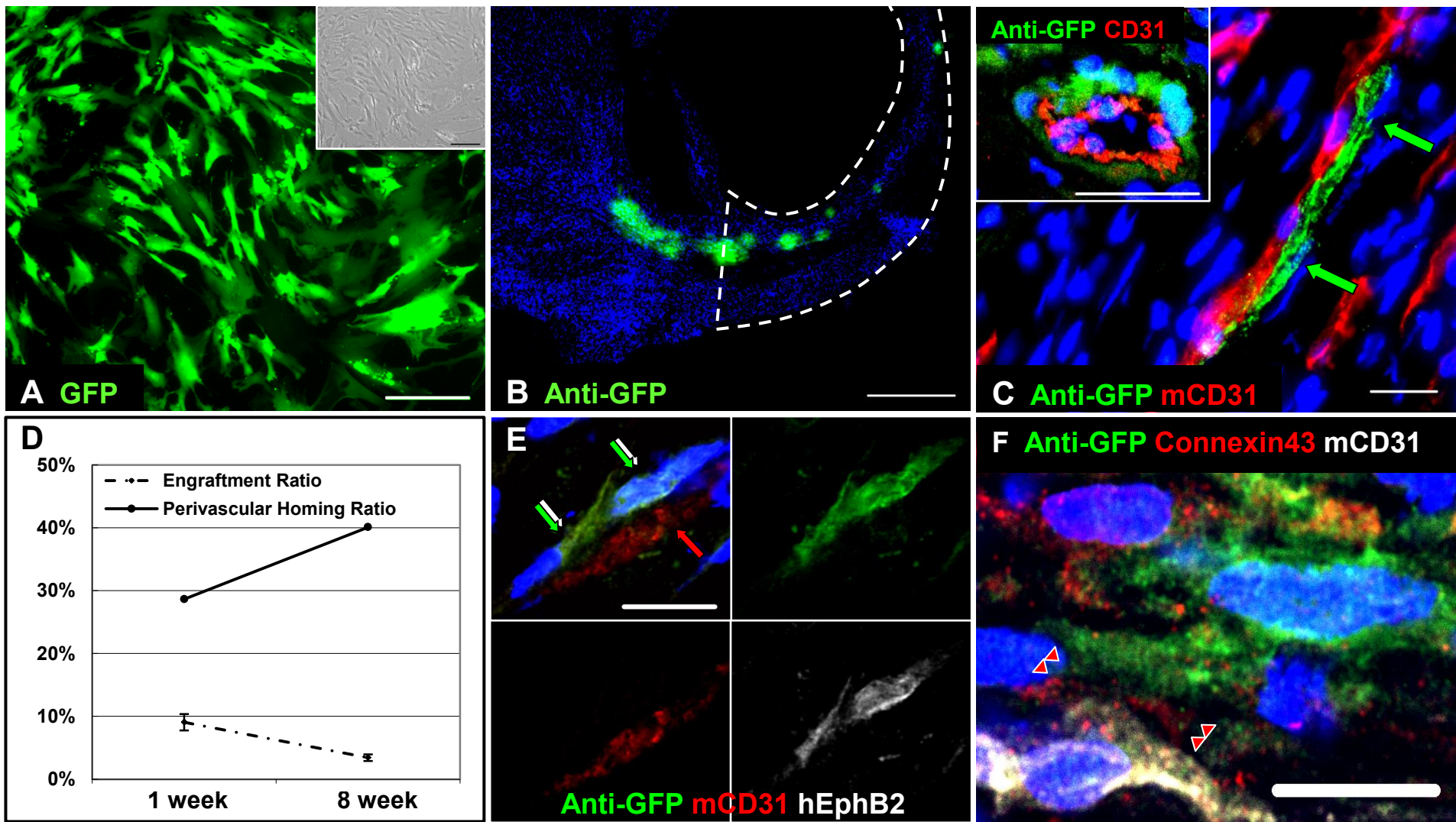
SUPPLEMENTAL MATERIAL

MATERIAL AND METHODS

Cell Isolation

Fresh muscle biopsies were mechanically minced and digested with a mixture of collagenases I, II and IV (all at 1 mg/mL, Sigma-Aldrich) at 37°C for 1 hour, according to a previously reported protocol.[1-3] Cells pellets were washed, resuspended in erythrocyte lysis buffer (155 mM NH_4Cl, 10mM $KHCO_3$, 0,1mM EDTA), and incubated for 10 min at room temperature (RT). Cells were then washed and sequentially filtered through 100- and 70-μm cell strainers (Becton-Dickinson Falcon) to obtain single cell suspension.

Fluorescence-activated Cell Sorting (FACS) and Flow Cytometry Analysis

Microvascular pericytes present in the adult and fetal skeletal muscles were purified by FACS following our published protocol.[1-3] Cells ($5-10 \times 10^6$) were incubated with one or all of the following directly conjugated mouse anti-human antibodies (all with 1:100 dilutions): anti-CD34-PE (DAKO), anti-CD45-APC-Cy7 (Santa Cruz), anti-CD56-PE-Cy7 and anti-CD146-FITC (both from AbD Serotec) at 4°C for 20 min in the dark. As negative controls, isotype-matched mouse IgGs conjugated to PE (Chemicon), APC-Cy7 (Becton-Dickinson), PECy7 and FITC (Chemicon), were used. After washing, all labelled cells were incubated with 7-amino-actinomycin D (7-AAD) (Becton-Dickinson, 1:100) for dead cell exclusion and subsequently sorted on a FACSAria flow cytometer (Becton-Dickinson).

For quality control, flow cytometry was employed to examine the expression of cell lineage markers. As we previously reported,[7] cultured pericytes at different passages were trypsinized and labelled with the following directly conjugated antibodies (all with 1:100 dilutions): anti-CD34-PE (Becton-Dickinson), anti-CD44-PE (Becton-Dickinson), anti-CD45-PE-Cy7 (Beckman Coulter), anti-CD56-PE (Chemicon), anti-CD73-PE (Zymed/Invitrogen), anti-CD90-APC (Becton-Dickinson), anti-CD105-PE (ImmunoTools) and anti-CD146-FITC (AbD Serotec) for 20 min at 4°C in the dark and subsequently analyzed on a FACSAria flow cytometer. For analysis of alkaline phosphatase (ALP) expression, cells were incubated with anti-human ALP (Biogenesis, 1:30) and then with donkey anti-sheep Ig-FITC (AbD Serotec), each for 20 min at 4°C.

Cell Culture and Cell Labeling

Sorted human microvascular pericytes were expanded and maintained in DMEM high glucose (Gibco, Invitrogen) supplemented with 20% FBS and 1% PS as we have previously described.[2,3] Cell morphology, proliferation, and surface marker expression were monitored in long-term culture to ensure the quality of cells, using formerly published methods and criteria.[2,3] Single donor-derived human umbilical cord vein endothelial cells (HUVECs) were purchased from Lonza and cultured in endothelial cell growth medium 2 (EGM-2, Lonza), following the manufacturer's instructions.

For gene transfer of green fluorescence protein (GFP), cultured pericytes at passages 7-10 were detached with 0.25% trypsin-EDTA (Gibco) and seeded at a density of 10,000 cells per cm^2. After 24-48 hours, when the culture reached 60-70% confluence, the medium was replaced with transduction medium (α-MEM, 10% FBS, 1% P/S, and 8 μg/mL polybrene), and a lentivirus-based CMV-driven eGFP expression vector was added at a MOI of 10 as previously described.[2] Following incubation for 16-18 hours at 37ºC, the transduction medium was removed and replenished by complete culture medium. Three days later, nearly 100% of cells expressed GFP. GFP-labeled cells were further expanded for 1-2 passages without significant adverse effect. For short-term *in vitro* experiments, cells were labelled with cell membrane dye, PKH26 (red) or PKH67 (green) (both from Sigma-Aldrich), following the manufacturer's instructions. Dye-labeled cells were used for experiments immediately after labelling without further expansion.

Intramyocardial Cell Transplantation in Acute Myocardial Infarction (AMI) Model

The Institutional Animal Care and Use Committee at Children's Hospital of Pittsburgh of UPMC and University of Pittsburgh approved the animal usage and surgical procedures performed in this study (Protocol 37-04, 55-07, and 0901681A-5). A Total of 78 male NOD/SCID mice (Jackson Laboratory, Bar harbor, ME, USA) were used for this study.

After the induction of anesthesia, mice were intubated and inhalationally anesthetized with 2% isoflurane gas throughout the surgery. Myocardial infarction (MI) and cell injection have been performed as we previously reported.[4-6] In brief, MI was induced by ligation of the left anterior descending coronary artery (LAD). Five minutes after the induction of infarction, $3x10^5$ cells in 30μl of PBS were injected at three sites of the ischemic myocardium (center and two borders of the infarct). Control mice received injections of 30μl PBS following MI. The investigator creating the infarction injury and performing the injection was blinded to the content of the injectant.

Echocardiography

Echocardiographic studies were performed by a blinded investigator repeatedly before surgery and at 2 and 8 weeks post-surgery to assess the cardiac function as described previously.[4-6] Concisely, mice were anesthetized with 2% isoflurane gas and immobilized on a heated stage equipped with electrocardiography. Murine heart rate and respiratory rate were continuously monitored while the body temperature was maintained at 37°C. Echocardiographic parameters were measured using a high resolution echocardiography system (Vevo 770, Visual Sonics). End-systolic dimension (ESD) and end-diastolic dimensions (EDD) were determined from the short axis images of the LV and measured from at least six consecutive beats using the M-mode tracing. End-systolic area (ESA) and end-diastolic area (EDA) were measured from short-axis images of the LV. Functional parameters, including LV fractional shortening (LVFS), LV fractional Area Change (LVFAC), and LV ejection fraction (LVEF), were determined as previously described.[7-9] Mice died or sacrificed for histological analysis prior to 8 weeks post-injection were not included in the echocardiographic study.

Histological and Immunohistochemical Analyses

Animals were sacrificed at 1, 2, and 8 weeks post-surgery. Hearts were arrested in diastole by intraventricular injection of 1M potassium chloride (KCl) and processed as formerly described.[4-6] Harvested hearts were flash frozen in 2-methylbutane (Sigma) pre-cooled in liquid nitrogen and serially cryosectioned at 6-8 μm thickness from apex to the ligation level (approximately 0.5 mm in length). Each series contains 21-24 heart sections, which are roughly 200 um apart originally and collected on one glass slide. Sections were fixed in a pre-cooled (-20°C) mixture of methanol and acetone (1:1) for 5 min or in 4% paraformaldehyde for 8 min prior to staining. Hematoxylin and eosin (H&E) staining was performed following the standard protocol. Non-specific antibody binding was blocked with 5% donkey or goat serum for 1 hour at room temperature (RT) and, if necessary, with the Mouse-on-Mouse (M.O.M.) antibody staining kit (Vector).

For homing and cell fate tracing, anti-GFP immunofluorescent staining was employed to detect GFP signals. Briefly, after fixation in paraformaldehyde and blocking, sections were permeablized with 0.1% Triton in PBS and incubated at 37°C for 1 hour with rabbit anti-GFP antibody (Abcam, 1:1000) or at 4°C overnight with goat anti-GFP antibody (Abcam, 1:200), followed by incubation with donkey anti-rabbit-Cy3 IgG (Jackson Immunoresearch, 1:250) or donkey anti-rabbit-Alexa™488 IgG (Molecular Probes, 1:250) for 1 hour at RT. To examine homing of donor cells, sections were

then incubated overnight at 4°C with rat anti-mouse CD31 antibody (Becton-Dickinson Biosciences, 1:100), followed by goat anti-rat-Alexa™488 IgG (Molecular Probes, 1:400) or donkey anti-rat-Alexa™555 IgG (Molecular Probes, 1:400). To examine expression of cardiomyocyte, smooth muscle cell, pericyte, and endothelial cell markers as well as Ki-67, MMP-2, connexin43, and human $VEGF_{165}$, sections were first stained for GFP and then incubated overnight at 4°C with goat anti-cardiac troponin I (Abcam, 1:200), mouse anti-human SM-MHC (DAKO, 1:50), goat anti-NG2 (chondroitin sulphate, Santa Cruz, 1:50), sheep anti-human CD31 (R&D systems, 1:50), mouse anti-human EphB2 (Abgent, 1:200), rabbit anti-Ki-67 (Abcam, 1:200), goat anti-MMP2 (R&D systems, 1:50), rabbit anti-connexin43 (Millipore, 1:200), or goat anti-human $VEGF_{165}$ (R&D systems, 1:50) primary antibody, followed respectively by donkey anti-goat Alexa™555 IgG, donkey anti-mouse Alexa™555 IgG, and rabbit anti-sheep Alexa™555 IgG (Molecular Probes, all 1:400). For evaluation of chronic inflammation, sections were incubated overnight at 4°C with rat anti-mouse CD68 primary antibody (Abcam, 1:200), followed by goat anti-rat-Alexa™488 IgG. Nuclei were stained with 4',6-diamidino-2-phenylindole (DAPI) (Molecular Probes, 1:1000) at RT for 5 min

Measurement of Cardiac Fibrosis and Infarct Wall Thickness

Masson's trichrome staining kit (San Marcos) was used to reveal collagen deposition on heart sections, following the manufacturer's instructions. The area of the collagen deposition, representing cardiac fibrosis, and the area of the entire cardiac tissue (excluding the void space in the chamber cavity) were measured using a digital image analyzer (Image J). Fibrotic area fraction was estimated as the ratio of fibrotic tissue to the entire cross-sectional area of cardiac tissue and averaged from 6 randomly selected sections at comparable infarct levels per heart. Left ventricular wall thickness at the center of the infarct was estimated as the mean of 3 adjacent measurements (0.25mm apart) and was averaged from 6 randomly selected sections at comparable infarct levels per heart.

Measurement of Cellular Apoptosis

To detect apoptotic cells, terminal dUPT nick end-labeling (TUNEL) staining was carried out according to the manufacturer's protocol (ApopTag Plus Peroxidase In Situ Apoptosis Detection Kit; Chemicon, Temecula, California) and counter-stained with hematoxylin. Apoptotic cell number was estimated from 3-5 randomly selected low power fields of the infarct area at comparable infarct levels per heart, using image J. The results were normalized to cardiac tissue area.

Quantification of Host Angiogenesis and Chronic Inflammation

To quantify host angiogenesis in the heart, immunohistochemistry using anti-mouse endothelial cell marker, CD31, was performed on cryosections. The capillary density, represented by the number of CD31-positive capillary structures per mm^2, was subsequently computed from 6 randomly selected images of the peri-infarct area or infarct region of each heart at the mid-infarct level, using Image J, as described previously.[4-6] To evaluate chronic inflammation within the infarct region, we performed immunofluorescent staining of anti-mouse CD68 on cryosections and subsequently computed the infiltration index, represented by the number of CD68-positive host cells per mm^2, from 8-10 randomly selected images of the entire infarct region of each heart at the mid-infarct level, using Image J.

Quantification of Donor Cell Engraftment and Perivascular Homing

To estimate the number of donor cells engrafted in the infarcted heart, quantification was performed on anti-GFP immunostained serial cryosections, using Image J. The number of GFP-positive cells (nuclei identified by DAPI) present in each heart cryosection was computed. The total number of GFP-positive cells within each heart was extrapolated as the sum of the number of GFP-positive cells in all serial sections (21-24 sections) times the number of section series, corrected by a section-collection-loss coefficient of 20%. The engraftment ratio was defined as the extrapolated total number of engrafted GFP-positive cells to the initial injection of $3x10^5$ cells. To estimate the number of donor cells that exhibited perivascular homing, quantification was performed on anti-GFP and anti-mouse endothelial cell marker, CD31, dual-immunostained serial cryosections, using Image J. Perivascular homing was defined as GFP-positive cells juxtapose CD31-positive mouse endothelial cells. The number of perivascular homing GFP-positive cells in each heart cryosection was computed. The total number of perivascular homing GFP-positive cells within each heart was extrapolated using the same formula described above. The perivascular homing ratio was defined as the extrapolated number of perivascular homing GFP-positive cells to the extrapolated total number of engrafted cells.

Hypoxia Assay

To assess the influence of the hypoxic microenvironment in human pericytes, we cultured cells under 2.5% O_2 hypoxic conditions (with 5% CO_2 and 92.5% N_2) *in vitro* as formerly described.[4,5] Concisely, pericytes were seeded in 6-well culture plates at 10,000 cells/cm^2 and allowed the cells to reach 80-90% confluence under normoxia. Upon the transition to low O_2 conditions, the complete culture medium was

removed and cells were washed twice with PBS before defined, serum-free DMEM medium was added. Twenty-four hours later, cells were trypsinized and counted. The culture supernatant and cell pellets were collected for analysis. Cells cultured under normoxia with the serum-free medium served as controls.

Semi-quantitative RT-PCR and Real-time Quantitative PCR (real-time qPCR)

For semi-quantitative RT-PCR (sqRT-PCR), cells were lysed with RLT-plus lysis buffer supplemented with beta-mecaptoethanol. Total RNA (N=3) were extracted with the Qiagen RNeasy plus-mini-kits. RNA concentration was measured using TECAN plate reader system with the NanoQuant measurement program. From each sample, 500ng of total RNA were reverse transcribed with SuperScript^{TM} III cDNA synthesis kits (Invitrogen) in 20 µl reactions. PCR was performed in 25 µl reaction with Promega Gotaq system and reacted in Vapo.Protect PCR machine (Eppendorf) using the following program: 3 minutes for the initial denature, 32 cycles at (94°C for 30 seconds, 55°C for 30 seconds, 72°C for 45 seconds) and final extension for 6 minutes. PCR products were verified by 1% agarose gel electrophoresis. Images were captured using the GelDoc system with Quantify One 4.6.2 software. The intensities of the target gene bands were quantified using the same software, and normalized to those of the house keeping gene β-actin.

For real-time qPCR, total RNA (N=6) was extracted from $1x10^5$ cells using the Nucleospin RNA kit (Clontech). cDNA was synthesized with SuperScript^{TM} II reverse transcriptase (Invitrogen), according to the manufacturer's instructions. cDNA and primers were added to SYBR Green PCR master mix (Applied Biosystems) according to the manufacturer's instructions. The quantitative analyses were carried out in triplicate on an ABI Prism 7900HT sequence detection system in the core facility of the Genomics and Proteomics Core Laboratories of the University of Pittsburgh. All data were normalized to human cyclophilin, which was used as an internal control. Gene expression levels were analyzed using SDS 2.2 Software (ABI) and calculated based on the comparative ΔC_T method (separate tubes). Data are presented as normalized expression level (in arbitrary units). Sequences of target gene primers/probes (IDT-Integrated DNA Technologies) used in real-time qPCR and sqRT-PCR are listed below in Supplemental Table T1 and T2 respectively.

Supplemental Table T1. Primer sequences for real-time qPCR

Gene	Forward	Reverse
bFGF NM002006	ccgttacctggctatgaagg	tttccttgaccggtaagtattg
HGF NM000601	atatgtgctggggctgaaaa	cacgaccaggaacaatgaca
VEGF-A NM001025368	gcgaggcagcttgagttaaa	ctttcctggtgagagatctgg
EGF NM001963	ggtactctcgcaggaaatgg	tccaccaccaattgctcata
PDGF-β CU013138	tcccgaggagctttatgaga	gggtcatgttcaggtccaac
TGF-β1 NM000660	cgactactacgccaaggaggt	cggagctctgatgtgttgaa
Flt-1 NM002019	cttcacctggactgacagca	acagctggaatggcagaaac
Flk-1 NM002253	tgctcaagacaggaagacca	cttcgatgctttccccaata
PDGFRβ NM002609	catcagcagcaaggacaccat	gaccttggtgtctagagagtcc
IGF-1 X57025	gctggtggatgctcttcagt	aagcagcactcatccacgat
MMP-2 NM004530	gctcccggaaaagattgatgc	acctagatgagtcggtcgtg
MMP-9 BC006093	ttccctggagacctgagaac	ctacgcacctctcagcttta
Cyclophilin	catctgcactgccaagactga	gcaaagtgaaagaaggcatgaa

Supplemental Table T2. Primer sequences for Semi-quantitative RT-PCR

Gene	Forward	Reverse
IL-6 NM000600.3	ccacaagcgccttcggtcca	gtggctgtctgtgtgggggcg
LIF M63420.1	acgccaacggcacggagaag	tacccgaggtgtcagggccg
COX-2 NC000001.10	gcgagggccagctttcacca	cctgccccacagcaaaccgt
HMOX1 NM002133.2	cgtccgcaacccgacagcat	cagccttgcggtgcagctct
MCP-1 NM002982.3	agctcgcactctcgcctcca	gcatctggctgagcgagccc
IL10 NM000572.2	gctgcacccacttcccaggc	gacagcgccgtagcctcagc
iNOS NM000625.4	acccgagatggccagggtcc	ccgcactcccttgtgctggg
IL-1α NM000575.3	aatgacgccctcaatcaaag	tgggtatctcaggcatctcc
IL-4 BC067514.1	gccaccatgagaaggacact	actctggttggcttccttca
IFNγ BC070256	tgaccagagcatccaaaaga	ctcttcgacctcgaaacagc
2,3-IDO NM194294	ctggtcctgagcttcctcac	cagcaccaagtctgagtgga
HIF1α NM001530	tccatgtgaccatgaggaaa	ccaagcaggtcataggtggt
TNFα HQ201306	agcccatgttgtagcaaacc	tgaggtacaggccctctgat
Actin NM001101.3	agcgggaaatcgtgcgtg	cagggtacatggtggtgcc

In vitro Vascular Network Formation

To demonstrate the vascular cell characteristics and the supportive function of cultured pericytes, we performed cell culture and co-culture experiments using 2D and 3D Matrigel systems and observed capillary-like network formation. In brief, 350μl of Matrigel (Becton-Dickinson) was placed in each well of a 24-well plate and incubated at 37°C for 30 min. Fifty thousand pericytes were resuspended in 700μl of EGM2 and seeded onto the Matrigel-coated well. Experiments using 5×10^4 HUVECs were performed as controls. A 2D co-culture system using cells pre-labeled with cell membrane dye (PKH fluorescent dye, Sigma-Aldrich) was developed to observe pericyte-HUVEC interactions. Briefly, 5×10^4 PKH26-labeled HUVECs (red) and 5×10^4 PKH67-labeled pericytes (green) were well mixed, resuspended in 700μl of EGM2, seeded onto Matrigel in a 24-well plate, and further cultured for 24 hours. An *in vitro* 3D Matrigel culture system was used to investigate vascular support by pericytes. In short, 25×10^4 pericytes were resuspended in EGM2 and well mixed with 350μl of Matrigel in a 3:1 ratio before being encapsulated into one well of a 24-well plate and subsequently incubated for 72 hours. A small amount of EGM2 was added after gelation and exchanged every 24-48 hours. Experiments using 25×10^4 HUVECs were performed as controls. A 3D co-culture system using 25×10^4 PKH26-labeled HUVECs (red) and 25×10^4 PKH67-labeled pericytes (green) was performed in the same manner and subsequently cultured for 72 hours. All images were taken using an epi-fluorescence microscope (Nikon Eclipse TE 2000-U).

Enzyme-linked immunosorbent assay (ELISA)

The secretion of growth factors and cytokines in culture supernatant was quantified by enzyme-linked immunosorbent assay (ELISA). Vascular endothelial growth factor (VEGF) secretion by microvascular pericytes was measured by human VEGF ELISA Kit (KHG0111, Invitrogen), following the manufacturer's instructions. The secretion of angiopoietins-1 (Ang-1), angiopoietins-2 (Ang-2), and transforming growth factor (TGF)-β1 by pericytes was measured by human Ang-1 (DANG10, R&D Systems), Ang-2 (DANG20, R&D Systems), and TGF-β1 (DB100B, R&D Systems) ELISA Kits respectively, following the manufacturer's instructions. Data are presented as pg/ml per 100,000 cells per 24 hours.


Measurement of Cell Proliferation

Murine RAW264.7 monocyte/macrophage-like cells (TIB-71, ATCC) or primary muscle and cardiac fibroblasts as well as skeletal myoblasts were quadruplicately plated (10^4 cells/well) in a 96-well plate.[10] Four hours later, the culture media were

changed to normoxic or hypoxic pericyte-culture conditioned media, or fresh serum-free media for control wells. Cells were subsequently cultured under ambient conditions for 72 hours. At this time, wells were washed and CellTiter 96® AQueous One Solution Cell Proliferation Assay (MTS) Reagent (G3582, Promega) in DMEM was added. The plate was incubated in 5% CO_2 at 37 °C for 3 hrs, at which point the absorbance at 490 nm was read with a 96-well plate reader. For each cell type/culture condition, experiments were performed in quadruplicates and repeated 3 times independently. Results were averaged. One-way ANOVA with Bonferroni post-hoc test was used for statistical analysis.

RESULTS

Supplemental Figure S1
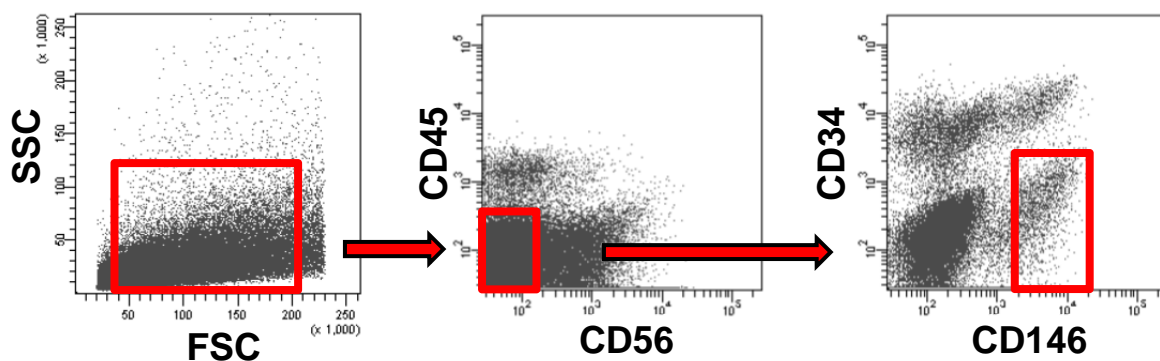
Supplemental Figure S1. Fluorescence-activated cell sorting (FACS) of human muscle pericytes. Human muscle biopsies were mechanically dissociated and digested with collagenase. After labeling, single cells suspension was subjected to FACS to purify the pericyte population based on their differential expression of cell lineage markers, including robust expression of the pericyte/endothelial cell marker CD146 and absence of the myogenic, endothelial/stem, and hematopoietic cell markers: CD56, CD34 and CD45, respectively. Skeletal muscle-derived pericytes (CD146$^+$/34$^-$/45$^-$/56$^-$) sorted to homogeny were collected and expanded *in vitro*.

Supplemental Figure S2

A

B
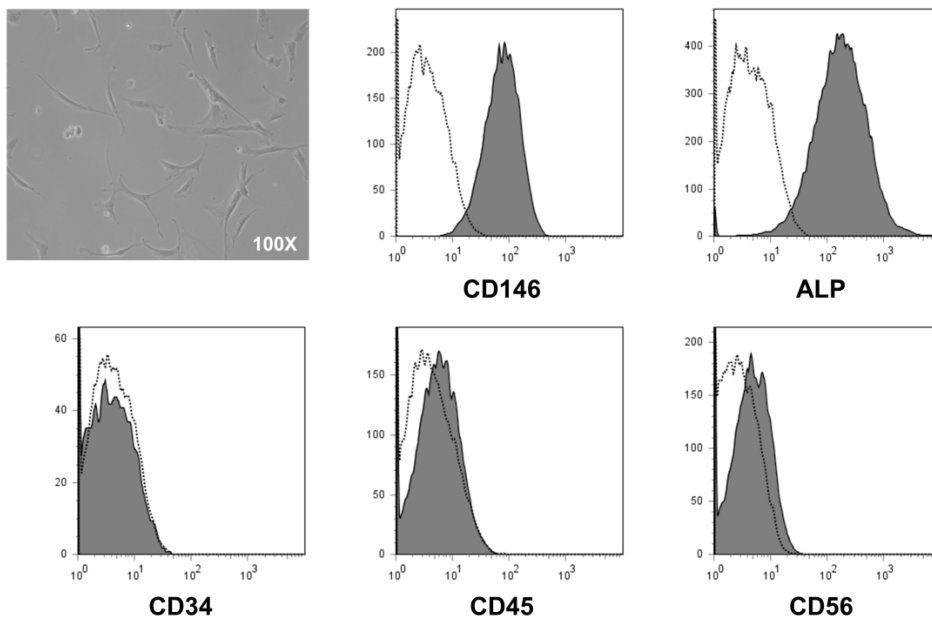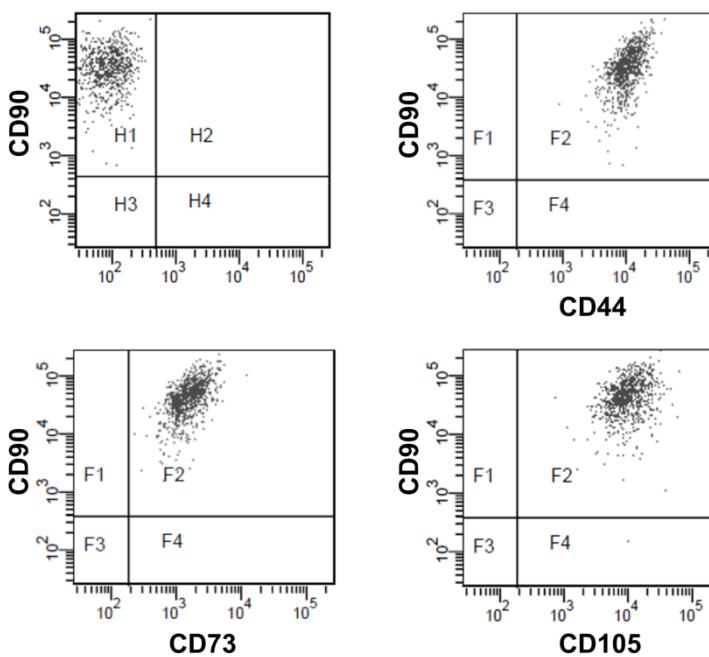
Supplemental Figure S2. (A) Morphology of purified pericytes in long-term culture. Flow cytometry analysis revealed that cultured pericytes retain original cell surface marker expression, including the robust expression of CD146 and alkaline phosphatase (ALP) with the absence of CD34, CD45, and CD56. **(B)** Flow cytometry analysis showed that long-term cultured pericytes strongly express classic MSC markers: CD90, CD44, CD73 and CD105.

Supplemental Figure S3
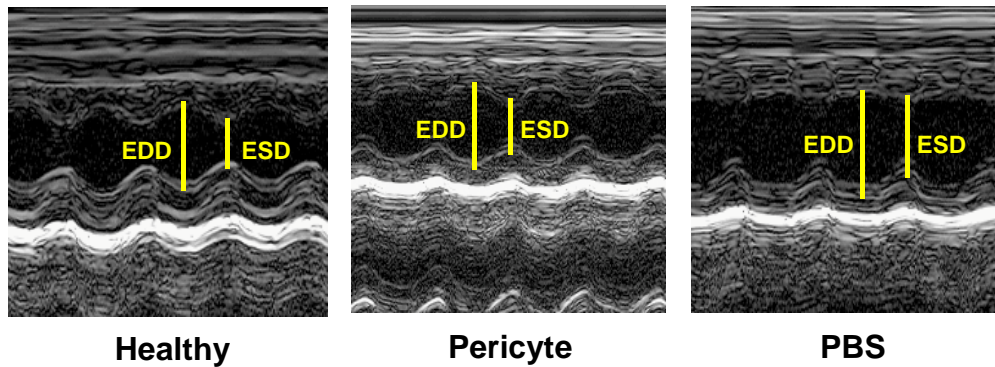
Supplemental Figure S3. Representative echocardiographic M-mode images of left ventricle (LV). End-systolic dimension (ESD) and end-diastolic dimension (EDD) were indicated.

Supplemental Table T3

Group	Healthy	Pericyte (averaged)		PBS (control)	
Time (Post-MI)	Pre-MI	2 weeks	8 weeks	2 weeks	8 weeks
LVESD (mm)	2.1±0.1	2.9±0.1	3.3±0.1	3.6±0.1	4.5±0.3
LVEDD (mm)	3.5±0.1	4.1±0.1	4.4±0.1	4.4±0.1	5.2±0.3
LVESA (mm^2)	3.3±0.3	6.1±0.2	7.4±0.5	8.5±0.4	12.4±0.8
LVEDA (mm^2)	6.6±0.4	9.4±0.2	10.6±0.6	11.0±0.4	15.1±0.9
LVFS (%)	40.6±1.5	28.7±1.0	26.0±1.1	17.8±1.2	13.9±0.9
LVFAC (%)	50.1±1.5	34.5±2.0	31.7±1.5	22.9±1.1	18.7±1.1
LVEF (%)	70.2±1.6	53.8±1.3	49.1±1.8	36.5±1.7	29.9±1.7

Supplemental Table T3. Echocardiographic parameters of pre- and post-MI NOD/SCID mouse hearts treated with or without pericytes. LV, left ventricle; ESD, end-systolic dimension; EDD, end-diastolic dimensions; ESA, end-systolic area; EDA, end-diastolic area; FS, fractional shortening; FAC, fractional area change; EF, ejection fraction.

Supplemental Figure S4

Group	CD146	CD56	Stat. Sig.
LVESD (mm)	2.6±0.2	3.7±0.2	
LVEDD (mm)	3.7±0.3	4.6±0.1	
LVESA (mm^2)	6.4±0.3	8.7±0.4	P=0.002
LVEDA (mm^2)	10.7±0.4	12.7±0.4	P=0.004
LVFS (%)	29.8±1.6	20.2±1.9	P=0.003
LVFAC (%)	40.6±1.6	31.7±1.7	P=0.003
LVEF (%)	58.4±0.8	45.4±2.4	P≤0.001
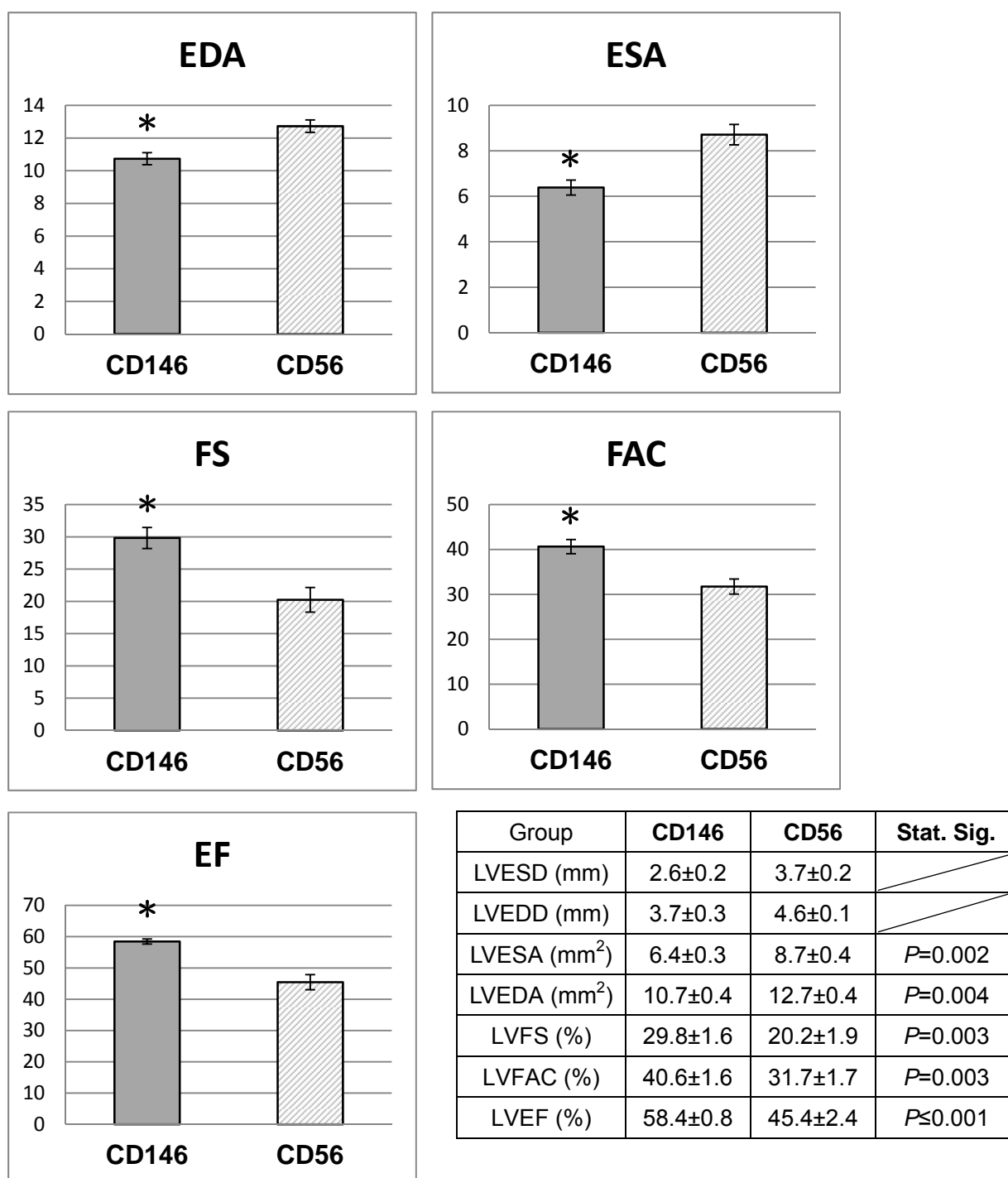
Supplemental Figure S4. Echocardiographic measurement of cardiac function in acutely infarcted hearts injected with either APs (CD146) or CD56+ myogenic progenitors (CD56) at 2 weeks post-infarction. APs and CD56+ myogenic progenitors were simultaneously sorted from a single adult muscle biopsy. Pericyte-treated hearts (N=6) exhibited significantly better LV function than CD56+ progenitor-treated ones (N=6) in multiple categories, including LVEDA (p=0.004), LVESA (p=0.002), LVFS (p=0.003), LVFAC (p=0.003), and LVEF (p≤0.001).

Supplemental Figure S5

A Infarct Region
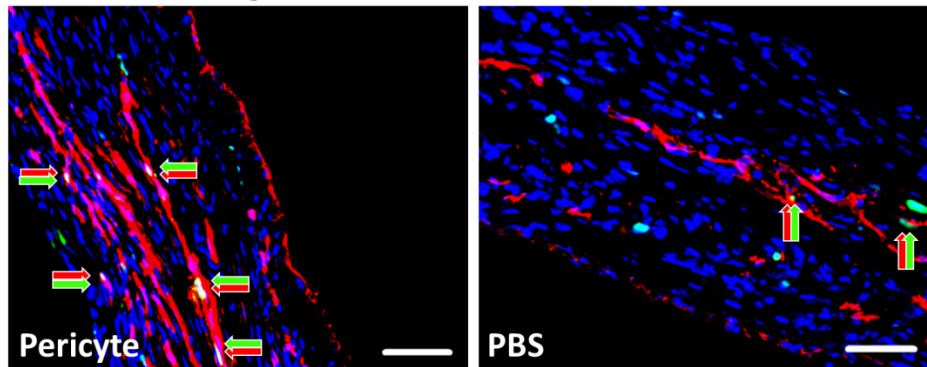
**B** Peri-infarct Area

C
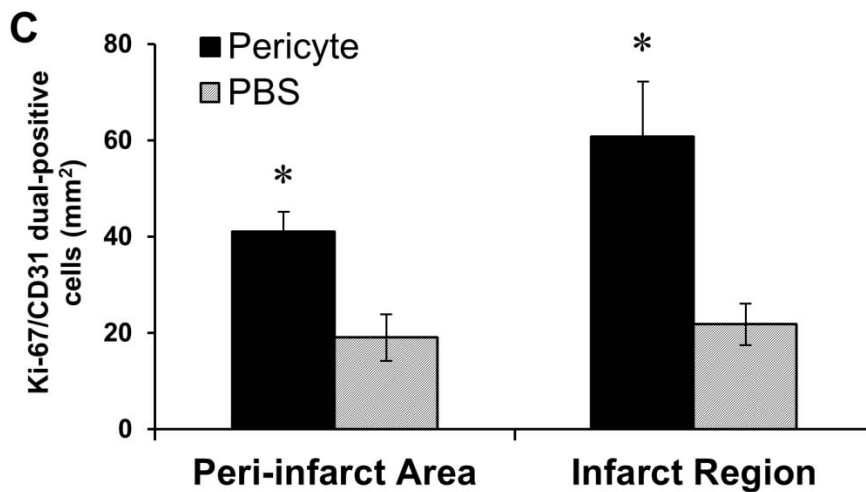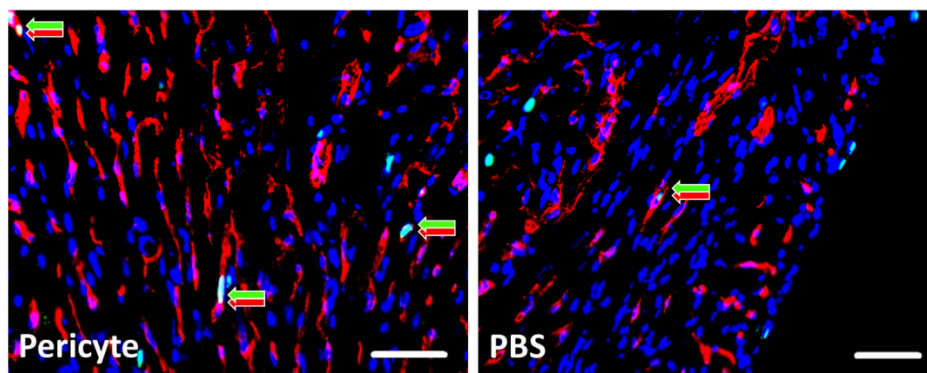
Supplemental Figure S5. Detection of host EC proliferation at 2 weeks post-infarction. Representative images of Ki-67 (green) and mouse CD31 (red) co-immunostaining **(A)** within the infarct region and **(B)** in the peri-infarct area of hearts injected with pericytes or PBS (scale bars=50μm). Proliferating host ECs were identified as Ki-67/CD31 dual-positive cells (green/red arrows). **(C)** Pericyte-treated group had a significantly larger number of proliferating ECs both within the infarct region (p=0.034) and in the peri-infarct area (p=0.025) than PBS control group (N=3 per group).

Supplemental Figure S6
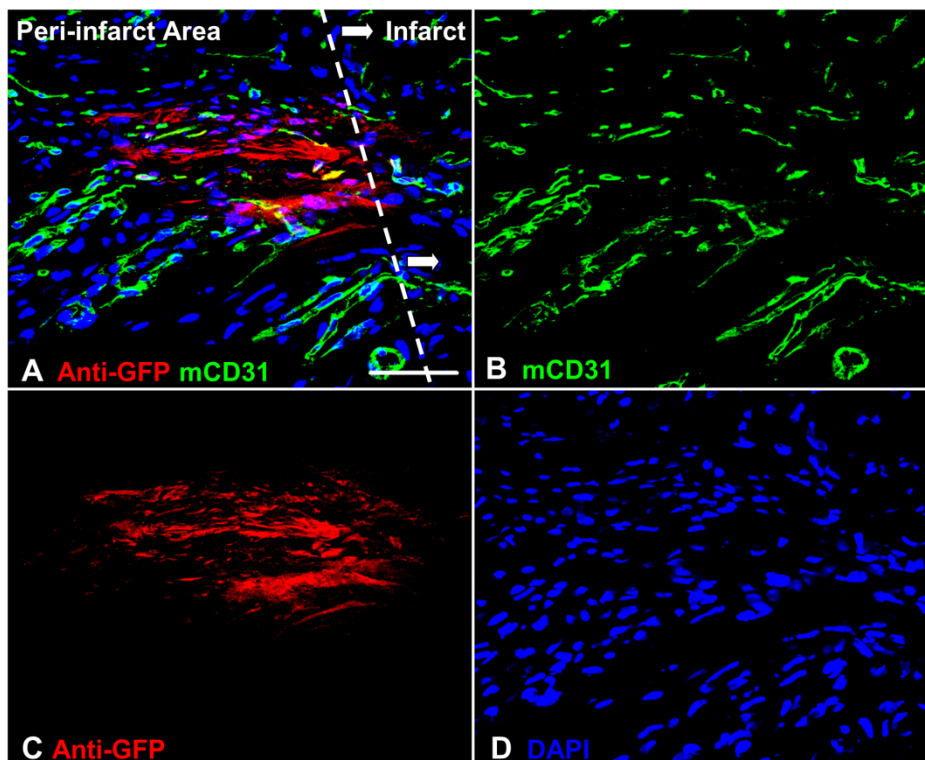
Supplemental Figure S6. (A-D) Donor pericytes (stained in red by anti-GFP) were particularly abundant in the peri-infarct area where host CD31(+) capillaries (mouse CD31 stained in green) remained largely intact (scale bar=50μm).

Supplemental Figure S7
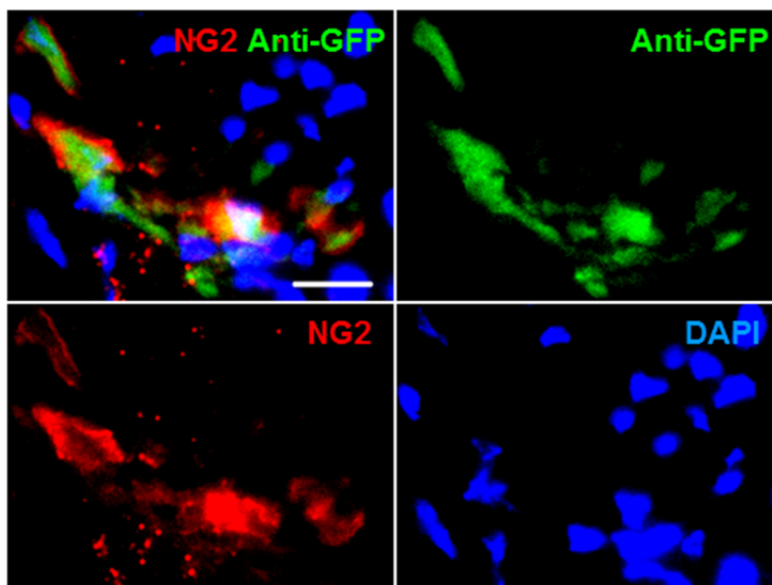
Supplemental Figure S7. Expression of the pericyte marker NG2 (chondroitin sulphate) was detected in the majority of, but not all, GFP-positive donor pericytes at 2 weeks post-infarction (scale bar=10μm).

Supplemental Figure S8
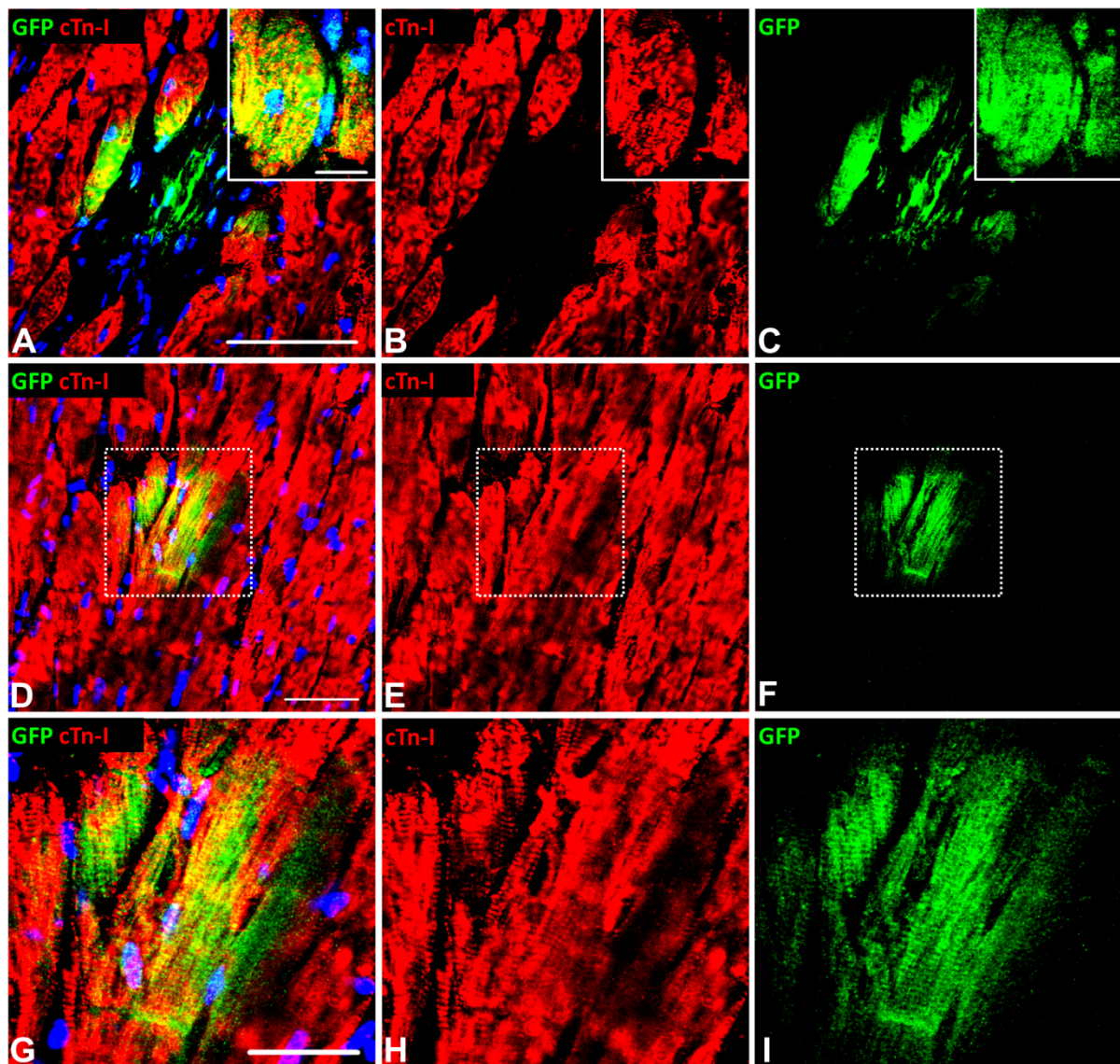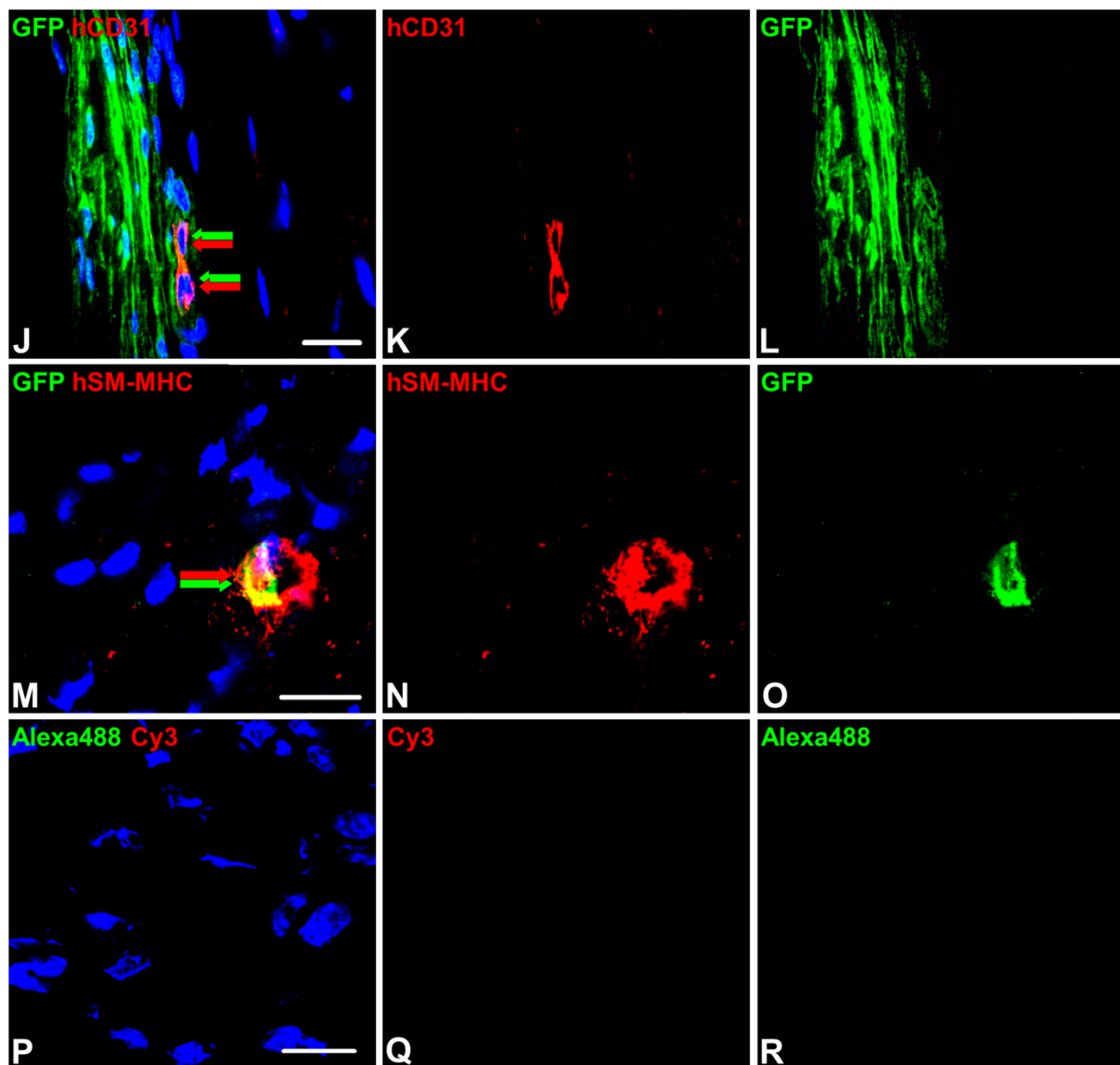
Supplemental Figure S8. Tracking cardiac cell lineage fates of donor pericytes. Confocal microscopy revealed that in the peri-infarct area **(A-C)** a minor fraction of GFP-labeled pericytes co-expressed a mature cardiomyocyte marker, cardiac troponin-I (cTn-I), while additional GFP(+) cells remained in the interstitium ([A], main, scale bar=50μm); a few of them appear single-nucleated ([A], inset, scale bar=10μm) (cTn-I in red, Anti-GFP in green). **(D-F)** Immunofluorescent detection of GFP-cTn-I dual-positive cardiomyocytes integrating within the residual myocardium (scale bar=50μm) with dotted area enlarged in **(G-I)** showing sarcomeric patterns (scale bar=20μm). **(J-L)** A very small number of GFP(+) pericytes (<1%) co-expressed human-specific CD31 (hCD31 in red, Anti-GFP in green; scale bar=10μm). **(M-O)** Few donor pericytes (<0.5%) expressed human-specific SM-MHC (hSM-MHC in red, Anti-GFP in green; scale bar=10μm). **(P-R)** Negative control images were taken from sections immunostained only with matching fluorescence-conjugated secondary antibodies (no primary antibody) (Cy3 in red, Alexa[TM]488 in green; scale bar=10μm).

Supplemental Figure S9

A

Infarct Area Total Cell Density

cells/mm^2

B

### Infarct Area Proliferating Cell Density

cells/mm^2
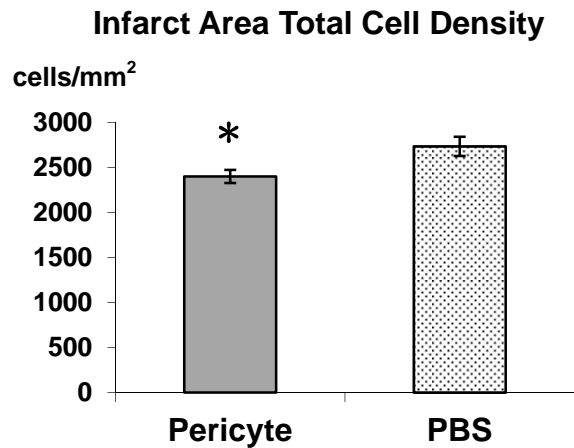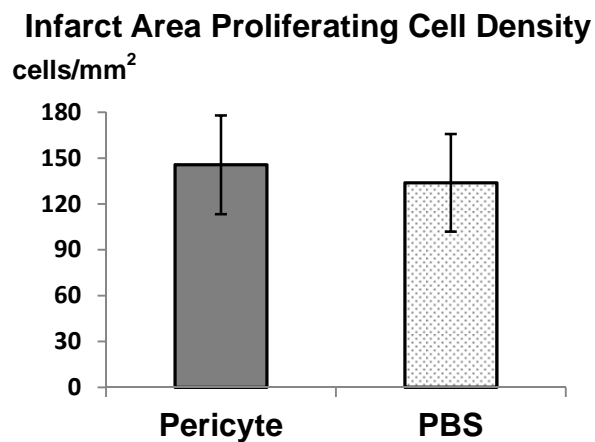
Supplemental Figure S9. Comparison of total and proliferating cell density within the infarct area at 2 weeks post-infarction. **(A)** Pericyte-injected hearts had a significantly less number of cells within the infarct area than the PBS-injected controls ($p<0.05$, N=5 per group). **(B)** A cell proliferation marker, Ki-67, was used to detect proliferating cells within the infarct area. No statistical difference in Ki-67(+) proliferating cell density was observed between pericyte- and PBS-injected hearts ($p=0.808$, N=3 per group).

Supplemental Figure S10

A

B
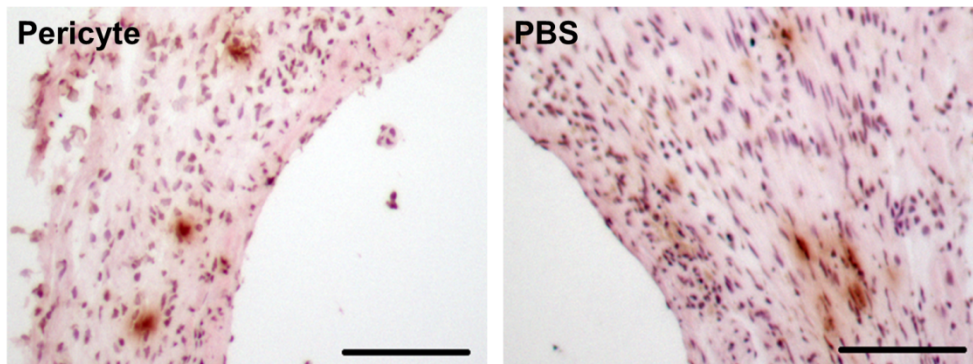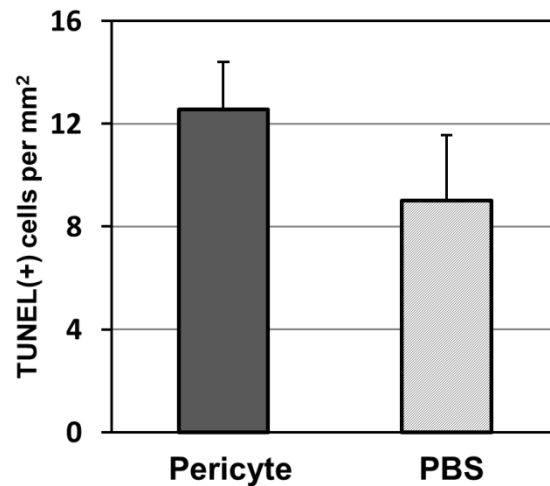
Supplemental Figure S10. (A) Terminal dUPT nick end-labeling (TUNEL) staining revealed the apoptotic cells within the infarct region of pericyte- or PBS-injected hearts. **(B)** Quantification of the apoptotic cell number (N=5 per group) showed no statistical difference between pericyte treatment (12.55±1.87 cells/mm^2) and PBS injection (9.01±2.55 cells/mm^2) at 2 weeks post-infarction (p=0.296).

REFERENCES

1. **Crisan M, Huard J, Zheng B, et al. Purification and Culture of Human Blood Vessel–Associated Progenitor Cells. *Current Protocols in Stem Cell Biology*: John Wiley & Sons, Inc.; 2007.**
2. **Crisan M, Yap S, Casteilla L, et al. A Perivascular Origin for Mesenchymal Stem Cells in Multiple Human Organs. *Cell Stem Cell.* 2008;3(3):301-313.**

3.   Crisan M, Deasy B, Gavina M, et al. Purification and Long-Term Culture of Multipotent Progenitor Cells Affiliated with the Walls of Human Blood Vessels: Myoendothelial Cells and Pericytes. In: Dr. Jennie PM, ed. *Methods in Cell Biology.* Vol Volume 86: Academic Press; 2008:295-309.

4.   Payne TR, Oshima H, Okada M, et al. A Relationship Between Vascular Endothelial Growth Factor, Angiogenesis, and Cardiac Repair After Muscle Stem Cell Transplantation Into Ischemic Hearts. *Journal of the American College of Cardiology.* 2007;50(17):1677-1684.

5.   Okada M, Payne TR, Zheng B, et al. Myogenic Endothelial Cells Purified From Human Skeletal Muscle Improve Cardiac Function After Transplantation Into Infarcted Myocardium. *Journal of the American College of Cardiology.* 2008;52(23):1869-1880.

6.   Okada M, Payne TR, Drowley L, et al. Human Skeletal Muscle Cells With a Slow Adhesion Rate After Isolation and an Enhanced Stress Resistance Improve Function of Ischemic Hearts. *Mol Ther.* 2012;20(1):138-145.

7.   Manning WJ, Wei JY, Katz SE, Litwin SE, Douglas PS. In vivo assessment of LV mass in mice using high-frequency cardiac ultrasound: necropsy validation. *American Journal of Physiology - Heart and Circulatory Physiology.* April 1, 1994 1994;266(4):H1672-H1675.

8.   Pollick C, Hale SL, Kloner RA. Echocardiographic and cardiac doppler assessment of mice. *Journal of the American Society of Echocardiography.* 1995;8(5, Part 1):602-610.

9.   Wandt B, Bojö L, Tolagen K, Wranne B. Echocardiographic assessment of ejection fraction in left ventricular hypertrophy. *Heart.* August 1, 1999 1999;82(2):192-198.

10.   Rando TA, Blau HM. Primary mouse myoblast purification, characterization, and transplantation for cell-mediated gene therapy. *The Journal of Cell Biology.* June 15, 1994 1994;125(6):1275-1287.

original article

Human Skeletal Muscle Cells With a Slow Adhesion Rate After Isolation and an Enhanced Stress Resistance Improve Function of Ischemic Hearts

Masaho Okada[1,2], Thomas R Payne[1–4], Lauren Drowley[1,2], Ron J Jankowski[4], Nobuo Momoi[5], Sarah Beckman[1], William CW Chen[1], Bradley B Keller[5], Kimimasa Tobita[5] and Johnny Huard[1–3,6]

[Q1] [1]Stem Cell Research Center, Children's Hospital of Pittsburgh, Pittsburgh, Pennsylvania, USA; [2]Department of Orthopaedic Surgery, University of Pittsburgh, Pittsburgh, Pennsylvania, USA; [3]Department of Bioengineering, University of Pittsburgh, Pittsburgh, Pennsylvania, USA; [4]Cook Myosite, Pittsburgh, Pennsylvania, USA; [5]Department of Pediatrics, Children's Hospital of Pittsburgh, Pittsburgh, Pennsylvania, USA; [6]Department of Molecular Genetics and Biochemistry, University of Pittsburgh, Pittsburgh, Pennsylvania, USA

Identification of cells that are endowed with maximum potency could be critical for the clinical success of cell-based therapies. We investigated whether cells with an enhanced efficacy for cardiac cell therapy could be enriched from adult human skeletal muscle on the basis of their adhesion properties to tissue culture flasks following tissue dissociation. Cells that adhered slowly displayed greater myogenic purity and more readily differentiated into myotubes *in vitro* than rapidly adhering cells (RACs). The slowly adhering cell (SAC) population also survived better than the RAC population in kinetic *in vitro* assays that simulate conditions of oxidative and inflammatory stress. When evaluated for the treatment of a myocardial infarction (MI), intramyocardial injection of the SACs more effectively improved echocardiographic indexes of left ventricular (LV) remodeling and contractility than the transplantation of the RACs. Immunohistological analysis revealed that hearts injected with SACs displayed a reduction in myocardial fibrosis and an increase in infarct vascularization, donor cell proliferation, and endogenous cardiomyocyte survival and proliferation in comparison with the RAC-treated hearts. In conclusion, these results suggest that adult human skeletal muscle-derived cells are inherently heterogeneous with regard to their efficacy for enhancing cardiac function after cardiac implantation, with SACs outperforming RACs.

INTRODUCTION

[Q2] Skeletal muscle is an attractive source of progenitor cells for autologous cell therapy due to its abundance and accessibility. Progenitor cells in skeletal muscle, generally referred to as myoblasts (or satellite cells), are numerous and heterogeneous in nature.[1] The potential use of myoblasts for treating muscle disorders has been hindered, at least in part, by high rates of cell death after transplantation.[2–4] Recently, there has been interest in the identification and purification of populations of skeletal muscle-derived cells with the greater potential for cell-based therapies.[1,2,4–16]

We and others have used the preplate isolation technique to fractionate skeletal muscle progenitor cells from rodent skeletal muscle on the basis of selective adhesion characteristics to tissue culture flasks.[17] Isolating cells with this method yields cell populations that are classified by a rapid or slow adherence to the culture flask. Skeletal myoblasts derived from the rapidly adhering cell (RAC) fraction of rodent skeletal muscle were poor at muscle regeneration when transplanted into both skeletal and cardiac muscles.[14–16] In contrast, murine skeletal muscle-derived stem cells (MDSC) derived from the slowly adhering cell (SAC) fraction demonstrated a significant improvement in skeletal muscle regeneration in comparison with the rapidly adhering myoblast population.[14,15] In addition, after intramyocardial injection into a murine model of an acute myocardial infarction (MI), hearts transplanted with MDSCs demonstrated a greater improvement in cardiac function in comparison with hearts transplanted with myoblasts.[16] The mechanisms underlying the functional difference between MDSC and myoblasts were attributed to the ability of the MDSCs to survive and engraft significantly better than the myoblasts.[16] The survival of MDSCs may have led to improvements in the attenuation of adverse remodeling and capillary density throughout the infarcted tissue. These effects were presumably mediated through long-term secretion of factors by the engrafted MDSCs, since differentiation into *de novo* cardiomyocytes was an extremely rare occurrence.[16] Although these promising results were observed with rodent skeletal muscle, it remained to be determined whether RAC and SAC isolated from human skeletal muscle would produce similar outcomes after cell transplantation into the heart.

Here, we isolated and characterized RAC and SAC from human skeletal muscle. The efficacy of both populations was evaluated in an MI model using immunodeficient mice. Our results indicate that the slowly adhering fraction of human skeletal muscle-derived cells more effectively improved cardiac function when compared with the rapidly adhering fraction. The SAC also demonstrated greater survival under conditions of oxidative and inflammatory conditions of stress *in vitro* when compared with the RAC.

Correspondence: Johnny Huard, 450 Technology Drive, 2 Bridgeside Point, Suite 206, Pittsburgh, Pennsylvania 15219, USA. E-mail: jhuard@pitt.edu

RESULTS

### Myogenic purity of RAC and SAC populations

Each cell population was analyzed for myogenic purity as determined by CD56 flow cytometry analysis. SAC populations contained a higher percentage of CD56-expressing cells when compared with the RAC populations (**Figure 1a**, SAC 83 ± 3% CD56-positive, RAC 39 ± 17%, $n = 3$ populations per group, $P = 0.07$).

Myogenic gene expression profiles

Evaluation of myogenic lineage genes in both the RAC and SAC populations demonstrated substantial expression of the myogenic cell markers desmin (*DES*) and m-cadherin (*CDH15*) as well as the myogenic determination gene *MYOD1* and the myogenic regulatory factor *MYF5* relative to the endogenous control gene *IPO8* (**Figure 1b**, average values of $n = 3$ donors). A modest expression of the *PAX7* transcription factor, which regulates the myogenic differentiation of satellite cells, was also detected (**Figure 1b**). Very low expression of the early satellite cell marker *PAX3* and the myogenic regulatory factors myogenin (*MYOG*) and *MYF6*, which are both involved in the specification of skeletal myoblasts into terminally differentiated myotubes, ~~were~~ observed (**Figure 1b**). As expected, a very low level of the skeletal muscle myosin heavy chain 2 (*MYH2*) gene, which is specifically expressed by terminally-differentiated skeletal myotubes, was detected in both populations, confirming that the RAC and SAC populations did not undergo terminal differentiation during

expansion under normal culture conditions (**Figure 1b**). Of the myogenic genes expressed by both cell populations, the SAC populations demonstrated increased expression of the following myogenic lineage genes relative to the RAC populations: *DES* (SAC: 1.6 ± 0.4 relative to RAC, $n = 3$ donors, $P = 0.218$), *CDH15* (1.4 ± 0.5, $P = 0.454$), *PAX7* (3.5 ± 1.1, $P = 0.082$), *MYOD1* (2.0 ± 0.4, $P = 0.066$), and *MYF5* genes (1.7 ± 0.3, $P = 0.108$) (**Figure 1c**). These findings correlate with the higher levels of myogenic purity observed in the SAC populations in comparison with the RAC populations (**Figure 1a**).

The presence of other cell types in the RAC and SAC populations that could have been co-isolated from human skeletal muscle was evaluated based on the expression levels of lineage-specific genes. We observed undetectable or minimal expression of the endothelial cell-specific gene von Willebrand factor (*VWF*), the smooth muscle cell lineage gene calponin 1 (*CNN1*), the adipocyte-expressed gene glycerol-3-phosphate dehydrogenase 1 (*GPD1*), the preadipocyte gene delta-like homolog (*DLK1*, alias ~~*PREF-1*~~) and the pan-hematopoietic gene protein tyrosine phosphatase receptor type C (*PTPRC*, alias *CD45*) (**Figure 1d**). The SAC populations also displayed lower expression relative to the RAC populations of the extracellular matrix genes fibronectin (*FN1*, 0.53 ± 0.15, $P < 0.05$) and collagen type IV (*COL4A1*, 0.54 ± 0.11 ~~quantity relative to RAC~~, $P < 0.05$), which are highly expressed by fibroblasts.[18] Taken together, these results suggest that the nonmyogenic cells (CD56⁻) within the RAC and SAC populations were fibroblasts, as expected.
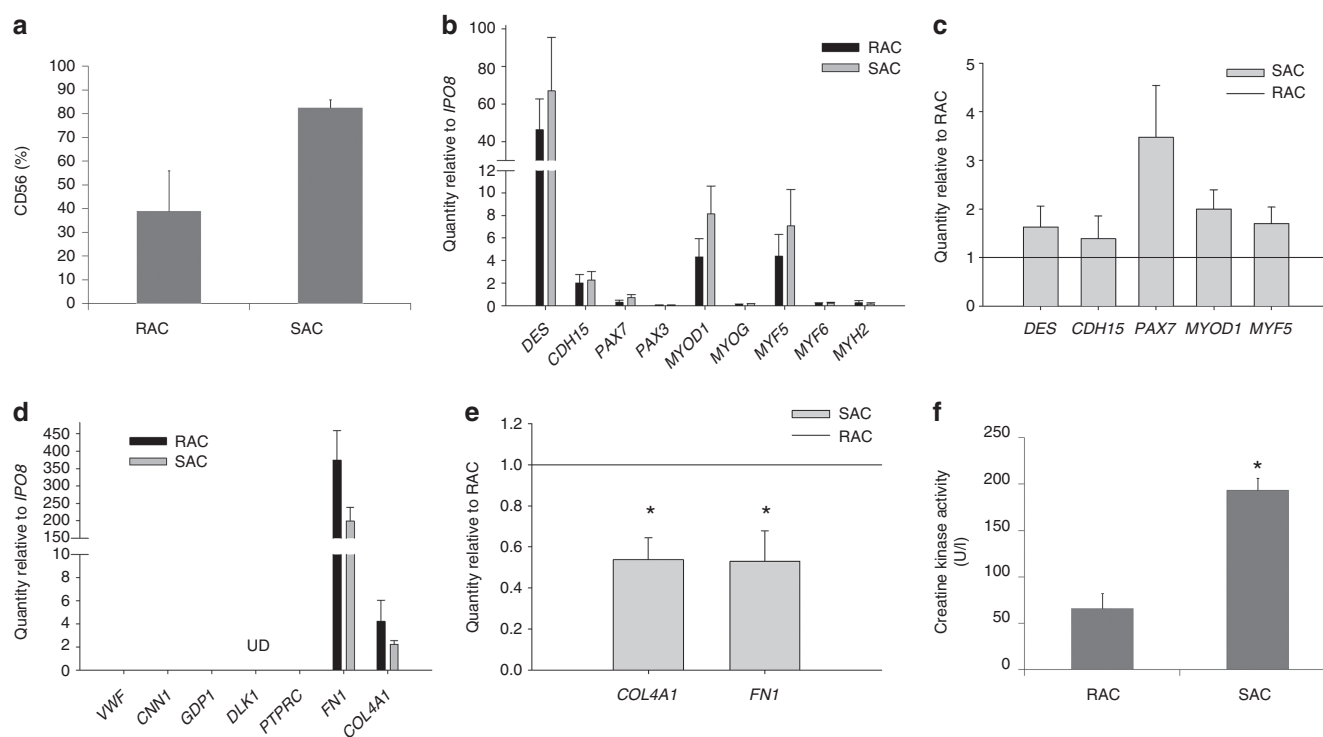
[Q3] **Figure 1 Characterization of the RAC and SAC after culture expansion.** (**a**) Each cell population was analyzed for myogenic purity by CD56 flow cytometry. (**b**) Myogenic gene expression profiles were measured in the RAC and SAC populations. Gene expression values are relative to the endogenous control gene *IPO8*. (**c**) SAC populations demonstrated increased expression of all expressed myogenic genes relative to the RAC populations. (**d**) Detection of other cell types within the RAC and SAC populations: *VWF* for endothelial cells, *CNN1* for smooth muscle cells, *GPD1* for adipocytes, *DLK1* for preadipocytes (UD, undetectable), *PTPRC* for blood cells, and *FN1* and *COL4A1* for fibroblasts. (**e**) SAC populations displayed decreased expression of *FN1* and *COL4A1* relative to the RAC populations (*$P < 0.05$). (**f**) SAC populations more rapidly differentiated into multi-nucleated myotubes than the RAC populations as signified by increased creatine kinase activity (*$P < 0.05$). RAC, rapidly adhering cell; SAC, slowly adhering cell.

Myogenic differentiation

The myogenic differentiation potential of RAC and SAC was measured *in vitro* by creatine kinase activity, an enzyme expressed in differentiated myogenic cells. When subjected to culture conditions that support terminal differentiation, the SAC populations displayed higher creatine kinase activity values when compared with the RAC populations, indicating that SAC more rapidly differentiated into skeletal myotubes than RAC (**Figure 1f**, SAC 194 ± 13 U/L, RAC 66 ± 16, *n* = 3 populations per group, *P* < 0.05).

[Q4]

Expression of paracrine factors

Under normal culture conditions, RAC and SAC highly expressed vascular endothelial growth factor A (*VEGFA*) and transforming growth factor-β1 (*TGFβ1*) genes. At lower levels, RAC and SAC populations also expressed fibroblast growth factor 2 (*FGF2*), platelet-derived growth factor-β (*PDGFβ*), angiopoietin 1 (*ANGPT1*), and hepatocyte growth factor (*HGF*) genes (**Supplementary Figure S1**). The RAC and SAC displayed minimal expression of insulin-like growth factor 1 (*IGF1*) and growth factors associated with neural development including nerve growth factor (*NGF*), brain-derived neurotrophic factor (*BDNF*), glial cell-derived neurotrophic factor (*GDNF*), and neuregulin 1 (*NRG1*) (**Supplementary Figure S1**). Overall, both cell populations displayed a similar gene expression profile of these paracrine factors.

Cell proliferation and survival under stress *in vitro*

The proliferation of RAC and SAC in culture was measured by a live cell imaging system every 12 hours for a period of 60 hours (**Figure 2a**). The SAC displayed a higher growth rate than the RAC (**Figure 2a**, 60 hours time point values: SAC 3.6 ± 0.4 cells normalized to initial cell number, RAC 2.4 ± 0.3, *n* = 3 populations per group; *P* < 0.05).

The cells' ability to survive conditions of oxidative and inflammatory stresses was evaluated *in vitro* with a cellular viability assay that was monitored in real-time with the live cell imaging system (**Figure 2b,c**). Under culture conditions of hydrogen peroxide-induced oxidative stress, a greater percentage of viable SAC were observed at all time points when compared with the RAC (**Figure 2b**, 72 hours time point values: SAC 48.1 ± 4.4% viability, RAC 27.7 ± 3.1%, *n* = 3 populations per group, *P* < 0.05). When exposed to inflammatory stress conditions with tumor necrosis factor-α, almost 40% of the RAC died whereas more than 85% of the SAC remained viable (**Figure 2c**, 72 hours time point values: SAC 86.1 ± 3.7% viability, RAC 61.2 ± 6.4%, *n* = 2 populations per group, *P* < 0.05). These results suggest that the SAC are more resistant to cellular death than the RAC when subjected to oxidative and inflammatory stresses, which are both likely conditions that cells will experience when injected directly into an acute MI.[19]

[Q5]

Intramyocardial injection and echocardiographic evaluation of cardiac function

The effect of human skeletal muscle-derived RAC and SAC for cardiac cell transplantation was assessed in an immunodeficient mouse model of an acute MI. We injected infarcted mice with cell populations isolated from three male donors (*n* = 27 mice for RAC, *n* = 22 for SAC, and *n* = 21 for control injections). The RAC
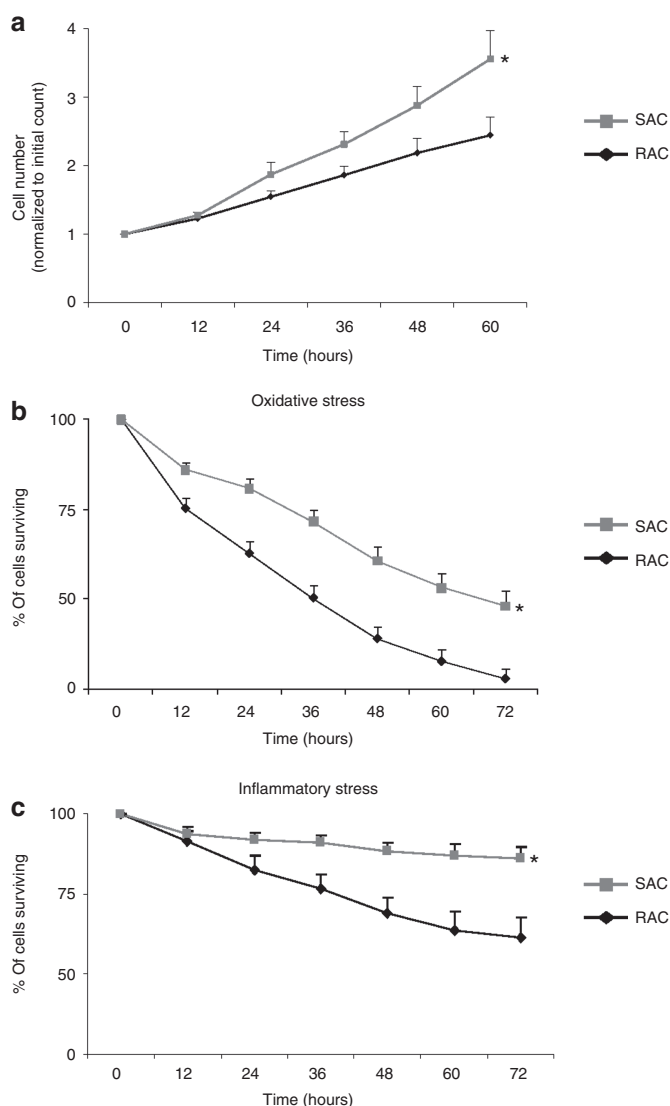
Figure 2 Cell proliferation and survival under oxidative and inflammatory stress. (**a**) Cell proliferation was measured in the RAC and SAC cultures (**P < 0.05). (**b**,**c**) SAC demonstrated greater survival under conditions of (**b**) oxidative and (**c**) inflammatory stress than the RAC (**P < 0.05). RAC, rapidly adhering cell; SAC, slowly adhering cell.

and SAC prepared for injection and frozen in cryopreservation medium displayed comparable viability and recovery post-thaw at the time of injection (post-thaw viability: RAC 89.4 ± 3.1%, SAC 89.6 ± 1.2%, *P* = 0.963; post-thaw recovery: RAC 68.4 ± 1.6%, SAC 74.9 ± 3.7%, *P* = 0.189).

Two weeks after infarction, cellular transplantation induced a modest decrease in left ventricular (LV) diastolic dimensions, as measured by end diastolic area, when compared with control vehicle injection (**Figure 3a**, SAC 11.9 ± 0.5 mm^2, RAC 12.6 ± 0.6, control 14.0 ± 0.7). Both cell groups had significantly smaller LV systolic dimensions when compared with the control group, as assessed by end systolic area (SAC 8.8 ± 0.4 mm^2, RAC 10.1 ± 0.6, control 11.9 ± 0.6; *P* < 0.05, RAC and SAC versus control). A greater improvement in LV contractility, as determined by fractional area change values, was observed in the cell-treated hearts when compared with the control vehicle-treated hearts 2 weeks after MI
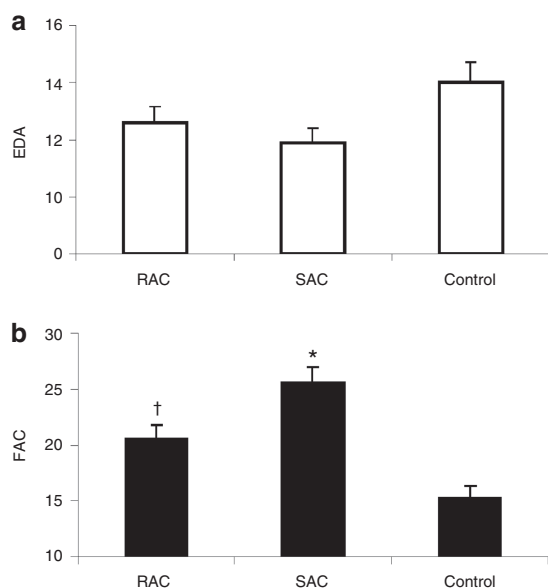
Figure 3 Functional assessments. (**a**) Left ventricular end diastolic area (EDA) was slightly reduced in hearts injected with the RAC and SAC populations when compared with control hearts injected with saline. (**b**) Hearts injected with SAC displayed stronger left ventricular contractility, as measured by percent fractional area change (FAC), when compared with hearts injected with RAC (*$P < 0.05$, SAC versus RAC and control; †$P < 0.05$, RAC versus control). RAC, rapidly adhering cell; SAC, slowly adhering cell.

(**Figure 3b**, SAC 25.6 ± 1.4%, RAC 20.6 ± 1.2%, control 15.3 ± 1.1%; $P < 0.05$, RAC and SAC versus control). The hearts injected with the SAC demonstrated significant improvement of LV performance when compared with the RAC (**Figure 3b**; $P < 0.05$, SAC versus RAC). When cardiac echocardiography data was separated by donor age, the SAC showed greater efficacy versus the RAC primarily in the older donors (57 and 70 year males) (**Supplementary Table S1**). In contrast, the SAC and RAC derived from the young donor (13-year-old male) demonstrated comparable outcomes, indicating that the selection of SAC may be the most critical from older donors (**Supplementary Table S1**). Overall, these results indicate that the SAC more effectively attenuated adverse remodeling and improved cardiac function when compared with the RAC, particularly when these cell populations were isolated from older donors.

Cardiac scar tissue

The extent of scar tissue formation within the LV was evaluated using Masson's trichrome stain (**Figure 4a–c**). Two weeks following a MI, a reduction in scar tissue was observed in both RAC- and SAC-injected hearts compared with control vehicle-injected hearts (**Figure 4d**, SAC 45.8 ± 6.6% scar, RAC 60.9 ± 7.1%, control 77.5 ± 5.3%). However, only the SAC significantly attenuated scar tissue formation following an acute MI when compared with the controls (**Figure 4d**, $P < 0.05$, SAC versus control).

Transplanted cell engraftment and proliferation

Donor myocytes were observed within the infarct zone by colocalization of Masson's trichrome stain (arrows, **Figure 5a**) and fast skeletal MYH immunostaining (arrows, **Figure 5b**). These engraftments were frequently surrounded by scar tissue along
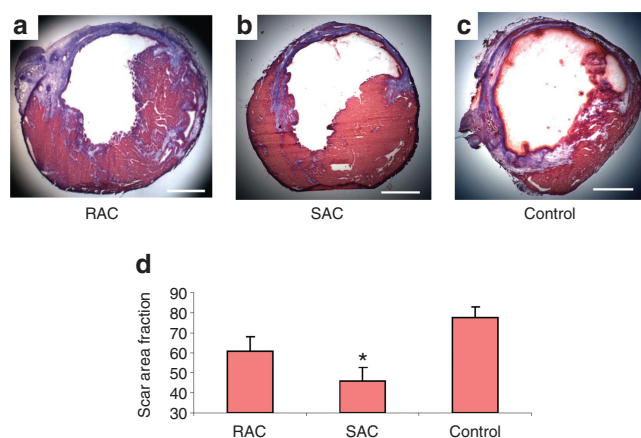

Figure 4 Infarct histology. (**a–c**) Representative images were taken from transverse sections of the Masson's trichrome–stained hearts. Muscle tissue is stained red, and collagenous tissue is stained blue. Bars equal 500 µm. (**d**) SAC-injected hearts demonstrated the greatest reduction of scar tissue when compared with the control (*$P < 0.05$, SAC versus control). SAC, slowly adhering cell.

the ischemic border zone (arrowheads, **Figure 5a,b**). The area of MYH⁺ tissue within the myocardium of the LV was comparable between hearts injected with the RAC and SAC (SAC 3.5 ± 1.2% MYH⁺ tissue in the myocardium, RAC 3.8 ± 0.8%, $P = 0.864$, SAC versus RAC). The presence of nuclei expressing proliferating cell nuclear antigen (PCNA) using a human-specific PCNA antibody further confirmed donor cell engraftment and indicated donor cell proliferation *in vivo* (**Figure 5c**). We observed proliferative, PCNA-positive donor cells more frequently in the SAC-injected hearts than in the RAC-injected hearts (**Figure 5d**, SAC 2.0 ± 0.3 PCNA⁺/MYH⁺ cells, RAC 0.4 ± 0.3; $P < 0.05$, SAC versus RAC). These findings confirm the engraftment of the injected human cells within the murine myocardium, and suggest that the SAC proliferate at higher levels than the RAC *in vivo*.

Angiogenesis

Capillary density within the infarct tissue was assessed by CD31 immunostaining (**Figure 6a–c**). More capillaries were observed within the infarct area of hearts treated with the SAC when compared with hearts injected with the RAC and the control vehicle (**Figure 6d**, SAC 723 ± 63 capillaries/mm², RAC 560 ± 21, control 548 ± 31; $P < 0.05$, SAC versus RAC and control). These findings indicate that transplanted SAC may induce a more potent angiogenic effect within the infarcted hearts when compared with transplanted RAC and the control.

Endogenous cardiomyocyte apoptosis and proliferation

Endogenous cardiomyocyte apoptosis and proliferation was evaluated at 3 days after MI. Multi-label staining for terminal dUPT nick end-labeling (TUNEL) and cardiac Troponin I (cTnI) was performed to determine the effect of cell implantation on endogenous cardiomyocyte apoptosis in the peri-infarct regions (**Figure 7a**). Hearts injected with SAC contained less apoptotic cardiomyocytes within the peri-infarct regions when compared with hearts transplanted with RAC and the control vehicle (**Figure 7b**, SAC 203 ± 29
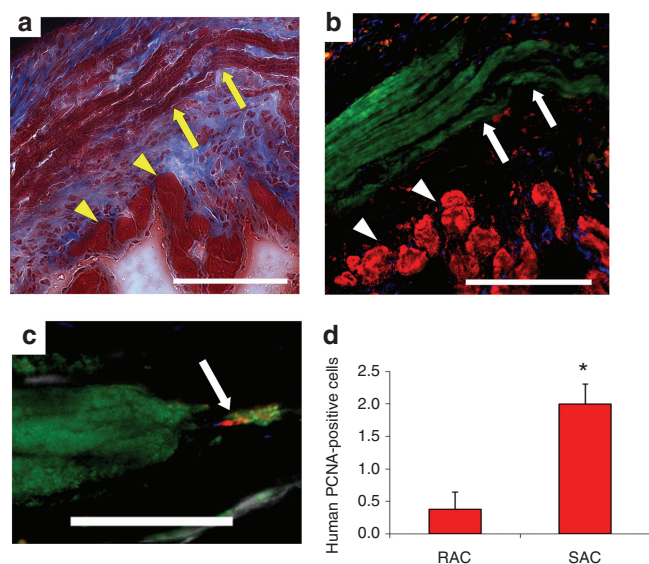
Figure 5 Engraftment and proliferation of injected cells *in vivo*. (**a**) The arrows designate the engraftment area of the SAC, and the arrowheads indicate host cardiac tissue in Masson's trichrome–stained hearts. Bar = 125 μm. Image **a** colocalizes with image **b**. (**b**) Fast skeletal myosin heavy chain (MYH)-positive myofibers (green stain, arrows) designate the SAC engraftment region. Cardiac troponin I-positive cardiomyocytes (red, arrowheads) identifies peri-infarct zone. Bar equals 125 μm. (**c,d**) Mitotic human PCNA-positive cells (red stain) that colocalized with the MYH-positive engraftment region (green stain) were more frequently observed in the SAC-injected hearts when compared with the RAC-injected hearts (*$P < 0.05$, SAC versus RAC). Cardiac troponin I-positive cardiomyocytes are stained grey, and nuclei are stained blue. PCNA, proliferating cell nuclear antigen; RAC, rapidly adhering cell; SAC, slowly adhering cell.
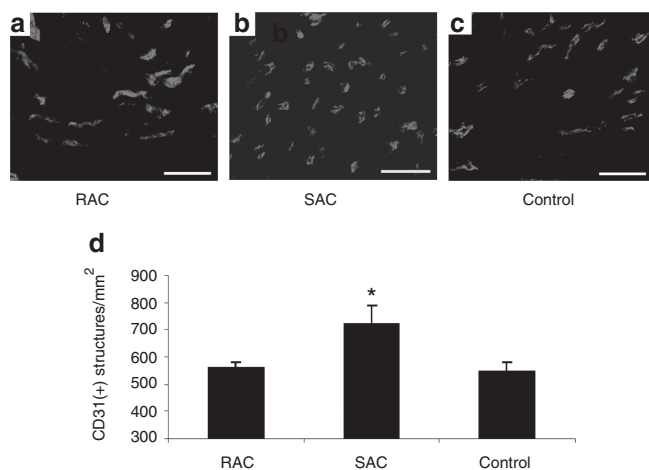

Figure 6 Angiogenesis. (**a**–**c**) Representative images are shown of CD31 immunostaining. Bars equal 50 μm. (**d**) The infarcts of hearts transplanted with SAC displayed higher capillary densities when compared with hearts injected with RAC and control vehicle (*$P < 0.05$, SAC versus RAC and control). RAC, rapidly adhering cell; SAC, slowly adhering cell.

TUNEL⁺/cTnI⁺ cells in four high power fields, RAC 321 ± 68, control 404 ± 81; $P < 0.05$, SAC versus control).

The number of proliferating cardiomyocytes present within the infarct border zone was measured by Ki-67 and cTnI dual label immunostaining (**Figure 7c**). Hearts injected with SAC contained more proliferating cardiomyocytes within the infarct border zone
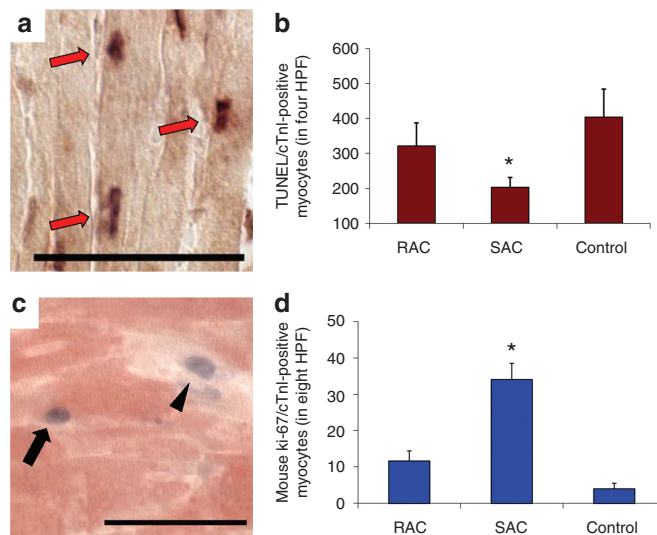

Figure 7 Endogenous cardiomyocyte apoptosis and proliferation. (**a**) Identification of apoptotic endogenous cardiomyocytes (arrows) by concomitant staining for cardiac troponin I (cTnI, light brown cytoplasmic stain) and TUNEL assay (arrows, dark nuclear stain). (**b**) The number of apoptotic cardiomyocytes was measured in four high power fields (HPF, *$P < 0.05$, SAC versus control). (**c**) Proliferating cardiomyocytes (arrow) within the peri-infarct region were identified by colocalization of both Ki-67 (blue nuclear stain) and cTnI (red) within the peri-infarct region. Some of the proliferating cells stained by Ki-67 did not colocalize with cTnI (arrowhead). Bars equal 50 μm. (**d**) The number of proliferating Ki-67-positive endogenous cardiomyocytes was measured in the peri-infarct region of the hearts (*$P < 0.05$, SAC versus RAC and control). RAC, rapidly adhering cell; SAC, slowly adhering cell, TUNEL, terminal dUPT nick end-labeling.

than hearts injected with either the RAC or the control (**Figure 7d**, SAC 34 ± 5 Ki-67⁺/cTnI⁺ cardiomyocytes in 8 high power fields, RAC 12 ± 3, control 4 ± 2; $P < 0.05$, SAC versus RAC and control). Taken together, these results suggest that the transplantation of SAC induced a beneficial effect on endogenous cardiomyocyte proliferation and apoptosis within the peri-infarct region.

DISCUSSION

The main finding in this study is that the SAC fraction is more effective at improving cardiac function than the RAC fraction derived from human skeletal muscle, which is a result that is consistent with our studies investigating progenitor cells from murine skeletal muscle for cardiac repair.[16] These results support the notion that human skeletal muscle-derived progenitor cells are heterogeneous not just in terms of cellular composition but of potency for cardiac cell transplantation.

Isolation of human skeletal muscle-derived cells on the basis of adhesion rates to tissue culture flasks using the preplate technique produced RAC and SAC populations that exhibit distinct characteristics and behavior. Our results *in vitro* demonstrate that myogenic progenitor cells with the highest myogenic purity and the strongest propensity for myogenic differentiation are purified in the SAC fraction rather than the RAC fraction. Interestingly, these findings in human skeletal muscle are consistent with the use of the preplate technique to isolate progenitor cells from murine skeletal muscle.[14] In the mouse, we observed that cells that adhered slowly also displayed greater myogenic purity based on *DES*

Remove Italics

expression when compared with cells that adhered rapidly.[14] In addition, the murine SAC population displayed a greater ability to regenerate skeletal muscle than the RAC population.[14] The mechanism underlying differential adhesion rates to tissue culture flasks is unknown at this point; however, these differences may result from a variety of factors including the expression of specific adhesion molecules and cellular density.[17] We are initiating research to determine whether other human skeletal muscle-derived cell populations, including CD34+CD90− cells,[5] myogenic endothelial cells[12,13] and pericytes,[10,11] are being collected preferentially in the slowly adhering fraction. Due to the limited number of cells (<100) contained within the slowly adhering fraction before expansion, and the known change in expression of many surface markers with time *in vitro*, flow cytometry characterization with a series of cell surface markers on the same populations used in this study for injection was not achievable.

The mechanism underlying the advantage of the SAC over RAC population for functional restoration after a MI may be multi-faceted.[7,16,20–25] A proposed aspect for the observed functional difference might be the varying ability of the transplanted cells to prevent adverse remodeling. SAC-treated hearts displayed a considerable reduction in end-systolic geometry when compared with RAC-injected hearts, suggesting that SAC induced a more effective attenuation of adverse remodeling. In clinical trials, skeletal myoblasts have shown a positive remodeling effect in the first randomized, placebo-controlled study of skeletal myoblast transplantation for cardiac repair (MAGIC trial).[26] The observed differences in end-systolic dimensions between the SAC and RAC could be attributed to the greater reduction in scar tissue in SAC-treated hearts when compared with hearts treated with RAC.

The reduced size of the infarct scar may be due to the preservation of at-risk cardiomyocytes, stimulation of endogenous cardiomyocyte proliferation, vascularization of the infarct scar, and/or the secretion of paracrine factors that regulate fibrosis. Three days after MI, we observed a significant increase in the number of proliferating cardiomyocytes and decrease in the number of apoptotic cardiomyocytes within the peri-infarct zone of hearts injected with SAC when compared with hearts injected with RAC and the control vehicle. We did not determine how the injected cells stimulated proliferation and protection of at-risk myocardium; however, at such an early time point after MI (3 days), a reasonable hypothesis is that this effect is due to the release of paracrine factors by the injected cells that stimulate cell survival and proliferation. Furthermore, various reports have shown that implanted cells promote infarct angiogenesis and have established a correlation between neovascularization and functional recovery of the heart after MI.[13,16,27,28] Here, we also observed a greater induction of angiogenesis within the infarct in SAC-treated hearts than in RAC-treated hearts, which may also support the attenuation of adverse infarct remodeling.[26,29]

The cells' ability to influence the host cells within the microenvironment through the release of paracrine molecules may represent a major determinant in the healing capacity of transplanted cells.[30,31] Here, we showed that both RAC and SAC express similar levels of various angiogenic and neurogenic genes under normal culture conditions. Many of the angiogenic factors expressed by the RAC and SAC, especially *VEGFA*, *HGF*, *TGFB1*, and *FGF2*,

have been shown to be expressed by human skeletal myoblasts, bone marrow mononuclear cells, adipose stromal cells, and bone marrow stromal cells.[32–37] In addition to stimulating angiogenesis, factors secreted by transplanted cells may activate signaling cascades that regulate fibrosis and the survival and proliferation of recipient cells in and around the infarct zone. Human skeletal muscle-derived cells likely express a wide variety of paracrine factors that far surpass the small battery of genes evaluated by others and us.[32,33] It is not unexpected that both the RAC and SAC populations express similar levels of the tested paracrine factors under normal culture conditions, since the level of cellular secretion of these factors may be primarily dependent on the cells' response to the environmental cues of the myocardial microenvironment and disease state (e.g., ischemia).[13,16,27,28]

Furthermore, the magnitude of the paracrine effect may be contingent on cell survival post-transplantation. The ability of transplanted cells to survive and proliferate, particularly when implanted directly into the harsh *milieu* of a myocardial infarct, may be critical for the cells to exert a lasting and significant biological effect, including the extended release of paracrine factors.[19] In our research with muscle progenitor cells isolated from human and murine skeletal muscle, we have consistently observed that transplanted SAC regenerate larger and more durable engraftments of skeletal myocytes than transplanted RAC.[14–16] We hypothesize that the preplate technique inherently selects for stress-resistant cells in the slowly adhering fraction, since these cells are able to tolerate suspension-induced stresses and anoikis during isolation.[38,39] Therefore, the SAC may represent a cell population endowed with an elevated resistance to stress. We have recently shown that muscle stem cells derived from the SAC fraction of murine skeletal muscle have an ability to survive under stress due to elevated levels of antioxidant expression.[40,41] Future research will evaluate whether human SAC also display similar antioxidant characteristics.

A limitation of this study is of the fact that the skeletal muscle-derived cells were injected immediately after a MI, which is not entirely relevant to an actual clinical scenario for autologous transplantation. In reality, the cells would require at least several weeks in order to cultivate a sufficient number of cells before treatment. Although we could not replicate the exact clinical conditions with this animal model, these findings may still provide meaningful information regarding the heterogeneity of human skeletal muscle-derived cells for cardiac cell transplantation.

In conclusion, the isolation of adult human skeletal muscle-derived cells on the basis of adhesion rates to tissue culture flasks enriches for cell fractions that support distinct levels of functional improvement when transplanted into ischemic myocardium. Selection of the best progenitor cell population from human skeletal muscle may aid in the translation of cell-based products for clinical applications of tissue repair.

MATERIALS AND METHODS

Animals. The Institutional Animal Care and Use Committee at the Children's Hospital of Pittsburgh approved the animal and surgical procedures performed in this study (Protocol 37/04). A total of 70 male nonobese diabetic/severe combined immunodeficient mice (NOD/SCID, strain NOD. CB17-*Prkdc^scid*/SzJ, The Jackson Laboratory, Bar Harbor, ME) between

13 and 22 weeks of age were used for this study. Creation of the acute MI model in adult mice and injection of thawed cells (3×10^5 cells in 30 μl) or control medium (30 μl) was performed in a blinded fashion, as previously described.[16] Echocardiography was also conducted in a blinded fashion to assess heart function, as previously described.[13,16] Additional information can be found in the **Supplementary Materials and Methods**.

Cells. RAC and SAC populations were isolated from human rectus abdominus skeletal muscle biopsies (50–250 mg) using the preplate technique.[17] Tissues were procured from 13, 57, and 70-year-old male donors (13M, 57M, and 70M, respectively). Isolation, culture expansion, and preparation of cells for injection are further detailed in **Supplementary Materials and Methods**. Cell populations from each donor were cryopreserved for injection at the following culture passages: 13M–RAC passage 4 and SAC passage 5–7, 57M–RAC passage 6 and SAC passage 5, 70M–RAC passage 8 and SAC passage 7. Post-thaw recovery and viability were evaluated from aliquots of the frozen cell suspensions that were prepared and cryopreserved for injection using the Viacount viability stain (Millipore, Hayward, CA) and Guava PCA flow cytometry system (Millipore).

Gene expression profile. RNA was purified from 1×10^5 cells for gene expression analysis immediately following the thaw of the cryopreserved stocks of cultured cells. The number of passages of the RAC and SAC were closely matched for the populations derived from the 13M (passage 7 for RAC and passage 6 for SAC), 57M (passage 6 for both populations), and 70M donor tissues (passage 3 for both populations).

Total RNA was isolated using the RNeasy Mini kit (Qiagen, Valencia, CA) and was reverse transcribed to cDNA (Applied Biosystems, Foster City, CA). Gene expression was measured using real-time quantitative PCR (see **Supplementary Materials and Methods** for detailed methods). All target genes were normalized to the reference housekeeping gene *IPO8* (Applied Biosystems, Hs00183533_m1). Relative quantity of gene expression was calculated as total amount of RNA based on the comparative ΔC_T (*i.e.*, relative expression level to endogenous control gene *IPO8*) and $\Delta\Delta C_T$ methods (i.e., relative expression level to the RAC population for each donor).

[Q6]

Myogenic assays. Myogenic purity analysis was performed on cellular suspensions using a PE-conjugated CD56 antibody (1:50; BD Pharmingen, San Diego, CA). The Guava PCA flow cytometry system measured the percentage of cells expressing CD56. Cell populations from each donor were evaluated at the following culture passages: 13M–RAC passage 4 and SAC passage 5–7, 57M–RAC passage 6 and SAC passage 5, 70M–RAC passage 8 and SAC passage 7.

To determine the myogenic differentiation potential of each population, cells were seeded onto a culture plate with low-serum differentiation medium and allowed to differentiate. Cell populations from each donor were evaluated at the following culture passages: 13M–RAC passage 4–5 and SAC passage 6–7, 57M–RAC passage 6 and SAC passage 5, 70M–RAC passage 4 and SAC passage 4. Terminal differentiation into multi-nucleated myotubes was measured with an assay that measured creatine kinase (CK) activity levels of differentiated cultures using the CK Liqui-UV Test Kit (Stanbio Laboratory, Boerne, TX) according to the manufacturer's instructions.[42]

[Q7]

Cell proliferation and survival assays. Cell proliferation under normal culture conditions and cell viability under stress conditions were evaluated with kinetic assays.[12,40,41] Cells were cultured for 60 hours in a live cell imaging system (Automated Cell, Pittsburgh, PA), which contains an incubation chamber for controlling temperature, humidity and CO_2 gas levels. The number of cells was measured in images acquired at 12-hour intervals.

Cell viability under stress conditions was analyzed as previously described.[12,40,41] Briefly, cells were cultured in a live cell imaging system for 72 hours in medium supplemented with propidium iodide (1:500, Sigma, St Louis, MO) to stain dead cells and either hydrogen peroxide (300 μmol/l;

[Q8]

Sigma) or tumor necrosis factor-α (10 ng/ml; Sigma) to induce cell death by oxidative and inflammatory stresses, respectively. Brightfield and fluorescent images were captured repeatedly at 10-minute intervals in the live cell imaging system for the entire 72-hour period. The percentage of viable cells (*i.e.*, propidium iodide exclusion) was measured from images acquired at 12-hour intervals using imaging software.

Histology and immunohistochemistry. Mice were sacrificed at 3 days, 2 weeks or 6 weeks after cell transplantation. We harvested the hearts, froze the tissue in 2-methylbutane precooled in liquid nitrogen, and serially sectioned the hearts from the apex to the base, as previously described.[13] Sections were then stained for fast skeletal MYH (1:200–1:400; Sigma) expression, as previously described.[20] The engraftment area ratio was defined as the area of MYH-positive tissue divided by the total area of the LV myocardium, which was identified by co-staining for cTnI (1:20,000; Scripps, San Diego, CA). To detect proliferating cells within the engraftment, tissue was stained with human anti-human PCNA antibody (1:400; US Biological, Swampscott, MA).[13] In sections stained with Masson's trichrome (IMEB, San Marcos, CA), scar area fraction was defined as the ratio of scar area to the cardiac LV muscle area and was averaged from five sections per heart, as previously described.[13] To measure capillary density, we stained heart muscle sections with an anti-mouse CD31 (platelet/endothelial cell adhesion molecule-1) antibody (BD Pharmingen).[16] The TUNEL assay was performed using the ApopTag Plus Peroxidase In Situ Apoptosis Detection Kit (Chemicon, Temecula, CA) according to manufacturer's instructions.[13] We carried out the Ki-67 (1:50; Dako, Glostrup, Denmark) and cTnI dual label immunostaining, as previously described, using the SG substrate kit (blue stain, Vector Laboratories, Burlingame, CA) and the AEC (3-amino-9-ethylcarbazole) substrate kit (red stain, Vector Laboratories), respectively.[13] Additional immunostaining methods are provided in the **Supplementary Materials and Methods**.

[Q9]

[Q10]

[Q11]

[Q12]

Statistical analysis. All measured data are presented as the mean ± SE of the mean. A *t*-test or a one-way analysis of variance was performed when comparing two groups or more than two groups, respectively. Analysis of variance *post hoc* analysis was conducted with the Tukey multiple comparison test. Statistical significance was defined by a value of $P < 0.05$. All calculations were performed using SigmaStat (Systat Software, San Jose, CA).

SUPPLEMENTARY MATERIAL
Figure S1. Cytokine gene expression profile.
Table S1. Echocardiographic data separated by donor cell populations.
Materials and Methods.

REFERENCES
1. Péault, B, Rudnicki, M, Torrente, Y, Cossu, G, Tremblay, JP, Partridge, T *et al.* (2007). Stem and progenitor cells in skeletal muscle development, maintenance, and therapy. *Mol Ther* **15**: 867–877.
2. Menasché, P (2004). Cellular transplantation: hurdles remaining before widespread clinical use. *Curr Opin Cardiol* **19**: 154–161.
3. Huard, J, Acsadi, G, Jani, A, Massie, B and Karpati, G (1994). Gene transfer into skeletal muscles by isogenic myoblasts. *Hum Gene Ther* **5**: 949–958.

4. Beauchamp, JR, Morgan, JE, Pagel, CN and Partridge, TA (1999). Dynamics of myoblast transplantation reveal a discrete minority of precursors with stem cell-like properties as the myogenic source. *J Cell Biol* **144**: 1113–1122.

5. Proksch, S, Bel, A, Puymirat, E, Pidial, L, Bellamy, V, Peyrard, S *et al.* (2009). Does the human skeletal muscle harbor the murine equivalents of cardiac precursor cells? *Mol Ther* **17**: 733–741.

6. Negroni, E, Riederer, I, Chaouch, S, Belicchi, M, Razini, P, Di Santo, J *et al.* (2009). *In vivo* myogenic potential of human CD133+ muscle-derived stem cells: a quantitative study. *Mol Ther* **17**: 1771–1778.

7. Sarig, R, Baruchi, Z, Fuchs, O, Nudel, U and Yaffe, D (2006). Regeneration and transdifferentiation potential of muscle-derived stem cells propagated as myospheres. *Stem Cells* **24**: 1769–1778.

8. Morosetti, R, Mirabella, M, Gliubizzi, C, Broccolini, A, Sancricca, C, Pescatori, M *et al.* (2007). Isolation and characterization of mesoangioblasts from facioscapulohumeral muscular dystrophy muscle biopsies. *Stem Cells* **25**: 3173–3182.

9. Motohashi, N, Uezumi, A, Yada, E, Fukada, S, Fukushima, K, Imaizumi, K *et al.* (2008). Muscle CD31(-) CD45(-) side population cells promote muscle regeneration by stimulating proliferation and migration of myoblasts. *Am J Pathol* **173**: 781–791.

10. Dellavalle, A, Sampaolesi, M, Tonlorenzi, R, Tagliafico, E, Sacchetti, B, Perani, L *et al.* (2007). Pericytes of human skeletal muscle are myogenic precursors distinct from satellite cells. *Nat Cell Biol* **9**: 255–267.

11. Crisan, M, Yap, S, Casteilla, L, Chen, CW, Corselli, M, Park, TS *et al.* (2008). A perivascular origin for mesenchymal stem cells in multiple human organs. *Cell Stem Cell* **3**: 301–313.

12. Zheng, B, Cao, B, Crisan, M, Sun, B, Li, G, Logar, A *et al.* (2007). Prospective identification of myogenic endothelial cells in human skeletal muscle. *Nat Biotechnol* **25**: 1025–1034.

13. Okada, M, Payne, TR, Zheng, B, Oshima, H, Momoi, N, Tobita, K *et al.* (2008). Myogenic endothelial cells purified from human skeletal muscle improve cardiac function after transplantation into infarcted myocardium. *J Am Coll Cardiol* **52**: 1869–1880.

14. Qu, Z, Balkir, L, van Deutekom, JC, Robbins, PD, Pruchnic, R and Huard, J (1998). Development of approaches to improve cell survival in myoblast transfer therapy. *J Cell Biol* **142**: 1257–1267.

15. Qu-Petersen, Z, Deasy, B, Jankowski, R, Ikezawa, M, Cummins, J, Pruchnic, R *et al.* (2002). Identification of a novel population of muscle stem cells in mice: potential for muscle regeneration. *J Cell Biol* **157**: 851–864.

16. Oshima, H, Payne, TR, Urish, KL, Sakai, T, Ling, Y, Gharaibeh, B *et al.* (2005). Differential myocardial infarct repair with muscle stem cells compared to myoblasts. *Mol Ther* **12**: 1130–1141.

17. Gharaibeh, B, Lu, A, Tebbets, J, Zheng, B, Feduska, J, Crisan, M *et al.* (2008). Isolation of a slowly adhering cell fraction containing stem cells from murine skeletal muscle by the preplate technique. *Nat Protoc* **3**: 1501–1509.

18. Pilling, D, Fan, T, Huang, D, Kaul, B and Gomer, RH (2009). Identification of markers that distinguish monocyte-derived fibrocytes from monocytes, macrophages, and fibroblasts. *PLoS ONE* **4**: e7475.

19. Suzuki, K, Murtuza, B, Beauchamp, JR, Smolenski, RT, Varela-Carver, A, Fukushima, S *et al.* (2004). Dynamics and mediators of acute graft attrition after myoblast transplantation to the heart. *FASEB J* **18**: 1153–1155.

20. Payne, TR, Oshima, H, Sakai, T, Ling, Y, Gharaibeh, B, Cummins, J *et al.* (2005). Regeneration of dystrophin-expressing myocytes in the mdx heart by skeletal muscle stem cells. *Gene Ther* **12**: 1264–1274.

21. Reinecke, H, Poppa, V and Murry, CE (2002). Skeletal muscle stem cells do not transdifferentiate into cardiomyocytes after cardiac grafting. *J Mol Cell Cardiol* **34**: 241–249.

22. Reinecke, H, Minami, E, Poppa, V and Murry, CE (2004). Evidence for fusion between cardiac and skeletal muscle cells. *Circ Res* **94**: e56–e60.

23. Reinecke, H, MacDonald, GH, Hauschka, SD and Murry, CE (2000). Electromechanical coupling between skeletal and cardiac muscle. Implications for infarct repair. *J Cell Biol* **149**: 731–740.

24. Leobon, B, Garcin, I, Menasche, P, Vilquin, JT, Audinat, E and Charpak, S (2003). Myoblasts transplanted into rat infarcted myocardium are functionally isolated from their host. *Proc Natl Acad Sci USA* **100**: 7808–7811.

25. Rubart, M, Soonpaa, MH, Nakajima, H and Field, LJ (2004). Spontaneous and evoked intracellular calcium transients in donor-derived myocytes following intracardiac myoblast transplantation. *J Clin Invest* **114**: 775–783.

26. Menasché, P, Alfieri, O, Janssens, S, McKenna, W, Reichenspurner, H, Trinquart, L *et al.* (2008). The Myoblast Autologous Grafting in Ischemic Cardiomyopathy (MAGIC) trial: first randomized placebo-controlled study of myoblast transplantation. *Circulation* **117**: 1189–1200.

27. Kocher, AA, Schuster, MD, Szabolcs, MJ, Takuma, S, Burkhoff, D, Wang, J *et al.* (2001). Neovascularization of ischemic myocardium by human bone-marrow-derived angioblasts prevents cardiomyocyte apoptosis, reduces remodeling and improves cardiac function. *Nat Med* **7**: 430–436.

28. Payne, TR, Oshima, H, Okada, M, Momoi, N, Tobita, K, Keller, BB *et al.* (2007). A relationship between vascular endothelial growth factor, angiogenesis, and cardiac repair after muscle stem cell transplantation into ischemic hearts. *J Am Coll Cardiol* **50**: 1677–1684.

29. White, HD, Norris, RM, Brown, MA, Brandt, PW, Whitlock, RM and Wild, CJ (1987). Left ventricular end-systolic volume as the major determinant of survival after recovery from myocardial infarction. *Circulation* **76**: 44–51.

30. Gnecchi, M, Zhang, Z, Ni, A and Dzau, VJ (2008). Paracrine mechanisms in adult stem cell signaling and therapy. *Circ Res* **103**: 1204–1219.

31. Cheng, AS and Yau, TM (2008). Paracrine effects of cell transplantation: strategies to augment the efficacy of cell therapies. *Semin Thorac Cardiovasc Surg* **20**: 94–101.

32. Perez-Ilzarbe, M, Agbulut, O, Pelacho, B, Ciorba, C, San Jose-Eneriz, E, Desnos, M *et al.* (2008). Characterization of the paracrine effects of human skeletal myoblasts transplanted in infarcted myocardium. *Eur J Heart Fail* **10**: 1065–1072.

33. Ebelt, H, Jungblut, M, Zhang, Y, Kubin, T, Kostin, S, Technau, A *et al.* (2007). Cellular cardiomyoplasty: improvement of left ventricular function correlates with the release of cardioactive cytokines. *Stem Cells* **25**: 236–244.

34. Kinnaird, T, Stabile, E, Burnett, MS, Shou, M, Lee, CW, Barr, S *et al.* (2004). Local delivery of marrow-derived stromal cells augments collateral perfusion through paracrine mechanisms. *Circulation* **109**: 1543–1549.

35. Kinnaird, T, Stabile, E, Burnett, MS, Lee, CW, Barr, S, Fuchs, S *et al.* (2004). Marrow-derived stromal cells express genes encoding a broad spectrum of arteriogenic cytokines and promote *in vitro* and *in vivo* arteriogenesis through paracrine mechanisms. *Circ Res* **94**: 678–685.

36. Tse, HF, Siu, CW, Zhu, SG, Songyan, L, Zhang, QY, Lai, WH *et al.* (2007). Paracrine effects of direct intramyocardial implantation of bone marrow derived cells to enhance neovascularization in chronic ischaemic myocardium. *Eur J Heart Fail* **9**: 747–753.

37. Rehman, J, Traktuev, D, Li, J, Merfeld-Clauss, S, Temm-Grove, CJ, Bovenkerk, JE *et al.* (2004). Secretion of angiogenic and antiapoptotic factors by human adipose stromal cells. *Circulation* **109**: 1292–1298.

38. Feng, J, Yang, S, Xu, L, Tian, H, Sun, L and Tang, X (2007). Role of caspase-3 inhibitor in induced anoikis of mesenchymal stem cells in vitro. *J Huazhong Univ Sci Technol Med Sci* **27**: 183–185.

39. Luebke-Wheeler, JL, Nedredal, G, Yee, L, Amiot, BP and Nyberg, SL (2009). E-cadherin protects primary hepatocyte spheroids from cell death by a caspase-independent mechanism. *Cell Transplant* **18**: 1281–1287.

40. Urish, KL, Vella, JB, Okada, M, Deasy, BM, Tobita, K, Keller, BB *et al.* (2009). Antioxidant levels represent a major determinant in the regenerative capacity of muscle stem cells. *Mol Biol Cell* **20**: 509–520.

41. Drowley, L, Okada, M, Beckman, S, Vella, J, Keller, B, Tobita, K *et al.* (2010). Cellular antioxidant levels influence muscle stem cell therapy. *Mol Ther* **18**: 1865–1873.

42. Kumar, A, Mohan, S, Newton, J, Rehage, M, Tran, K, Baylink, DJ *et al.* (2005). Pregnancy-associated plasma protein-A regulates myoblast proliferation and differentiation through an insulin-like growth factor-dependent mechanism. *J Biol Chem* **280**: 37782–37789.